SAT-WIND project. Final report

Hasager, Charlotte Bay; Astrup, Poul; Nielsen, Morten; Badger, Merete; Badger, Jake; Nielsen, P.; Sørensen, P.B.; Barthelmie, Rebecca Jane; Pryor, Sara; Bergström, H.

Publication date:
2007

Document Version
Publisher's PDF, also known as Version of record

Risø-R-Report

SAT-WIND project
Final report

C.B. Hasager, P. Astrup, M. Nielsen, M. B. Christiansen, J. Badger (Risø), P. Nielsen (EMD), P. B. Sørensen (DONG energy), R. J. Barthelmie (Univ. Edinburgh and Risø), S.C. Pryor (Indiana Univ. and Risø), H. Bergström (Univ. Uppsala)

Risø-R-1586(EN)

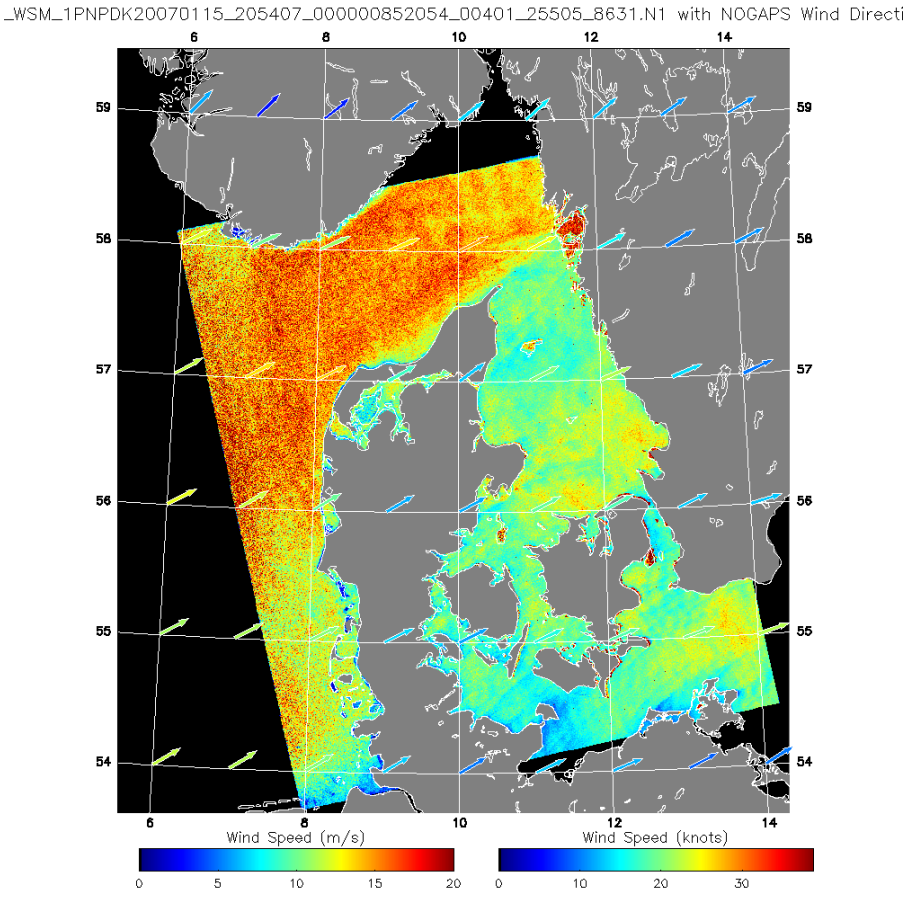

Risø National Laboratory
Technical University of Denmark
Roskilde, Denmark
April 2007

Author: C.B. Hasager, P. Astrup, M. Nielsen, M. B. Christiansen, J. Badger (Risø), P. Nielsen (EMD), P. B. Sørensen (DONG energy), R. J. Barthelmie (Univ. Edinburgh and Risø), S.C. Pryor (Indiana Univ. and Risø), H. Bergström (Univ. Uppsala)
Title: SAT-WIND project Final report

Risø-R-1586(EN)
April 2007

Abstract (max. 2000 char.):

The SAT-WIND project 'Winds from satellites for offshore and coastal wind energy mapping and wind-indexing' was a research project funded by STVF/DSF in the years 2003 to 2006 (Sagsnr. 2058-03-0006). The goal of the project was to verify the applicability of satellite wind maps derived from passive microwave, altimeter, scatterometer and imaging Synthetic Aperture Radar (SAR) technologies for wind energy tools for wind resources and wind-indexing. The study area was the Danish Seas including the North Sea, interior seas and the Baltic Sea. The report describes technical details on the satellite data sources including

- passive microwave (SSM/I, AMSR-E),
- passive microwave polarimetric (WindSat),
- scatterometer (ERS, QuikSCAT, Midori-2 and NSCAT),
- altimeter (ERS, Topex, Poseidon, GFO-1, Jason-1),
- SAR (ERS, Envisat).

The SAR wind maps were treated in S-WAsP developed by Risoe National Laboratory in cooperation with GRAS A/S in the innovative project SAT-WIND-SMV (Sagsnr. 2104-05-0084) in the years 2005 and 2006 in parallel with SAT-WIND. The results from the SAT-WIND project are presented. These include ocean wind statistics, offshore wind resource estimates and comparison results for wind-indexing.

ISSN 0106-2840
ISBN 87-550-3570-1

Contract no.: 2058-03-0006 &
Contract no.: 2104-05-0084

Group's own reg. no.: 1130308-01 & 1130315-01

Sponsorship: Danish agency for science technology and innovation. STVF/DSF

Cover :
ESA Envisat ASAR wind map from JHU/APL, Risø DTU observed 15 January 2007 at 20.54 UTC. The arrows are from the NOGAPS meteorological model indicating wind speed and direction.

Pages: 131
Tables: 17
References: 60

Information Service Department
Risø National Laboratory
Technical University of Denmark
P.O.Box 49
DK-4000 Roskilde
Denmark
Telephone +45 46774004
bibl@risoe.dk
Fax +45 46774013
www.risoe.dk

1 Introduction **5**

1.1 Project goal 5
1.2 Cooperation 5
1.3 Report structure 6

2 Background **6**

3 Satellite data **7**

3.1 Scatterometer 7
3.1.1 History 7
3.1.2 Measurement principles 8
3.1.3 Data access for wind products 10
3.1.4 QuikSCAT (scatterometer data) 11
3.1.5 Midori-II (scatterometer data) 15
3.1.6 NSCAT (scatterometer data) 15
3.1.7 ERS SCAT (scatterometer data) 16
3.1.8 ASCAT (scatterometer data) 16
3.2 Passive microwave 17
3.2.1 History 17
3.2.2 Measurement principle 17
3.2.3 SSM/I (passive microwave data) 19
3.2.4 AMSR-E (passive microwave data) 20
3.3 Passive microwave polarimetric 22
3.3.1 History 22
3.3.2 Measurement principle 22
3.3.3 WindSat (passive microwave polarimetric data) 22
3.4 SAR 23
3.4.1 History 23
3.4.2 Measurement principle 23
3.4.3 ERS-2 SAR (SAR data) 25
3.4.4 Envisat ASAR (SAR data) 28
3.4.5 ALOS PALSAR (SAR data) 32
3.5 Altimeter 33
3.5.1 History 33
3.5.2 Measurement principle 33
3.5.3 ERS RA (altimeter data) 33
3.5.4 Topex/Poseidon ALT (altimeter data) 33
3.5.5 GFO 34
3.5.6 Jason-1 34
3.6 Summary on satellite wind observations 34

4 Tools development (S-WAsP) **35**

4.1 S-WAsP for SAR (S-WAsP is short for Satellite WAsP) 35
4.2 S-WAsP for scatterometer and passive microwave 36

5 Wind resource results **38**

5.1 Results using QuikSCAT 38
5.1.1 Denmark 38
5.1.2 North Sea and Baltic Sea 49
5.1.3 Sweden 52
5.2 Results using Midori-II 57
5.3 Results using NSCAT 59
5.4 Results using ASCAT 59

5.5 Results using ERS-2 SCAT 59
5.6 Results using SSM/I 62
5.7 Results using AMSR-E 64
5.8 Results using WindSat 66
5.9 Results using ERS SAR 68
5.10 Results using Envisat ASAR 70
5.10.1 Denmark 70
5.10.2 Sweden 77
5.11 Results using ERS altimeter 80
5.12 Results using Topex altimeter 81
5.13 Results using Poseidon altimeter 82
5.14 Results using several satellites 83
5.15 Summary on satellite results 85

6 Mesoscale modeling and comparison 87

6.1 KAMM/WAsP method 87
6.1.1 Results – wind climate in Denmark 90
6.2 MIUU model 95
6.2.1 The MIUU meso-scale model 95
6.2.2 Wind climate modelling 96
6.2.3 Model domain 97
6.2.4 Geostrophic wind statistics 98
6.2.5 Results - wind climate in Sweden 100
6.2.6 Model verifications 101
6.2.7 Results from QuikSCAT and SAR in Sweden 102

7 Wind-indexing 105

7.1 Introduction 105
7.2 Wind-index results using SSM/I 107

8 Discussion 117

9 Conclusion 119

Acknowledgements 119

Appendix A (List of SAT-WIND publications) 125

Appendix B (Bitmap color scale) 128

Appendix C (Technical details on SAR systems) 129

1 Introduction

1.1 Project goal

The SAT-WIND project period was from January 2004 to October 2006. The SAT-WIND project was funded by the Danish agency for science technology and innovation, STVF (Sagsnr. 2058-03-006).

SAT-WIND is short for 'Winds from satellites for offshore and coastal wind energy mapping and wind-indexing'.

The goal of the SAT-WIND project was to verify the applicability of satellite wind maps derived from passive microwave, altimeter, scatterometer and imaging SAR technologies for wind energy tools for wind resources and wind-indexing. This has been achieved.

The study area was the Danish Seas including the North Sea, interior seas and the Baltic Sea.

1.2 Cooperation

The project was a joint cooperation between Risoe National Laboratory- DTU, Wind Energy Department (co-ordinator), Energi- and Miljødata (EMD) and DONG energy (former Elsam Engineering). During the project collaborations were established with the Johns Hopkins University, Applied Physics Laboratory in the USA, Uppsala University in Sweden and GRAS in Denmark.

The role of Risoe beyond coordination was extraction of all types of satellite data, analysis and presentation. Tool development was also undertaken by Risoe during the project. This includes the new S-WAsP for wind resource mapping from SAR and other satellite wind data. EMD analyzed satellite data in regard to wind-indexing, i.e. long-term wind observations, wind power production and changes in wind and wind power between years. DONG energy participated with the experience and data from the Horns Rev offshore wind farm. The cooperation allowed important comparison results between high-quality wind observations from offshore masts to the satellite wind data.

Cooperation with the Johns Hopkins University, Applied Physics Laboratory included hosting Ph.D. student Merete Bruun Christiansen for 4 months in the USA and supervision by Dr. Frank Monaldo and Dr. Don Thompson. After this a continued close cooperation with Risoe has taken place. In particular, the APL/NOAA SAR Wind Retrieval System (ANSWRS) has been installed at Risoe and this - in combination with access to the ESA rolling archive on Envisat ASAR - allow near-real-time wind mapping from SAR at Risoe.

The cooperation with Uppsala University includes a workshop at Risoe with Dr. Hans Bergström as invited speaker during the SAT-WIND project. The theme was mesoscale modeling of wind resources. It was agreed to cooperate and share data and make comparisons between model results and satellite wind maps. Also Uppsala University has provided a time-series of meteorological data for comparison to satellite wind data.

GRAS and Risoe cooperated closely on the tool development for SAR. The tool development was originally started in the EU project (WEMSAR, Wind Energy Mapping using SAR, contract ERK6-CT-1999-00017) and further elaborated in the ESA EOMD (European Space Agency, Earth Observation Market Development) project (EO-

windfarm, contract 17736/03/I-IW). The final tool as of today was produced in close cooperation with GRAS. The new tool is called S-WAsP. It is useful for wind resource calculation from satellite SAR wind maps. A similar routine, yet without the CHIPS interface, is run for low resolution satellite data such as scatterometer and passive microwave. The development for SAR-based wind resource mapping was supported by the project SAT-WIND-SMV (Sagsnr. 2104-05-0084) and the work was done jointly with M.Sc. Lars Boye Hansen.

Finally, the two ESA projects, EO-1356 (Wind mapping from SAR) and EO-3644 (Scandia-SAR) have been very important for the SAR wind mapping part. In EO-1356 the first analysis of ERS SAR and early Envisat ASAR analysis was done. The project EO-3644 is the source of Envisat ASAR data for the entire region of interest from the rolling archive. In the future, we foresee offshore wind results from other types of SAR data, e.g. Terra-X (science project with DLR/GKSS) and ALOS PALSAR (EO-3729). This is X-band and L-band, respectively, in contrast to C-band SAR.

1.3 Report structure

The structure of the report is given with the general background in chapter 2, description of all investigated satellite data types in chapter 3 and the tool development in chapter 4. Results from satellite wind data are presented in chapter 5, and meso-scale modeling and comparison to satellite-based wind maps are presented in chapter 6. Chapter 7 presents the wind-indexing analysis and results. Chapter 8 is discussion and chapter 9 conclusion. Listing of publications from the SAT-WIND project is given in Appendix A.

2 Background

The design, layout and siting for offshore wind farms would optimally be based on extensive, climatologically and spatially representative in situ wind observations but such observations are typically not available. This lack of readily available data also places a severe constraint on our ability to evaluate simulations conducted with meteorological models. Current practices on the modeling offshore winds therefore introduce significant uncertainties. For wind farm owners the wind power production may deviate from the prospected output and wind-indexing becomes a necessary tool in surveying on-going wind farm projects as well as in recommendations for new offshore wind farm initiatives.

Until now offshore wind observations from satellites have not been used for offshore wind energy purposes even though wind maps from various technologies such as passive microwave, altimeter, scatterometer and imaging synthetic aperture radar (SAR) are available for more than one decade. The major reasons for not using satellite winds within offshore wind energy are

- satellite wind mapping accuracy
- satellite wind mapping frequency
- low resolution satellite wind maps ‘blank’ out the coastal zone
- technological methodologies to transfer satellite data to wind energy tools

For selection of the ‘right spots’ for planning offshore and coastal wind farms, the relative offshore wind speeds would be of importance. In (pre)-feasibility studies where a large region typically is under investigation, a lower absolute accuracy on the wind

estimate may be acceptable. The spatial wind variations mapped from satellites may be used for pointing out where to put up the relatively expensive offshore met-masts. In regard to wind-indexing continuous and frequent wind observations are necessary. This can be provided by satellite wind observations.

3 Satellite data

Satellite data measuring principles for ocean wind mapping include five basic methodologies

1. Scatterometer
2. Passive microwave
3. Passive microwave polarimetric
4. Synthetic Aperture Radar (SAR)
5. Altimeter.

An introduction to each of the five measurement principles and data types are given in this chapter.

3.1 Scatterometer

3.1.1 History

Satellite scatterometry started with the Seasat-A Satellite Scatterometer (SASS) that flew from June to October 1978 and observed ocean winds. It was followed by the satellite scatterometer ERS-1 SCAT in 1991 and scatterometer ERS-2 SCAT in 1995 both developed and operated by the European Space Agency (ESA). National Aeronautics and Space Administration (NASA) launched the NASA scatterometer (NSCAT) in 1996. Unfortunately NSCAT did not work for very long, only to 1997 and therefore, very quickly, the next scatterometer was launched. It is QuikSCAT. It was launched in 1999. QuikSCAT is the workhorse on ocean wind vectors today.

Midori-II SeaWinds was launched in 2002 but it was unfortunately lost during an episode of high solar activity October 2003. NSCAT, QuikSCAT and Midori-2 are co-operations between NASA and NASDA (National Space Development Agency (Japan)). The Advanced scatterometer (ASCAT) at MetOp satellite platform was launched 19 October 2006. MetOp is the meteorological operational satellites of Eumetsat (Figa-Saldana *et al.* 2002). Table 3.1 lists the scatterometers. Scatterometers have nominal accuracy rms. of ±2 ms^{-1} within 3 to 20 ms^{-1} (for ASCAT from 2 to 25 ms^{-1}) for wind speed and wind direction accuracy within 20°. However, as demonstrated in numerous publications, e.g. at http://winds.jpl.nasa.gov/publications/quikscat_publications.html the actual accuracy is better.

In the SAT-WIND project data from ERS, NSCAT, QuikSCAT and Midori-2 have been studied.

Table 3.1 List of scatterometers.The times are local time.

Platform	Sensor	Swath (km)	Grid cell (km)	Crossing times	Coverage	Period
Seasat	SASS	500	50	?	< daily	/6 to /10/1978
ERS-1	SCAT	500	25	10.30, 21.30	< daily	/7/1991 to /3/2000-
ERS-2	SCAT	500	25	10.30, 21.30	< daily	/3/1995 to present
ADEOS-1	NSCAT	600	25	6.00, 18.00	< daily	/9/1996 to /6/1997
QuikSCAT	SeaWinds	1800	25	6.00, 18.00	Bi-daily	/6/1999 to present
Midori-2	SeaWinds	1800	25	10.30, 21.30	Bi-daily	/12/2002 - /10/2003
MetOp-1	ASCAT	2*550	50	9.30, 21.30	Daily	/11/2006 to present
MetOp-2	ASCAT		50		Daily	2007
MetOp-3	ASCAT		50		Daily	2012

3.1.2 Measurement principles

Scatterometers are real aperture radars operating in the microwave spectrum either at ~ 5 GHz (C-band) or ~ 13 GHz (Ku-band). The European (ERS SCAT and ASCAT) scatterometers work at C-band whereas the American/Japanese scatterometers (SASS, NSCAT, QuikSCAT and Midori-2) work at Ku-band.

Scatterometers transmit pulses. The pulses are echoed back to the instrument and received. The transmitted pulse is a pulse with linear frequency modulation ('chirp'). When the received pulses are de-chirped, the backscattered signal can be analyzed. The frequency can be mapped into slant range when the chirp rate and the Doppler frequency are known. The normalized backscatter per resolution cell in slant range (across track) and ground range (along flight track) is the key information used for wind vector retrieval. Variations in the magnitude of the Normalized Radar Cross Section (NRCS) are a function of the centimeter-sized, wind-driven waves of the ocean surface. These short waves give a roughness of the sea surface that has a size similar to that of the microwave radiation. (The roughness is not identical to the aerodynamic roughness associated with large waves produced during wind and air-sea interaction during hours. In fact, the scatterometer and SARs are not viewing the wavelengths at the scale of meters).

ERS-1 and ERS-2 SCAT have single-swath (beam) with three antennae. The three antennas are fore-, mid- and aft measuring the upwind, downwind and crosswind components. NSCAT and ASCAT have 6 antennae in a mirrored pattern. Therefore these are able to map dual-swath.

Rotating antennae measure the same (minimum) three components. Rotating antennae are found at QuikSCAT and Midori-2. QuikSCAT has two pencil beam radar antennae both scanning in conical shape. The two antennae measure with two different incident

angles, two polarizations, and as the beams look forward and aft, also measure at two different aspect angles. Hence multiple NRCS observations are obtained at 25 km resolution.

An example of three antennae is shown for the ERS scatterometer (figure 3.1). The three antennae have radar beams looking 45º (forward), 90º (sideways), and 135º (backward) with respect to the satellite's flight direction. The beams continuously illuminate a 500 km wide swath as the satellite moves along its orbit. Thus three backscatter measurements of each grid point are obtained at different viewing angles and separated by a short time delay. These "triplets" are fed to a mathematical model that calculates surface wind speed and direction

(http://earth.esa.int/rootcollection/eeo4.10075/scatt_design.html).

The mathematical model is a geophysical model function (GMF) that relates the NRCS to the wind vector through empirical coefficients. The coefficients are found from collocated in-situ wind data and NRCS values, or a combination of in-situ wind data, meteorological model data and NRCS values (Stoffelen & Anderson 1997).

Wind from QuikSCAT and Midori-2 are provided in swath and gridded mode. Swath is the original coordinate system. Gridded mode is resampled to a geographical coordinate system. ERS SCAT and NSCAT are provided in swath mode only. ERS SCAT can be purchased from ARGOSS (http://www.argoss.nl/) in gridded mode.

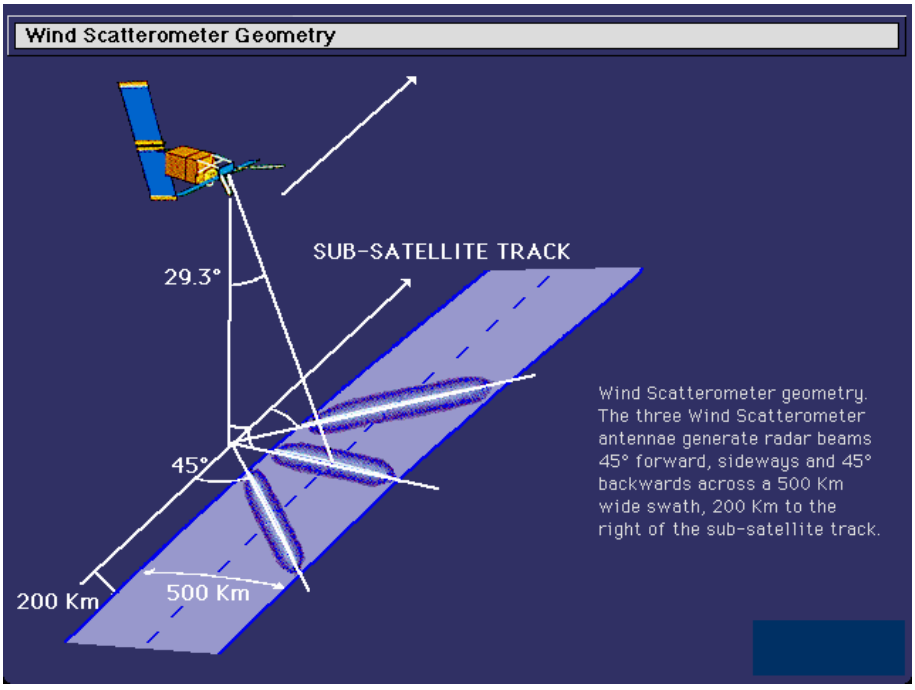

Figure 3.1 ERS wind scatterometer geometry. From

http://earth.esa.int/rootcollection/eeo4.10075/scatt_design.html

3.1.3 Data access for wind products

Satellite data are available from more sources. "The Physical Oceanography Distributed Active Archive Center (PO.DAAC)", part of NASA's Jet Propulsion Laboratory, "http://podac.jpl.nasa.gov", holds data from many satellites, but this seems all to be swath data. Remote Sensing Systems (RSS), "www.remss.com", also provide swath data, but additionally they have bitmaps for most of the interesting data, so of the 70 GByte compressed data downloaded for this project, close to 40 GByte have been bitmaps from Remote Sensing Systems. They have been downloaded by anonymous FTP from their FTP-server "ftp.ssmi.com" using UNIX-scripts to automate the process. The residual 30 GByte of data are swath data downloaded from PO.DAAC using their download tool "Aspera", "http://podaac.jpl.nasa.gov/aspera/". Approximately 250 MByte of new data from still operating satellites are downloaded from Remote Sensing Systems once a month.

The bitmaps

The RSS bitmaps cover the Earth with a resolution of 0.25 × 0.25 degree, i.e. with fields of 1440*720 pixels. The pixel sequence is west to east before south to north, i.e. 1st pixel lower left corner coordinates are 0.00 degree east, 90.00 degree south, second pixel lower left corner coordinates are 0.25 degree east, 90.00 degree south, 1441st pixel lower left corner coordinates are 0.00 degree east, 89.75 degree south, etc. The pixel values are single byte unsigned integers, IVAL, 0<=IVAL<=255, and the different field valus are appropriately scaled to get the best possible resolution with the interval 0<=IVAL<=250, the last five values being used as flags.

3.1.4 QuikSCAT (scatterometer data)

QuikScat data are produced by Remote Sensing Systems and sponsored by the NASA Ocean Vector Winds Science Team. Data are available at "www.remss.com".

The QuikScat data are recorded with a SeaWinds instrument. The recording started 19th July 1999, and is still ongoing (March 2007). Since 1.10.2006 the coastal mask has been made broader as shown in figure 3.2. Before 31.8.2006 data were from ver. 3, since then from ver. 4.

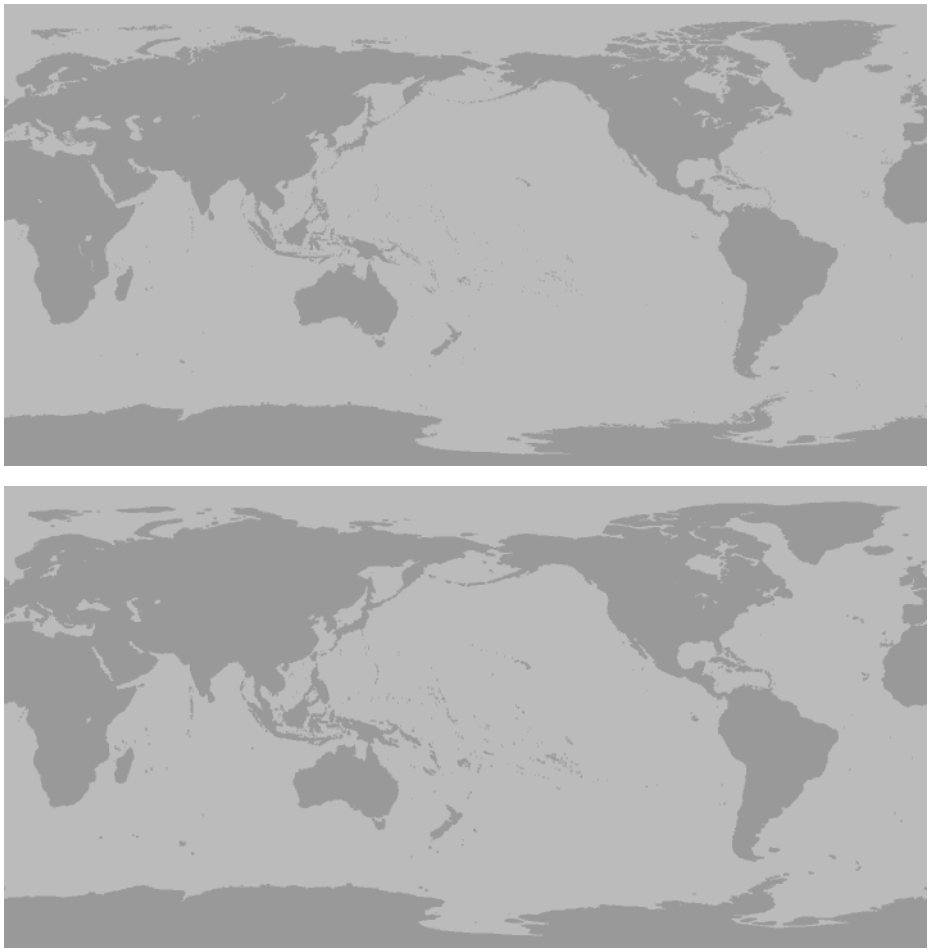

Figure 3.2 Land mask used in QuikSCAT from 1999 to 30.9.2006 (above) and since 1.10.2006 (below).

The bitmap pixel values are given as single byte unsiged integers, IVAL, i.e. 0 <= IVAL <= 255, used as follows:

```
0 <= IVAL <= 250: valid geophysical data
     IVAL  = 251: not used for scatterometers
     IVAL  = 252: not used for scatterometers
     IVAL  = 253: scatterometer observations exist, but are bad
     IVAL  = 254: no scatterometer observations
     IVAL  = 255: land mass
```

The bitmap files, one per day, contain eight data fields. The first four are for the ascending passes, i.e. recorded when the satellite travels north, the last four for the descending passes. Scaling is used to get the most out of the 1-byte resolution. The field parameters and the scaling read:

Fields	Parameter	Scaling
1st & 5th	Time [minutes of day GMT]	TIME = IVAL * 6
2nd & 6th	Wind Speed [m/s] at 10 m	WSPD = IVAL * 0.2
3rd & 7th (oceanic)	Wind Direction [deg]	WDIR = IVAL * 1.5
4th & 8th	Combination Rain Flag	bit combination

The "oceanic" wind direction is the direction of the wind vector, i.e. it is 180 degree different from the meteorological wind direction.

The combination rain flag contains a stand-alone scatterometer rain flag and available collocated radiometer rain data.

bit pos 0	SCATTEROMETER rain flag (0=no rain, 1=rain)
bit pos 1	1 for collocated SSMI, TMI observations (for QuikSCAT data) or AMSR observations (for Midori-II data) within 60 min, else=0
bit pos 2-7	0-63: radiometer rain (data from another satellite) where: 0: absolutely no rain 1: rain in one of the adjacent cells 2: Radiometer RR = 0.5 3: Radiometer RR = 1.0 4: Radiometer RR = 1.5 etc.

RR is the columar rain rate - rain rate times rain column height, unit [km mm/hour] - measured with a radiometer on another satellite. In the swath files this RR is given as a 1 byte integer, 255 meaning no measurement, and 0 to 254 meaning 0.0 to 25.4 km*mm/hour columnar rain rate, and it is recommended not to use the wind data if this rate exceeds 0.15, which must mean if it exceeds 0.1. As the bit map files are generated from the swath files, this must mean that the bit map wind shoud not be used if the "bit 2-7" value of the rain flag is 2 or higher. Neither should it be used, if the "bit 0" value is 1, i.e. if the scatterometer indicates rain.

It is important to remove rain-contaminated data from the processing, especially at lower wind speeds typical of the tropics, as this is where rain has the greatest effect. Rain causes SeaWind instruments to over-predict wind speeds in low wind situations.

Each pixel of each field holds the latest value of the day in question, i.e. at higher latitudes, where the satellite passes more times a day. The last recorded values are those retrieved. Example of QuikSCAT wind speed and wind direction maps are presented in figure 3.3.

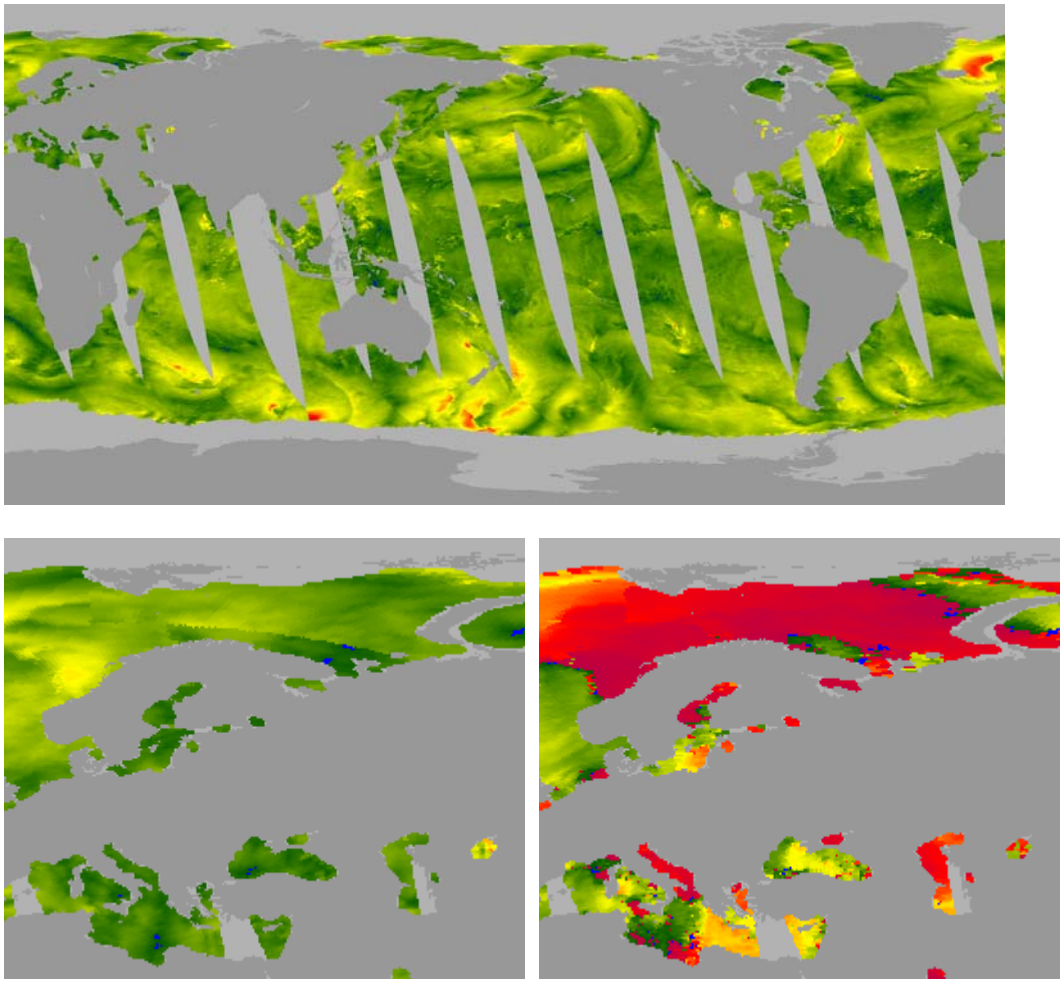

Figure 3.3 QuikScat wind speed map of 3rd October 2003, ascending passes, global map (top panel). Panels below: Cut-outs covering the European seas east of Greenwich. Left: wind speed; right: wind direction. Color scale in Appendix B.

QuikSCAT wind maps are produced at a higher spatial resolution of 12.5 km by 12.5 km at NOAA/NESDIS. Examples from the near-real-time (NRT) server with QuikSCAT winds at http://manati.orbit.nesdis.noaa.gov/hires/ are shown in figure 3.4. It includes a wind map with the standard 25 km by 25 km grid resolution and a wind map with the research quality 12.5 km by 12.5 km resolution. Data for research in the SAT-WIND project has been requested, however not yet provided at the high resolution. One advantage of this higher resolution may be that the data are obtained slightly closer to the coastline.

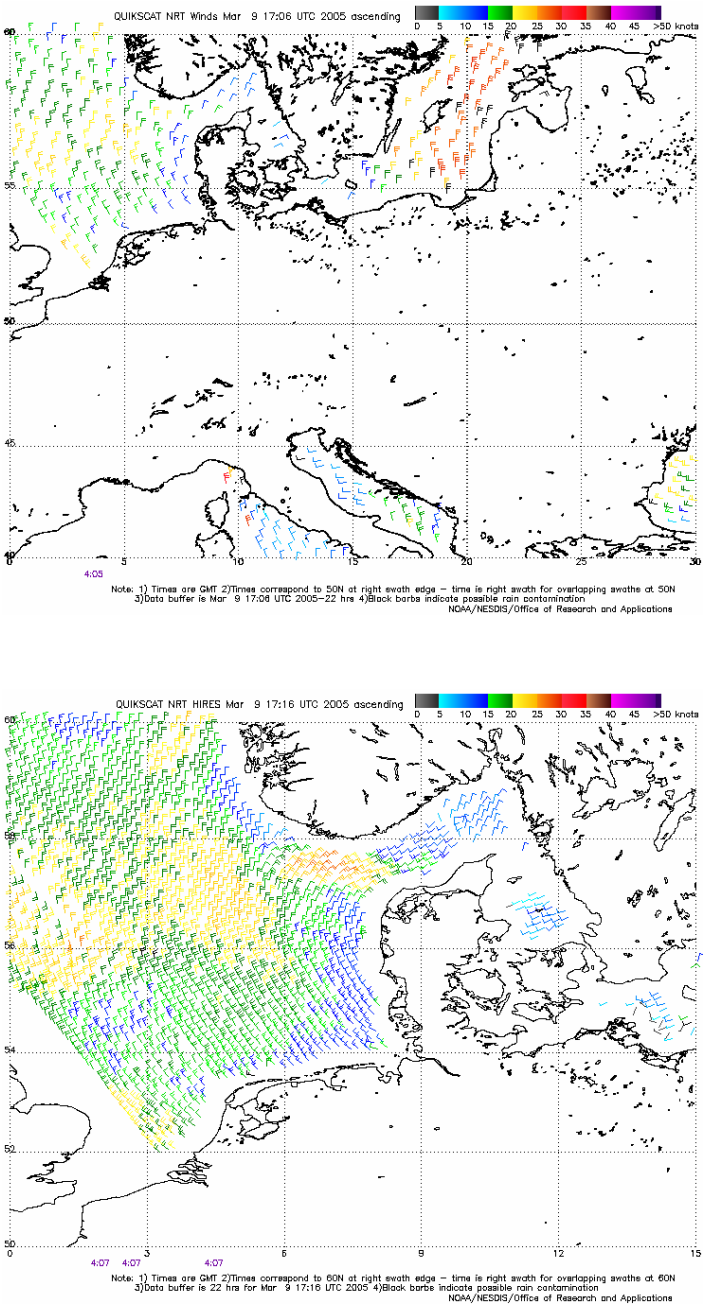

Figure 3.4 Wind maps from http://manati.orbit.nesdis.noaa.gov/hires/ shown in near-real-time from the QuikSCAT satellite. The upper panel shows the standard product of 25 km by 25 km. The lower panel shows the high-resolution research quality 12.5 km by 12.5 km grid cell wind map. Both wind maps are from March 9th, 2005.

3.1.5 Midori-II (scatterometer data)

Midori-II (Adeos-2, SeaWinds) data are produced by Remote Sensing Systems and sponsored by the NASA Ocean Vector Winds Science Team. Data are available at "www.remss.com".

The Midori-II data, also called Adeos-II or SeaWinds data are recorded by a SeaWinds instrument in the period 10th April to 24th October 2003. The data file format is exactly as for the QuikScat data. An example is shown in figure 3.5.

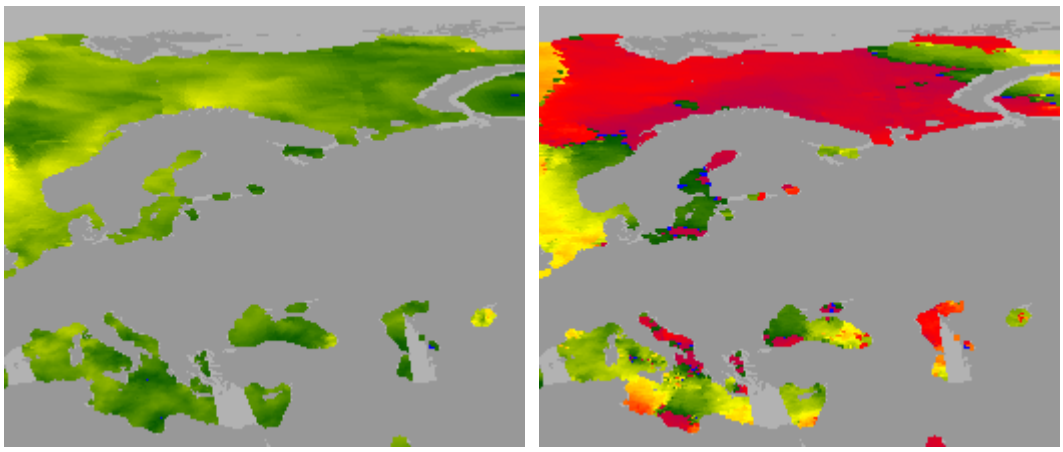

Figure 3.5 Cut-outs of Midori-II maps of 3rd October 2003, ascending passes, covering part of the European seas east of Greenwich. Left: wind speed; right: wind direction. Color scale in Appendix B.

3.1.6 NSCAT (scatterometer data)

NSCAT data are produced by Remote Sensing Systems and sponsored by the NASA Ocean Vector Winds Science Team. Data are available at "ftp.ssmi.com/nscat".

The NSCAT (NASA Scatterometer) data were recorded by the ADEOS-I satellite from 15th September 1996 to 29th June 1997. The data are available as swath files only, but have within the actual project been converted into fixed-grid bitmap files with the same data format as that directly retrived for the QuikScat and Midori-II data.

It is seen, that the NSCAT data do not go as close to the coasts as do the QuikScat and Midori-II data, and all in all contain much more voids than these. Wind speed and wind direction map examples are shown in figure 3.6.

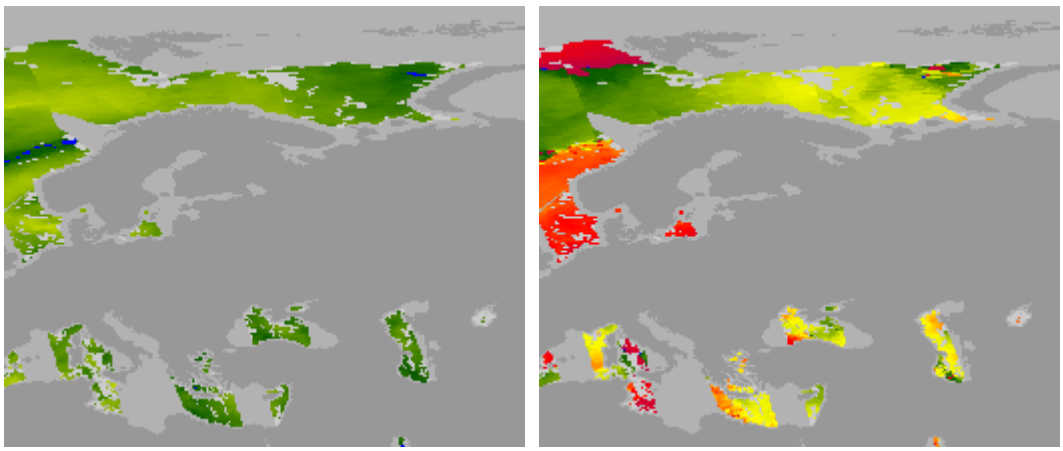

Figure 3.6 Cut-outs of NSCAT maps of 27th June 1997, ascending passes, covering part of the European seas east of Greenwich. Left: wind speed; right: wind direction. Color scale in Appendix B.

3.1.7 ERS SCAT (scatterometer data)

ERS-2 SCAT wind data were received from ARGOSS, http://www.argoss.nl in co-located ascii files providing latitude, longitude and wind speed for the North Sea in the period June 1999 to December 2000.

Wind data from ERS-1 and -2 SCAT were obtained by courtesy of Han Wensink, ARGOSS from a site (1° grid cell) near Horns Rev in the North Sea covering the period 1991 to 2003.

From http://www.ifremer.fr/cersat/ weekly and monthly products gridded at 1° were available but these were not studied. (It was preferred to study only observations available in form of individual observations, not time-averaged products).

3.1.8 ASCAT (scatterometer data)

The wind data products are not yet released for research. Since 17 February 2007 raw data dissemination has been initiated

http://www.eumetsat.int/Home/Main/Media/News/029482?l=en

3.2 Passive microwave

3.2.1 History

It is the Meteorological Program of the United States Department of Defense that is in charge of the Defense Meteorological Satellite Program (DMSP). Within DMSP a long series of Earth observing satellites have been active since the mid-70'ties. The series is called F-1 (from 1976), F-2 (from 1977), etc., up to currently operating satellite platforms F-13 (from 1995), F-14 (from 1997) and F-15 (from 1999). Since F-8 (from 1987) a passive microwave radiometer has been flown. This sensor is capable of measuring ocean wind speed (not direction). It is the Special Sensor Microwave Imager (SSM/I).

Also the Advanced Microwave Scanning Radiometer (AMSR) and AMSR-E, the Advanced Microwave Scanning Radiometer for Earth Observation System (at NASA) provides ocean wind speed from passive microwave. AMSR and AMSR-E were developed by Japan Aerospace Exploration Agency (JAXA). AMSR-E was launched in April 2002. AMSR was launched December 2002 but lost in October 2003. Table 3.2 list SSM/I and AMSR series. In the current project data from F-8, F-10, F-11, F-13, F-14, F-15 and AMSR-E were investigated.

3.2.2 Measurement principle

The SSM/I is a seven channel, four frequency, linearly-polarized, passive microwave radiometric system which measures atmospheric, ocean, and terrain microwave brightness temperatures at 19.35, 22.24, 37.00, and 85.80 GHz (from http://www.ncdc.noaa.gov/oa/satellite/satelliteresourcesabout.html#DMSP, (Kramer 1996)). The archived data consist of antenna temperatures recorded across a 1400 km swath. The electromagnetic radiation is polarized by the ambient electric field and scattered by the atmosphere and the surface of the Earth. SSM/I records both horizontally and vertically polarized electromagnetic emission at the four wavelengths.

The brightness temperature (T_B) in Kelvin is related to the instantaneous wind speed over the ocean. An empirical relationship is found between T_B and wind observations from buoys and radiosondes. It is now the wind speed at 10 m above sea surface that is calculated (Wentz 1995). Recently the SSM/I data series have been recalculated and the observations are also compared to NSCAT and QuikSCAT wind data (http://www.ssmi.com/ssmi/ssmi_description.html).

AMSR is an eight-frequency, total-power microwave radiometer with dual polarization (except two vertical channels in the 50GHz band). The bands are at 6.925, 10.65, 18.7, 23.8, 36.5, 89.0, 50.2, and 53.8 GHz

(http://sharaku.eorc.jaxa.jp/AMSR/products/index.htm).

The Advanced Microwave Scanning Radiometer - Earth Observing System (AMSR-E) is a twelve-channel, six-frequency, passive-microwave radiometer system. It measures horizontally and vertically polarized brightness temperatures at 6.9 GHz, 10.7 GHz, 18.7 GHz, 23.8 GHz, 36.5 GHz, and 89.0 GHz. The spatial resolution of AMSR-E data doubles that of SSM/I (http://nsidc.org/data/docs/daac/amsre_instrument.gd.html).

Table 3.2. List of passive microwave series.

Platform	Sensor	Swath (km)	Crossing times	Period	Resolution (º)	Dynamic range and target accuracy and rms
F-8	SSM/I	1400	6.00 18.00	/10/1087 to /12/1991	0.25	3-25 ms^{-1} ± 2 ms^{-1} 1.3 ms^{-1} rms
F-10	SSM/I	1400	6.00 18.00	/12/1990 to /11/1997	0.25	3-25 ms^{-1} ± 2 ms^{-1} 1.3 ms^{-1} rms
F-11	SSM/I	1400	5.00 17.00	/12/19991 to /5/2000	0.25	3-25 ms^{-1} ± 2 ms^{-1} 1.3 ms^{-1} rms
F-13	SSM/I	1400	6.00 18.00	/5/1995 to present	0.25	3-25 ms^{-1} ± 2 ms^{-1} 1.3 ms^{-1} rms
F-14	SSM/I	1400	9.30 20.30	/5/1997 to present	0.25	3-25 ms^{-1} ± 2 ms^{-1} 1.3 ms^{-1} rms
F-15	SSM/I	1400	10.30 21.30	/12/1999 to /8/2006	0.25	3-25 ms^{-1} ± 2 ms^{-1} 1.3 ms^{-1} rms
Aqua	AMSR-E	1445	10.30 21.30	/4/2002 to present	0.25	0-30 ms^{-1} ± 2 ms^{-1} rms (0-20 ms^{-1}) 10% rms (0-30 ms^{-1})
Midori-2	AMSR	1445	10.30, 21.30	/12/2002 to /10/2003	0.25	0-30 ms^{-1} 1.5 ms^{-1}

3.2.3 SSM/I (passive microwave data)

Wind from SSM/I and AMSR-E are available as swath and gridded mode.

SSM/I data are produced by Remote Sensing Systems and sponsored by the NASA Earth Science REASoN DISCOVER Project. Data are available at "www.remss.com". (Data from version 5 and 6 of wind maps have been studied.)

The SSM/I data are/has been recorded by 6 DMSP-satellites in polar orbits, 2 of which are still in operation (March 2007). The satellites are differentiated through the names F08, F10, F11, F13, F14, and F15, which also form part of the data filenames. The F08-satellite operated from 9th October 1987 to 31st December 1991, the F10-satellite from 8th December 1990 to 14th November 1997, and the F11-satellite from 3rd December 1991 to 16th May 2000. The still operating satellites are the F13-satellite, operating since 3rd May 1995 and the F14-satellite, operating since 8th May 1997. The F15-satellite was operating from 18th December 1999 to August 2006.

The data are given in the same bitmap manner and resolution as the other bitmap data - see description in section 3.1.3 and 3.1.4 - but the field parameters are somewhat different.

Each daily file holds 10 fields, the first five for the ascending passes, the last five for the descending passes. The field parameters, the scaling, and the flags read:

Fields	Parameter	Scaling
1st & 6th	Time [minutes of day GMT]	TIME = IVAL * 6.0
2rd & 7th	10m wind speed [m/s]	WSPD = IVAL * 0.2
3th & 8th	columnar water vapor [mm]	VAPOR = IVAL * 0.3
4th & 9th	cloud liquid water [mm]	CLOUD = IVAL * 0.01
5th & 10th	precipitation rate [mm/hr]	RAIN = IVAL * 0.1

```
0 <= IVAL <= 250: valid geophysical data
     IVAL  = 251: regions where wind speed was not derived or heavy
                  rain on water vapor map
     IVAL  = 252: sea ice (locations where >0% ice)
     IVAL  = 253: SSM/I observations exist, but are bad
     IVAL  = 254: no SSM/I observations
     IVAL  = 255: landmass
```

Remark: No wind direction. The data do not at all go close to the coasts. Examples of wind speed maps are shown from the 6 satellites (F8, F11, F10, F13, F14 and F15) in figures 3.7.

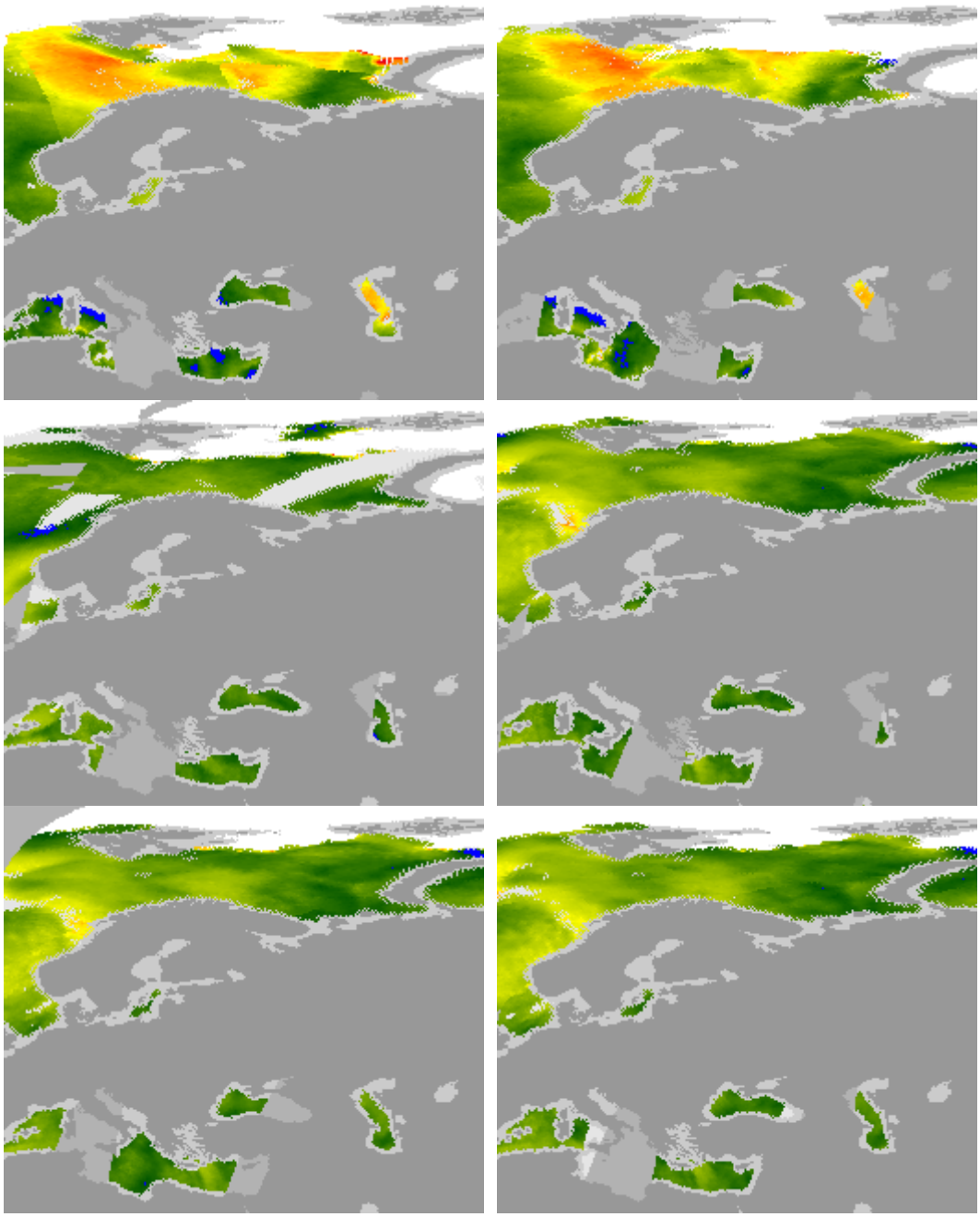

Figure 3.7 Cut-outs of SSM/I wind speed maps, ascending passes, covering part of the European seas east of Greenwich. Top panels: Left: satellite F08; right: satellite F11. Middle panels: Left: satellite F10, 27th June 1997; right: satellite F13, 3rd October 2003. Bottom panels: Left: satellite F14; right: satellite F15. Color scale in Appendix B.

3.2.4 AMSR-E (passive microwave data)

AMSR-E data are produced by Remote Sensing Systems and sponsored by the NASA Earth Science REASoN DISCOVER Project and the AMSR-E Science Team. Data are available at "www.remss.com".

The AMSR-E data has been recorded since 1st June 2002, and are available in the same fixed-grid format as the QuikScat data, the field parameters, however, being partly different. Again one file per day but here containing twelve fields, the first six for the ascending passes, the last six for the descending. The field parameters, the scaling, and the flags read:

Fields	Parameter	Scaling
1st & 7th	Time [minutes of day GMT]	TIME = IVAL * 6.0
2nd & 8th	sea surface temperature [C]	SST = IVAL * 0.15-3.0
3rd & 9th	10m surface wind [m/s]	WSPD = IVAL * 0.2
4th & 10th	columnar water vapor [mm]	VAPOR = IVAL * 0.3
5th & 11th	cloud liquid water [mm]	CLOUD = IVAL * 0.01
6th & 12th	rain rate [mm/hr]	RAIN = IVAL * 0.1

```
0 <= IVAL <= 250: valid geophysical data
     IVAL  = 251: missing SST or WSPD due to sun glint;
                  missing SST or WSPD near sea ice;
                  missing SST or WSPD due to rain;
                  missing WAPOR due to heavy rain;
                  missing SST due to high WSPD (> 20 m/s)
     IVAL  = 252: sea ice
     IVAL  = 253: observations exist, but are bad (not used in
                  composite maps)
     IVAL  = 254: no observations
     IVAL  = 255: land mass
```

Remark: No wind direction and no coverage near coasts. An example of a wind speed map is shown in figure 3.8.

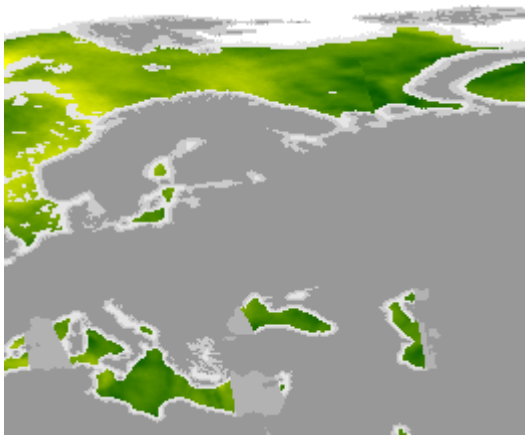

Figure 3.8 Cut-out of ASMR-E wind speed map of 3rd October 2003, ascending passes, covering part of the European seas east of Greenwich. Color scale in Appendix B.

3.3 Passive microwave polarimetric

3.3.1 History

The WindSat radiometer on-board the Coriolis satellite platform is the first space-borne multi-frequency polarimetric microwave radiometer. It was launched January 2003. WindSat was developed by the Naval Research Laboratory for the U.S. Navy and the National Polar-orbiting Operational Environmental Satellite System. It will be used instead of SSM/I after year 2010 when the DMPS and NOAA meteorological programs merge. Furthermore the European MetOp ASCAT will be part of this new system. The data are listed in table 3.3. Data from WindSat are studied in the current project.

Table 3.3 List of polarimetric passive microwave.

Platform	Sensor	Swath (km)	Period	Resolution (km)
Coriolis	WindSat	840	/1/2003 to present	25

3.3.2 Measurement principle

WindSat measures the principal polarizations (vertical and horizontal) and the cross-correlation of the vertical and horizontal polarizations. The microwave emission from the ocean surface depends on wind speed. The wind driven waves on the ocean surface are not isotropic and their distribution varies with wind direction. This non-isotropic effect is measured by the polarimetric passive microwave data. The radiometer operates at 6.8, 10.7, 18.7, 23.8, and 37.0 GHz. The brightness temperatures at vertical, horizontal, plus 45º, minus 45 º (the Stokes vector) are obtained. This provides the possibility to map the wind vector. It is the 10.7, 18.7 and 37.0 GHz bands that are fully polarimetric whereas the 6.8 and 23.8 GHz have dual-polarization. The swath is 840 km (http://www.nrl.navy.mil/content.php?P=04REVIEW87). Wind Sat data are provided in swath mode (and raw) only.

3.3.3 WindSat (passive microwave polarimetric data)

The WindSat data can be made available upon request and specification of use to NASA's Jet Propulsion Laboratory, see "http://podaac.jpl.nasa.gov/windsat".

The data are swath data and both Sensor Data Record (SDR) files containing raw data, and Experimental Data Record (EDR) files containing processed data, i.e. wind speed, wind direction, sea surface temperatures, and other parameters, are obtainable. A set of the latter covering the period 1st September 2003 to 28th February 2004 were downloaded, approximately 30 GByte in compressed form. The EDR data resolution is approximately 0.54 degree in the "look" direction, and 0.36 in the sweep direction, but for convenience the downloaded set has been converted into the same fixed-grid data structure of 0.25 degree resolution as the downloaded bitmap data, but with only 6 fields per daily file, i.e. time of day, wind speed, and wind direction, for ascending and descending passes. An example of a wind speed map is shown in figure 3.9.

```
Fields      Parameter                      Scaling
----------  -----------------------------  ------------------------------
1st & 4th   Time [minutes of day GMT]      TIME = IVAL * 6
2nd & 5th   Wind Speed [m/s] at 10 m       WSPD = IVAL * 0.2
3rd & 6th   Wind Direction [deg]           WDIR = IVAL * 1.5 (oceanic)

0 <= IVAL <= 250: valid geophysical data
     IVAL  = 251: no data
```

```
IVAL  = 252: not used
IVAL  = 253: not used
IVAL  = 254: not used
IVAL  = 255: land mass
```

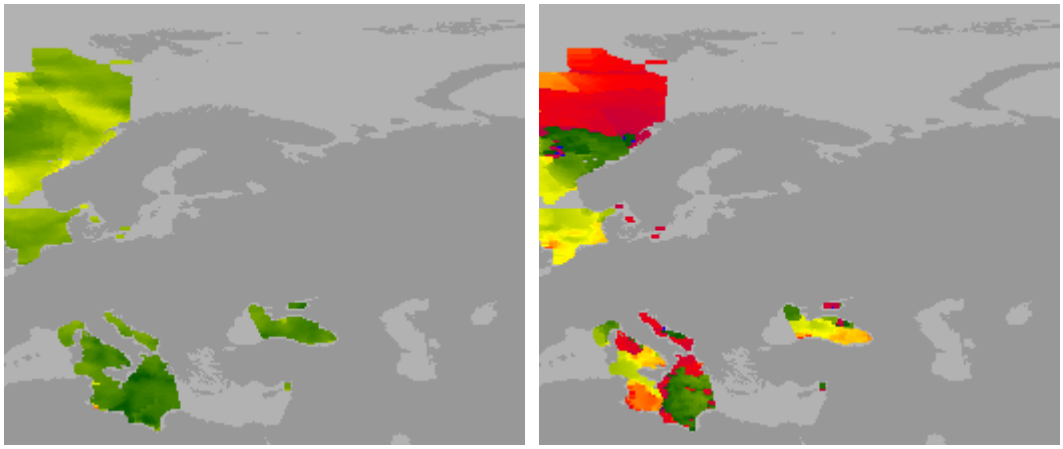

Figure 3.9 Cut-outs of WindSat maps of 3rd October 2003, ascending passes, covering part of the European seas east of Greenwich. Left: wind speed; right: wind direction. Color scale in Appendix B.

3.4 SAR

3.4.1 History

Seasat carried an L-band SAR with HH-polarization from June to October 1978. This was the first SAR sensor on-board a satellite platform. Seasat was followed by several shuttle missions with SAR sensors. In Russia, ALMAZ-1/-2 S-band (~3 GHz) SAR sensors were flown in 1987 and 1991-1992 (Hasager 2000; Kramer 1996). SAR images are available from ERS-1/-2 from ESA, JERS-1 (Japanese Earth Resources Satellite) from NASDA, Radarsat-1 from the Canadian Space Agencey (CSA), Envisat from ESA and PALSAR at the Advance Land Observing Satellite (ALOS) from NASDA (http://www.eorc.jaxa.jp/ALOS/about/palsar.htm) as listed in table 3.4. For the future are scheduled Radarsat-2 and -3 from CSA and ESA Sentienel-1. See table 3.4. A comparison of SAR systems is provided by http://www.nap.edu/html/ssb_html/SAR/sartab11.htm.

SAR data from ERS-2 and Envisat ASAR were studied in the current project.

3.4.2 Measurement principle

A SAR instrument is looking sideways between the angles from near-range to far-range (see Figure 3.10). In this dimension, the slant range observations are made. The distance on the ground between near- and far-range is the swath width. The across track resolution is obtained through frequency modulation (‘chirp’).

As the satellite moves along the flight track, the azimuth range observations are made. The azimuth resolution is specified as one-half the antenna length. The synthetic aperture is obtained by tracking the individual phase and amplitude of individual return signals during a given integration time interval. Hence the distance is much longer than the physical length of the instrument antenna. It is the Doppler shift in each individual

recorded signal in the backscatter signal that determines the position of the scatter in the azimuth position.

The SAR illuminates a footprint and the signals returned from the footprint area are the backscattered values, the NRCS.

It is again the relationship between NRCS and ocean wind speed, similar to the scatterometers, which is used to calculate the wind speed. The geophysical model functions can be used provided that the wind direction is known *a priori*, as the imaging SAR only observes one view of the surface (in contrast to e.g. 3 to 4 views from the antennae at scatterometers). However, it is possible in most SAR images to identify linear features aligned with the mean wind direction from techniques such as two-dimensional Fast Fourier analysis (Gerling 1986) or wavelets (Du *et al.* 2002).

SAR data are provided in swath (and raw) mode only.

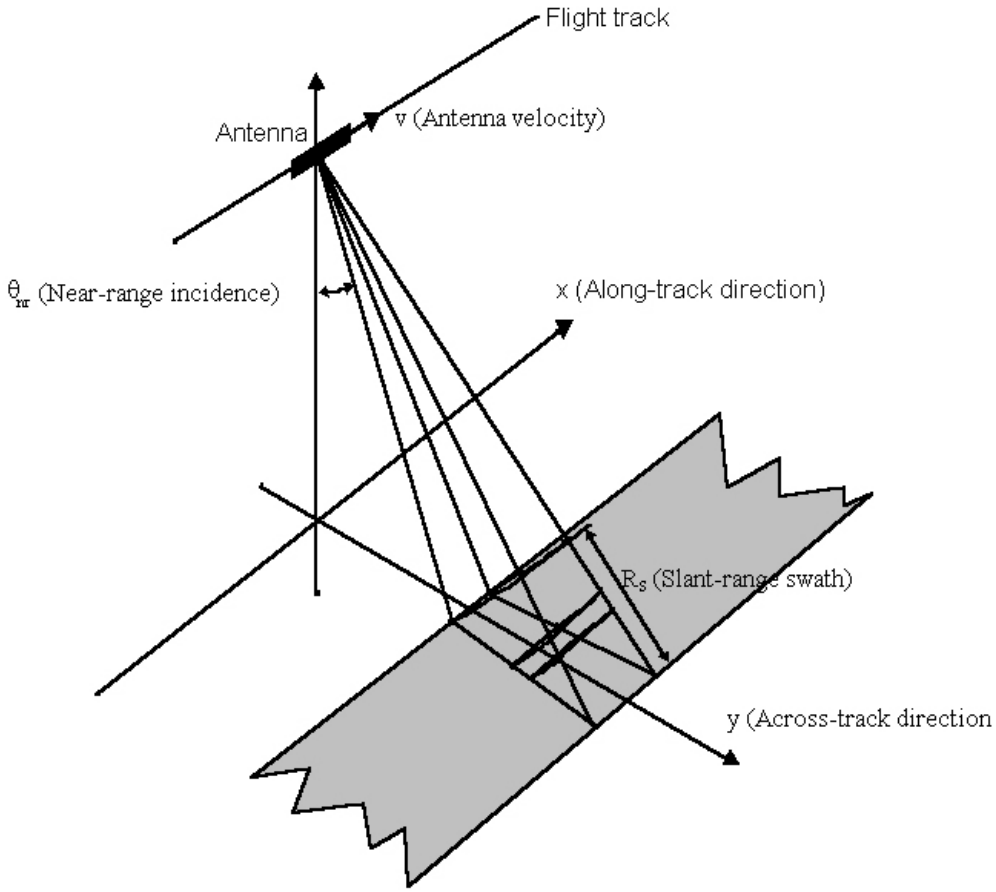

Figure 3.10 SAR system viewing geometry. From

http://www.emi.dtu.dk/aboutEMI/emi_presentation/images/hvad_er_en_sar.jpg

Table 3.4 List of SAR (Imaging radars)

Platform	Sensor	Period	Band	Pol.	Resolution (m)	Swath (km)
Seasat	SAR	/6/ to /10/1978	L	HH	25	100
ALMAZ-1	SAR	/3/ to /10/1991	S	HH	13-20	20-35
ALMAZ-2	SAR	/5/1991 to /10/1992	S	VV	?	?
ERS-1	SAR	/7/1991 to /3/2000	C	VV	25	100
JERS-1	SAR	/2/1992 to /11/1998	L	HH	18	75
ERS-2	SAR	/3/1995 to present	C	VV	25	100
Radarsat-1	ScanSAR	/11/1995 to present	C	HH	25-100	25-170
Envisat	ASAR	/3/2000 to present	C	VV, HH, VH, HV	25-250	100-400
ALOS	PALSAR	/11/2006 to present	L	VV, HH, VH, HV	7-88	
Radarsat-2	ScanSAR	2007 scheduled	C	VV, HH, VH, HV		
Radarsat-3	ScanSAR	2012 scheduled	C	VV, HH, VH, HV		
Sentinel-1	ASAR	?	C	VV, HH, VH, HV		
Radarsat-4	ScanSAR	2013 scheduled	C	VV		
Radarsat-5	ScanSAR	2014 scheduled	C	VV		

Further technical detail on satellite SAR is listed in Appendix C.

3.4.3 ERS-2 SAR (SAR data)

ERS-2 SAR scenes were received from ESA in the Cat. 1 research project EO-1356. The scenes were received in swath mode in the precision (PRI) format. It was 3-look at a resolution of 25 m by 25 m grid cells covering 100 km by 100 km.

ERS-2 is in sun-synchronous polar retrograde orbit at an altitude of 780 km. The local crossing time at equator is 10.30 am in ascending pass and at 21.30 o'clock local time in descending pass. The repeat cycle was 35 days. At mid-latitude there is ~10 days revisit

time. ERS-2 was launched April 21st, 1995. It had a 3-year mission design life. However, ERS-2 SAR is still operational under certain circumstances more than 11 years after launch. The data archive at ESA http://odisseo.esrin.esa.it/eoli/eoli.html contains a very large amount of SAR images from ERS-1 and ERS-2.

An example of a raw image covering the Baltic Sea between Lolland-Falster and Germany is shown in Figure 3.11. The processing of the SAR image included calibration with the BEST software from ESA, http://earth.esa.int/services/best/. The calibrated image was then calculated into a wind speed map using the Nansen Environmental and Remote Sensing Centre tool WEMSARtool, available through http://www.nersc.no/EO-WINDFARM/index.php. It is the CMOD-4 model by (Stoffelen & Anderson 1997) that was applied. The wind direction was either taken from offshore meteorological observations or from determination of the streak direction in the SAR image. An example of a wind speed map from the North Sea at Horns Rev is shown in Figure 3.12.

All SAR data from ERS-2 SAR that were analyzed in the SAT-WIND project are listed in table 3.6. Many of the ERS-2 SAR images (62) were recorded prior to construction of the Horns Rev wind farm. Wind maps from these images have been compared to meteorological observations (Hasager *et al.* 2004b). SAR images recorded after construction of the Horns Rev and Nysted offshore wind farms have been used for a study on wake effects (Christiansen & Hasager 2005b; Hasager *et al.* 2005b; Christiansen & Hasager 2005a). The two SAR data sets were combined in the SAT-WIND project for wind resource estimation (Hasager *et al.* 2005c).

Table 3.6 ERS-2 SAR and Envisat ASAR satellite images in the SAT-WIND project.

	ERS SAR	Envisat ASAR high-resolution (IMG & APP)	Envisat ASAR wide-swath-mode (WSM)	Total
Horns Rev before wind farm	62			62
Horns Rev after wind farm	28	8		36
Nysted after wind farm	2	4		6
Denmark			~150	150
Baltic Sea			~100	100
Total				~350

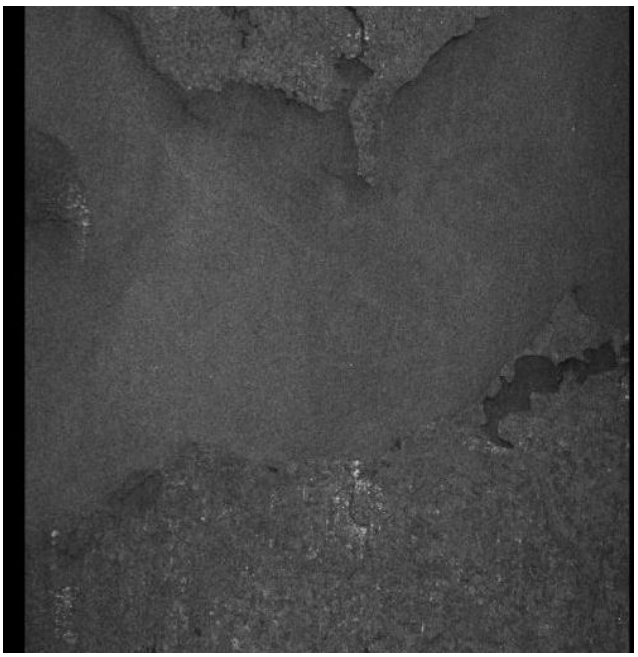

Figure 3.11 ERS-2 SAR image from the south Baltic Sea from ESA. The image is from 19 October 2003.

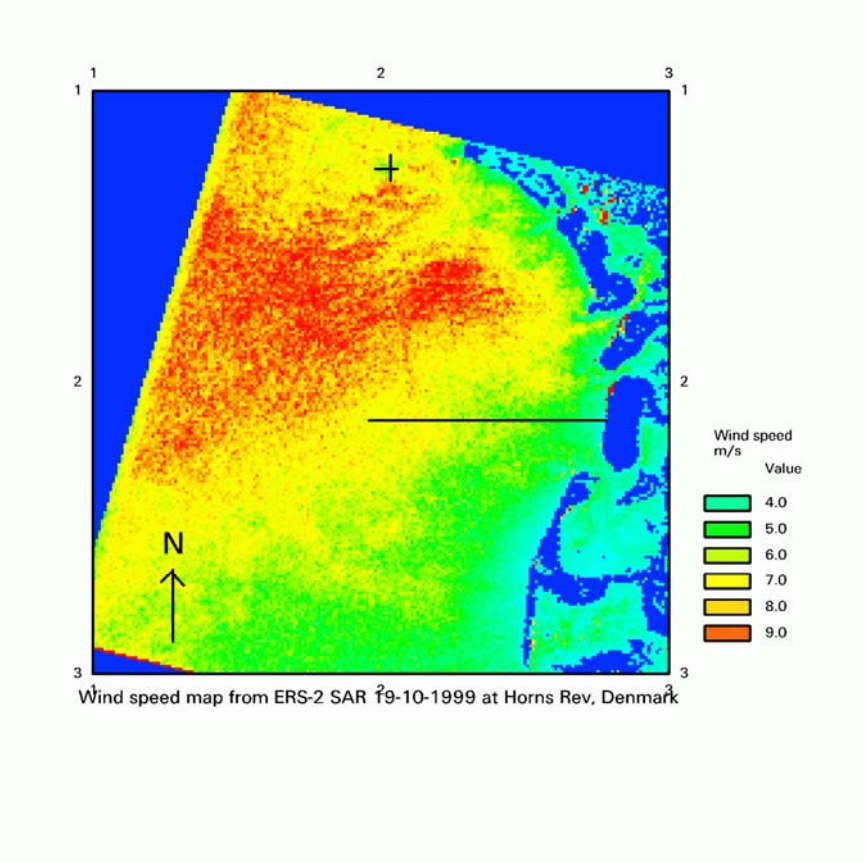

Figure 3.12. Wind speed map at Horns Rev based on ERS-2 SAR image.

3.4.4 Envisat ASAR (SAR data)

Envisat was launched March 1st, 2002 by ESA. It carries 12 instruments. One of these is an Advanced SAR (ASAR). Envisat has orbited Earth more than 26.000 times and the amount of data stored from all instruments is more than 500 Terrabyte (~ 260 Gb per day) as of February 28th, 2007. The data can be accessed through http://odisseo.esrin.esa.it/eoli/eoli.htm at ESA.

ASAR is an active phased array with incidence angles between 15º and 45º. The ASAR can be programmed to 27 different modes of operation. It is a ScanSAR as it can be programmed to two different spatial resolutions (high-resolution, wide swath and global monitoring mode) and to alternating polarization mode. The wide swath and global monitoring modes both have a 405 km swath whereas the high-resolution image mode and alternating polarization have < 100 km swath. See figure 3.13 for the swath resolutions of ASAR. Technical details on ASAR can be found in the ASAR Product Handbook at http://envisat.esa.int/dataproducts/asar/CNTR.htm.

The high-resolution (stripmap) mode is obtained when selecting an imaging swath by changing the beam incidence angle and the elevation beam-width. The antenna pointing is fixed normal the flight line. It is a < 100 km swath with 30 m by 30 m resolution. There are 7 sub-swaths available (IS1 to IS7) with the near-range numbered IS1 and the far-range numbered IS7. Table 3.7 lists the details. It is IS2 that resembles ERS-2 SAR the most in regard to incidence angle. Figure 3.14 shows the high-resolution swath geometry of image mode. It is a multi-looking of three in precision image format of image mode.

Table 3.7 Envisat ASAR image mode details.

From http://envisat.esa.int/dataproducts/asar/CNTR1-1-5.htm

Image swath	Swath (km)	Ground position from nadir (km)	Incidence angle range (º)
IS1	105	187 – 292	15.0 - 22.9
IS2	105	242 – 347	19.2 - 26.7
IS3	82	337 – 419	26.0 - 31.4
IS4	88	412 – 500	31.0 - 36.3
IS5	64	490 – 555	35.8 - 39.4
IS6	70	550 - 620	39.1 - 42.8
IS7	56	615 - 671	42.5 - 45.2

The wide swath and global monitoring mode both have a 405 km swath with incidence angles from 15º to 45º. In wide swath mode the spatial resolution is 150 m and the global monitoring 1000 m (however this mode has not functioned well).

The alternating polarization mode has a swath as that of image mode of < 100 km. Here the scanning within the swath alternates between two polarizations. It is possible to select any combination of two polarizations including co- and cross-polarization, e.g. HH and VV, or VV and HV, or HV and VH, etc.

Only one mode of the 27 modes can be recorded at a given site at a given time. The receiving mode is programmed in advance by ESA. In case that more than one user has a request for a specific mode, it is not possible to fulfill all requests. A priority system is set up. Also a few preferred modes have been selected as the 'Envisat background mission'. This mission includes especially the wide swath mode. This mode has the advantage of a broad swath, yet reasonably high spatial resolution. Also the revisit time is relatively high with a 405 km swath. For the wide swath mode the repeat track is ~ 3 days. For high resolution mode the repeat is of the order of ~ 10 days.

Envisat ASAR images available for the SAT-WIND project are listed in table 3.6. For the period 2002-2005, Envisat ASAR data were delivered by ESA on request. In April 2006, Risø National Laboratory gained access to ESA's rolling archive where data from the Envisat background mission are available at no cost. The data remain in the archive for approximately one week. Routines have been setup at Risø to download images over Denmark on a daily basis and in near-real-time. Similar routines can, with permission from ESA, be set up for any given area of interest.

The processing of Envisat ASAR scenes into wind speed maps was similar to that of ERS-2 SAR. The scenes in precision format were calibrated before a geophysical model function was applied for wind retrieval.

SAR measurements were obtained from a single look angle. As a consequence, several wind speed and direction pairs may correspond to a given backscatter coefficient (i.e. the

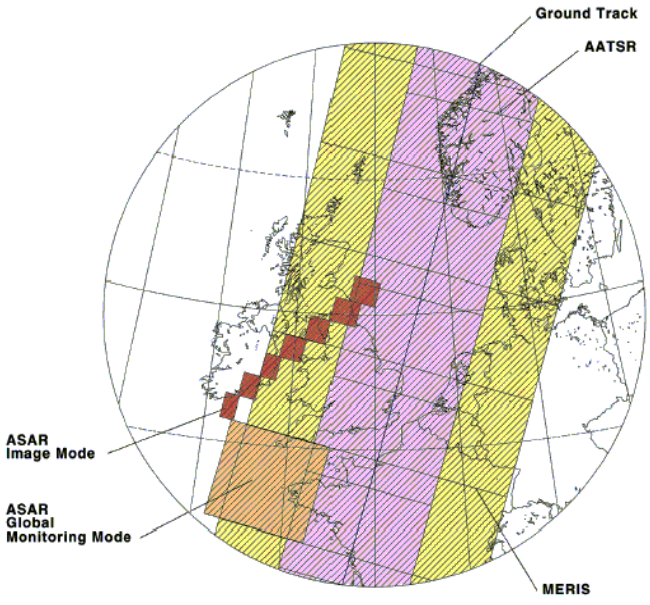

Figure 3.13. Envisat ASAR image mode (high-resolution) and global monitoring mode (low-resolution). The swath of low resolution of 405 km is also used in the medium-resolution product. The figure is from ESA.

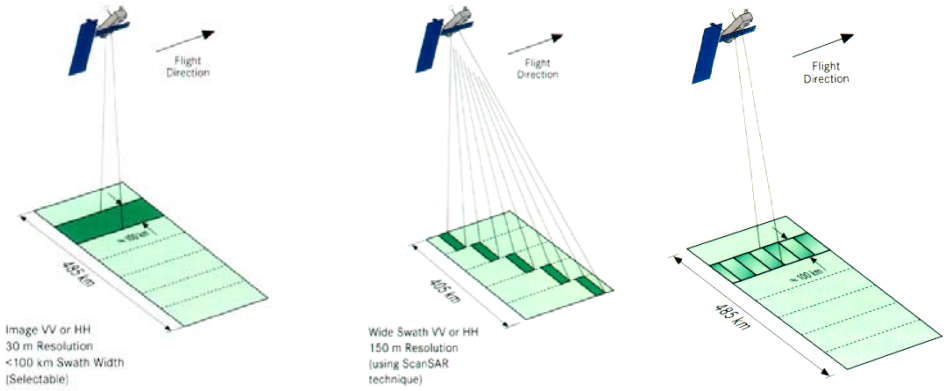

Figure 3.14 Envisat ASAR swath and resolution. Left) high-resolution (strip-mode). Middle) Wide Swath mode. Right) Alternating polarization mode. From http://envisat.esa.int/dataproducts/asar/CNTR1-1-2.htm

radar backscatter per area). To select the appropriate wind speed, the wind direction must SAR measurements were obtained from a single look angle. As a consequence, several wind speed and direction pairs may correspond to a given backscatter coefficient (i.e. the radar backscatter per area). To select the appropriate wind speed, the wind direction must be known a priori. Wind directions may be obtained from in situ measurements (Hasager *et al.* 2004b; Hasager *et al.* 2005c; Hasager *et al.* 2006b), scatterometry (Hasager et al. 2005a; Monaldo et al. 2004), or atmospheric models interpolated in time and space to match the SAR data acquisition (Monaldo et al. 2001; Monaldo 2000). Directions may also be retrieved with a 180° ambiguity from km-scale streaks found in most SAR images (Du et al. 2002; Fichaux & Ranchin 2002; Koch 2004). The streaks are aligned approximately with the wind direction and originate from atmospheric roll vortices impacting the sea surface. SAR winds have been retrieved to an accuracy of 1.1 m s-1 compared to high-quality in situ measurements from an offshore mast at Horns Rev, Denmark (Christiansen et al. 2006a; Christiansen & Hasager 2006; Christiansen et al. 2006b). From (Hasager *et al.* 2007).

The APL/NOAA SAR Wind Retrieval System (ANSWRS) developed at the Johns Hopkins University, Applied Physics Laboratory (JHU/APL) enables operational wind retrievals from Radarsat and Envisat data The ANSWRS software was developed in the Alaska SAR Demonstration project (Monaldo *et al.* 2003; Monaldo *et al.* 2001; Thompson *et al.* 2001; Monaldo 2000). In 2005-2006, the Ph.D. student Merete B. Christiansen, Risø visited JHU/APL for four months where she was trained in using ANSWRS. The software has been implemented at Risø since April 2006 as part of SAT-WIND-SMV project. Wind mapping from Envisat ASAR images is thus possible in near-real time for the Scandinavian seas.

The ANSWRS software uses, as default input, wind directions from the Navy Operational Global Atmospheric Predictions System (NOGAPS) on a one degree latitude/longitude grid. The wind directions are interpolated in time and space to match a given SAR data acquisition. Users have a choice between the model functions CMOD4 and CMOD5 for wind retrieval. Various other parameters may be adjusted (e.g. spatial resolution, map projection, and color scaling). Wind maps were output as netCDF files containing wind speed and directions on a uniform latitude/longitude grid. In addition, a

color map showing the wind field was produced. The color maps were posted at Risø's web site (http://www.risoe.dk/galathea/opslag/satellit_arkiv.htm) and they may also be viewed with Google Earth. Finally, a text file was produced for each wind map providing details on the SAR processing parameters.

An example of a raw Envisat ASAR wide-swath mode scene is shown in Figure 3.15. In this scene from June 11th, 2003, it is visible that the wind is from west as very long bands (boundary-layer rolls?) in the atmosphere reaches all the way from the East coast of Northern Jutland to Sweden. An example of the calculated wind speed map for this scene is shown in Figure 3.15.

Figure 3.15 Envisat ASAR wide-swath raw data from June 11th, 2003. Copy from the ESA quicklook archive.

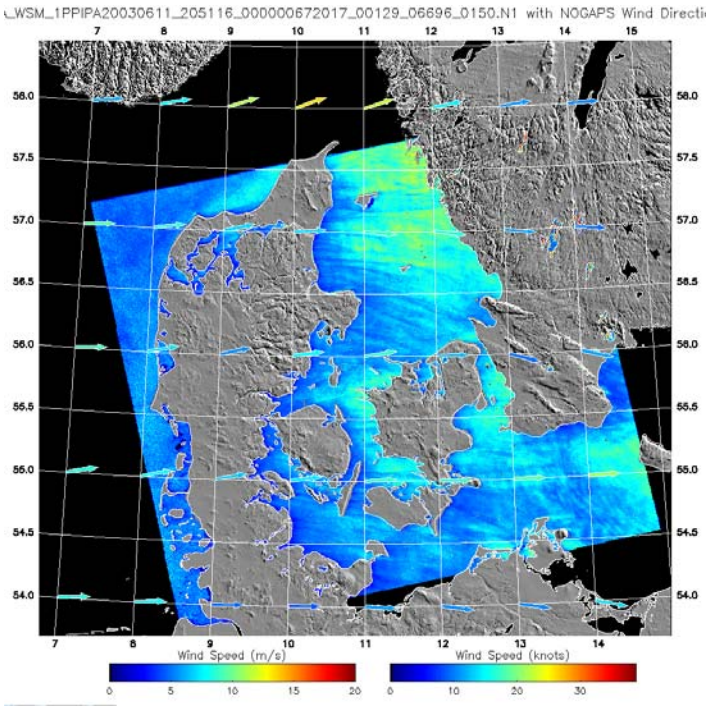

Figure 3.16 Envisat ASAR wide-swath wind map covering Denmark made from Risø-DTU - JHU/APL from June 11th, 2003. It is the NOGAPS model wind directions used in CMOD-4.

3.4.5 ALOS PALSAR (SAR data)

ALOS PALSAR images from JAXA were accessible from EOLI-SA. An example of a raw ALOS PALSAR image covering part of Denmark is shown in figure 3.17. The PALSAR ScanSAR mode is interesting due to the large coverage and frequent passing. A Geophysical Model Function algorithm for L-band using JERS-1 was developed by (Shimada *et al.* 2004; Shimada *et al.* 2003). Work is currently on-going to improve L-band wind retrieval. A necessary step is to validate the accuracy of PALSAR ocean wind maps before using the new wind maps in offshore wind resource mapping. Validation using offshore meteorological observations is planned for the future.

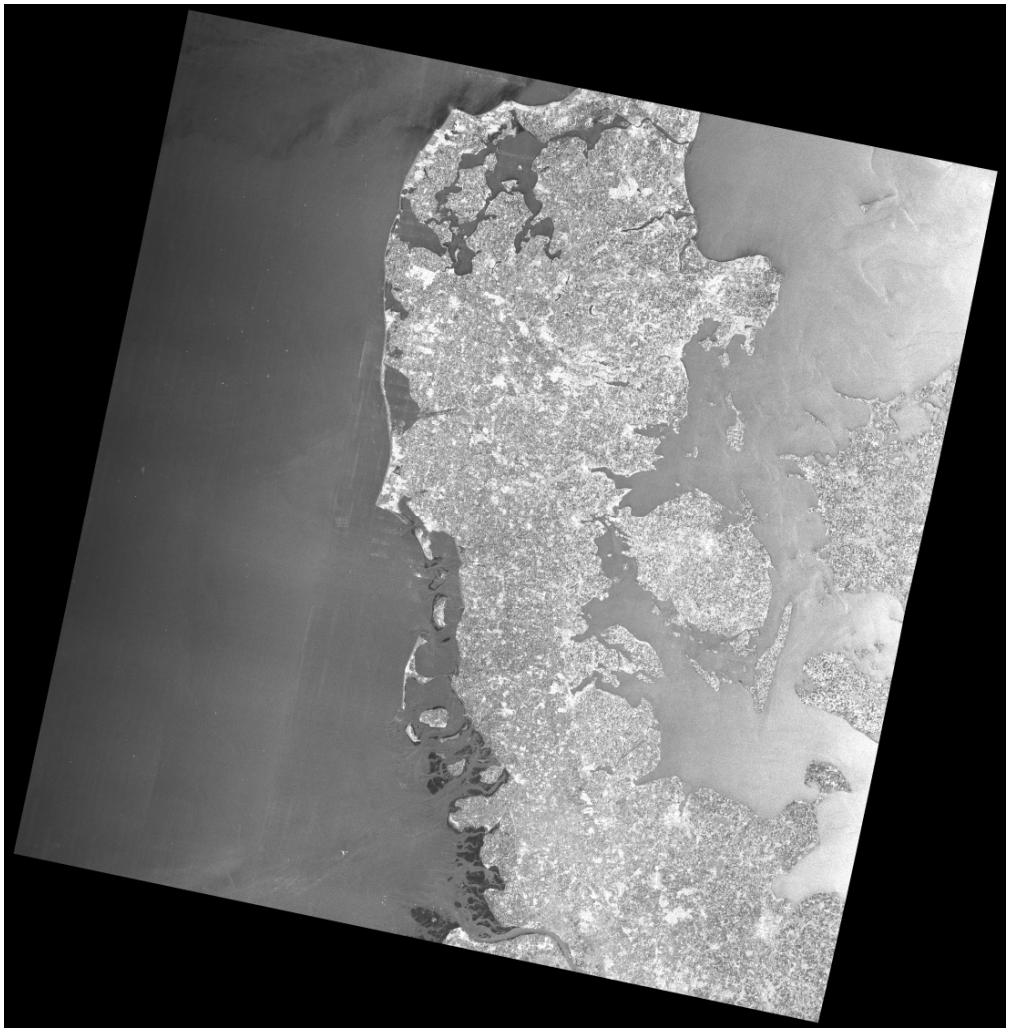

Figure 3.17. The ALOS PALSAR raw image is covering part of Denmark. It was observed 10.01.2007 at 10:16 UTC.

3.5 Altimeter

3.5.1 History

The first altimeter at a satellite platform was at GEOS-3 in 1975. Since then more than 10 altimeters have been in orbit. For a list see (Kramer 2002). Table 3.8 lists the altimeters from which data were used in the present project. GFO-1 operated 1998 to present. GFO-1 belongs to the US Navy. ERS-1 operated 1991-1995 and ERS-2 from 1995 to present. ERS belongs to ESA. Topex/Poseidon operated 1992 to 2002 and belongs jointly to NASA and CNES. Jason-1 operated 1991 to present and belongs jointly to NASA and CNES.

Table 3.8 List of altimeters used in the study.

Platform	Period
ERS-1	1991 - 1995
Jason-1	1991- now
Topex/Poseidon	1992- 2002
ERS-2	1995 - now
GFO-1	1998- now

3.5.2 Measurement principle

An altimeter looks nadir and it is mainly used to provide data on surface height of the ocean and land. It is a very accurate distance measurement. The radar altimeter pulse on the water surface is partly echoed back. The returned pulse received by the altimeter varies with the characteristics of the surface. The footprint illuminated at the surface will vary in response to wind speed variations. It is the scattering cross section that is used to calculate wind speed. The altimeter probes a small area (footprint) with some distance between.

GFO-1 is Ku-band (13.5 GHz) from the US Navy. ERS RA is Ku-band (13.8 GHz) from ESA. Topex ALT sensor is dual-frequency (C and Ku-band) from NASA and the Poseidon ALT from CNES is Ku-band. Jason-1 has C- and Ku-band. Gridded wind speed products are available at commercial cost from ARGOSS (http://www.argoss.nl). Wind direction cannot be determined from altimeter data.

3.5.3 ERS RA (altimeter data)

Wind speed data from ERS-2 RA were obtained from ARGOSS, http://www.argoss.nl in co-located ascii files providing latitude, longitude and wind speed for the North Sea for the period June 1999 to December 2000.

Wind speed data from ERS-1 and -2 RA were obtained by courtesy of Han Wensink, ARGOSS from a site (1° grid cell) near Horns Rev in the North Sea for the period 1991 to 2003.

3.5.4 Topex/Poseidon ALT (altimeter data)

Wind speed data from Topex and Posiedon altimeters were obtained from ARGOSS, http://www.argoss.nl in co-located ascii files providing latitude, longitude and wind speed for the North Sea for the period June 1999 to December 2000.

Wind speed data from Topex/Poseidon were obtained by courtesy of Han Wensink, ARGOSS from a site (1° grid cell) near Horns Rev in the North Sea for the period 1992 to 2003.

3.5.5 GFO

Wind speed data from GFO were obtained by courtesy of Han Wensink, ARGOSS from a site (1° grid cell) near Horns Rev in the North Sea for the period 1998 to 2003.

3.5.6 Jason-1

Wind speed data from Jason-1 were obtained by courtesy of Han Wensink, ARGOSS from a site (1° grid cell) near Horns Rev in the North Sea for the period 1991 to 2003.

3.6 Summary on satellite wind observations

Satellite wind maps studied in the SAT-WIND project are listed in table 3.9. It details the source (data owner), the spatial and temporal resolution, and period of satellite operation.

Table 3.9 List on satellite wind observations used in the SAT-WIND project.

	Source	Period	Resolution (km)	Frequency
Passive microwave				
SSM/I	DMSP	1987-now	25	6 per day
AMSR-E	NASA	2003-now	25	1 per day
Passive microwave polari.				
WindSat	NRL	2003- now	25	< 1 per day
Scatterometer				
ERS-1 SCAT	ESA	1991-1995	25	< 1 per day
ERS-2 SCAT	ESA	1995-2001	25	< 1 per day
NSCAT	NASA/NASDA	1996-1997	25	1 per day
QuikSCAT	NASA	1999-now	25	2 per day
Midori-2	NASA/NASDA	2002-2003	25	2 per day
Altimeter				
Jason-1	NASA/CNES	1991-now	10*	< 1 per day
TOPEX/Poseidon	NASA/CNES	1992-2002	10*	< 1 per day
ERS-2 RA	ESA	1995-now	10*	< 1 per day
GFO-1	US Navy	1998–now	10*	< 1 per day
SAR				< 1 per day
ERS-1 SAR	ESA	1991-1995	0.5	3 per month
ERS-2 SAR	ESA	1995-now	0.5	3 per month
Envisat ASAR (IMG, APP)	ESA	2002-now	0.5	3 per month
Envisat ASAR (WSM)	ESA	2002-now	2	8 per month

* Altimeter data were used from a grid cell of minimum 25 km.

Passive microwave (SSM/I, AMSR-E) and altimeter provide wind speed maps only. The other data types provide wind vector maps.

Most wind maps were stored at Risø at a resolution of 25 km by 25 km in gridded format (latitude and longitude coordinate system). The exceptions were ERS SCAT and all altimeter data. These were at a resolution of 25 km by 25 km data and were stored in ascii files with latitude and longitude.

As mentioned in section 3.1.3 the amount of data download was large. Approximately stored wind information is for SSM/I 29 GB, AMSR-E 4 GB, QuikSCAT 4 GB, Midori

0.3 GB, NSCAT 9 GB and WindSat 1 GB. In many cases much more data were downloaded and the relevant information for the study was extracted. As example, for WindSat 80Gb was downloaded and the relevant information then extracted to 1 GB.

SAR wind maps were stored at resolutions ranging from 400 m by 400 m to 1 km by 1 km. ERS was only stored at 400 m by 400 m whereas Envisat wind maps were stored at either 400 m by 400 m or 1 km by 1 km resolution in latitude and longitude corner coordinates (or UTM).

SAR wind maps studied in the SAT-WIND project include

- ~ 100 ERS SAR wind maps.
- ~ 15 Envisat high-resolution wind maps (IMG and APP).
- ~ 300 Envisat wide swath wind maps (WSM).

Most of the high-resolution wind maps covered Horns Rev (~ 100) and a few Nysted (~ 6). The low-resolution SAR wind maps covered the North Sea, interior seas of Denmark and the Baltic Sea. Raw ASAR data from the Envisat rolling archive have been downloaded since April 2006 to present.

4 Tools development (S-WAsP)

It was a technical challenge to provide reliable wind resource statistics based on the huge amount of satellite-based observations on surface ocean winds. First of all, the database with wind observations had to be structured well and the data herein had to be quality controlled. The data format differed between the various wind maps.

Gridded format files in a latitude and longitude grid was most prevalent. For some wind maps however, only swath data formats were available. These were recalculated to gridded format in the Risø satellite wind database. For a limited part of the data set, the wind maps were available only in ascii file with latitude and longitude. SAR wind maps were only available in swath format. Special software was needed for the analysis.

4.1 S-WAsP for SAR (S-WAsP is short for Satellite WAsP)

Risø developed the software for S-WAsP for wind resource mapping from SAR within SAT-WIND and SAT-WIND-SMV projects. The first proto-type software was RWT, short for Risø Wemsar Tool, developed in the EU-WEMSAR project (ERK6-CT-1999-00017) in years 2000 to 2003. It was described in (Nielsen *et al.* 2004; Hasager *et al.* 2004a; Hasager *et al.* 2004c). Further development took place in the EO-windfarm project (ESA EOMD 177736/03/I-IW) in years 2003 to 2006.

Briefly described, the new S-WAsP calculates wind resource statistical maps based on a series of wind maps from SAR. Each SAR wind map is a snapshot in time recorded either in the morning (~ 10.30 am) or in the evening (~ 21.30 pm local time). It is necessary to fit a Weibull distribution to a very limited number of observations in order to obtain the Weibull parameters (shape and scale) per grid cell. Special functions are available for that e.g. the maximum likelihood estimator that also has the advantage of treating censored data series (parts of the series are missing) (Pryor *et al.* 2004; Barthelmie & Pryor 2003). In our case this is winds < 2 ms^{-1} and > 24 m s^{-1} as the

CMOD algorithm cannot map winds beyond those limits currently. Work is ongoing to improve especially for high winds (Figa-Saldana *et al.* 2002) with CMOD5.

Each wind grid cell in the SAR wind maps is much smaller than the footprint area for 10 m winds. The footprint was described in (Nielsen *et al.* 2004). From Nielsen *et al.* 2004:

Citation start:

If we assume that momentum flux is analogue to the flux of a passive scalar like humidity, micrometeorology offers a theory for the relationship between winds at turbine hub height and close to the surface. With the moderate changes of the flow field, this assumed analogy is almost correct. The theory is known as the footprint model, because the sensitivity of a signal at an elevated point to upstream surface conditions is determined by the same equations as the case of surface exposure during continuous emission at the elevated point with reverse wind direction. Dispersion in the boundary layer depends on wind profile and eddy diffusivity and especially the latter of these conditions are quite sensitive to atmospheric stability. Horst and Weill (1994) developed a reasonably accurate footprint model based on surface-layer scaling, and this model demonstrates that the footprint area is smaller and closer to the observation point in convective conditions whereas it is much more extended during stable conditions. However, as long as boundary-layer stability information generally is unavailable, it seems safer to use the classical model of Gash (1986) describing the footprint in the neutral boundary layer.

Citation finished.

It is chosen to weigh the wind grid cells in respect to a footprint probability density function for the 10 m height. This is the height that all satellite wind maps now are available for (SSM/I used to be valid for 20 m but the data recently have been re-processed to 10 m values). S-WAsP calculates wind resource statistics at 10 m above sea level. The result is the Observed Wind Climate (OWC) and this information - in form of a tab-file - can be used in WAsP for site evaluation.

The present version of S-WAsP handles high-resolution SAR (from ERS) and Envisat ASAR high-resolution wind maps in an identical way. Envisat ASAR low-resolution wind maps are treated slightly differently as the spatial resolution is somewhat lower. However the wind resource statistics obtained will still cover exactly the site of interest. Footprint weighing is made (or other filtering). The number of observations will be relatively low (maximum will be a few hundred and most likely far fewer) and the data series is censored.

Envisat ASAR wide-swath wind maps were delivered to the SAT-WIND project through a close collaboration with JHU/APL. An import routine from the JHU/APL format to S-WAsP was finalized.

One of the technicalities of S-WAsP is also that the wind statistics are binned into only one sector for calculating the Weibull scale parameter. This is because the number of observation is too low if using e.g. 12 wind sector bins. The global scale parameter was then assumed valid for all bins.

4.2 S-WAsP for scatterometer and passive microwave

S-WAsP for scatterometer and passive microwave polarimetric is based on wind vector wind maps as for SAR wind maps. A major difference, however, is the spatial resolution. It is not relevant to use footprint averaging as the 25 km by 25 km grid cells are much

larger than the footprint area. This means a somewhat simpler calculation is made. The number of observations from scatterometer is much larger than for SAR. There are around 6000 observations available anywhere on the globe. This data set allows 12 bins for Weibull shape and scale parameters in S-WAsP. The result is the Observed Wind Climate (OWC) at ocean at a distance far from the coastline. The distance is > 25 km as this is the grid cell resolution.

The distance from the observed wind climate to the coastline may however be much larger in some cases. This is due to the method of processing of scatterometer wind maps so far. Initiatives to produce higher resolution wind maps from scatterometer e.g. at 12.5 km by 12.5 km resolution is in progress but not yet fully performed. It may be relevant to access this type of data if possible, especially to obtain wind statistics somewhat closer to the coast. However in all cases, it will definitely be necessary to use WAsP (Mortensen *et al.* 2000) with information on terrain orography and roughness combined with satellite-based OWC statistics. Orography and roughness maps may be obtained from the WAsP contouring software recently developed by Morten Nielsen, Risø. It provides an easy way to use satellite-based orography and roughness maps in WAsP.

S-WAsP is also upgraded to import passive microwave wind maps. These are gridded wind speed maps at 25 km by 25 km resolution. It is maps with wind speed only. The number of observations is very large, of the order of ~10.000 wind maps. Some assumptions on wind direction may be taken either from scatterometer or other sources. It is necessary to combine the information. Studies by (Aicken *et al.* 2002) show one type of methodology for this. (Unfortunately this group from QinetiQ could not participate in the SAT-WIND project even though it was originally planned).

5 Wind resource results

The work in SAT-WIND focuses on results based on satellite wind observations. These are in part compared to meteorological observations and model results.

5.1 Results using QuikSCAT

5.1.1 Denmark

QuikSCAT wind maps from CERSAT/IFREMER (www.ifremer.fr/cersat) as monthly values were studied. Figure 5.1 shows the area of interest (Hasager *et al.* 2004a).

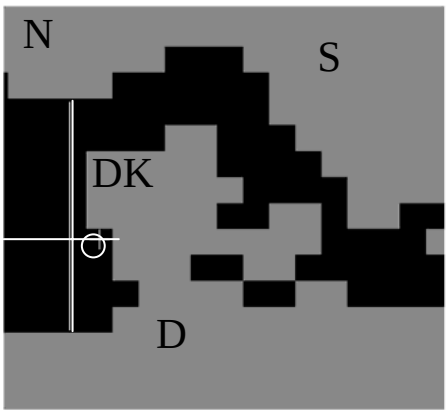

Figure 5.1 Map of Denmark. The circle indicates the Horns Rev wind farm and meteorological mast. The horizontal and vertical transects indicate the graphs shown in Figure 5.2. Country codes were included for Denmark, Sweden, Norway and Germany. Each wind map grid cell is 50 km by 50 km.

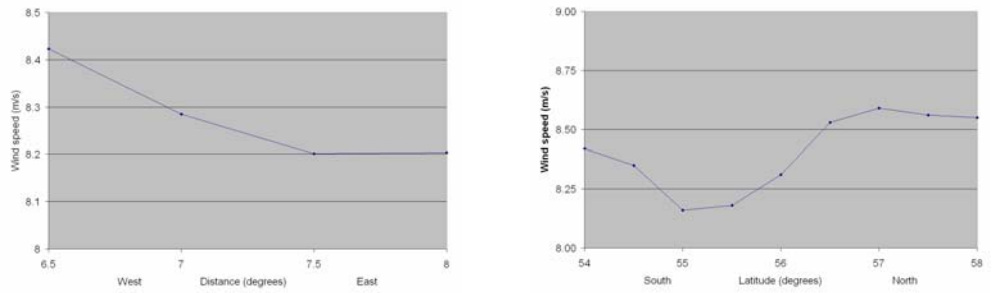

Fig. 5.2 Left) Vertical transect of mean wind speed from West to East along latitude 55.5º. Right) Horizontal transect of mean wind speed from South to North along longitude 7.5º based on 5 years of gridded monthly Quikscat data from IFREMER/CERSAT. Figure from(Hasager et al. 2006b).

The results in Fig 5.2 were based on nearly five years of bi-daily QuikSCAT wind maps in the period August 1999 to December 2003. The results compared reasonably to

knowledge on the wind climate in the North Sea. The Horns Rev wind farm is located a few km further north at longitude ~ 7.52°.

An example of seasonal and inter-annual wind speed variations over the ocean observed from QuikSCAT is given in Fig. 5.3. The data are from a grid cell near the wind farm. The distance to the wind farm was around 100 km.

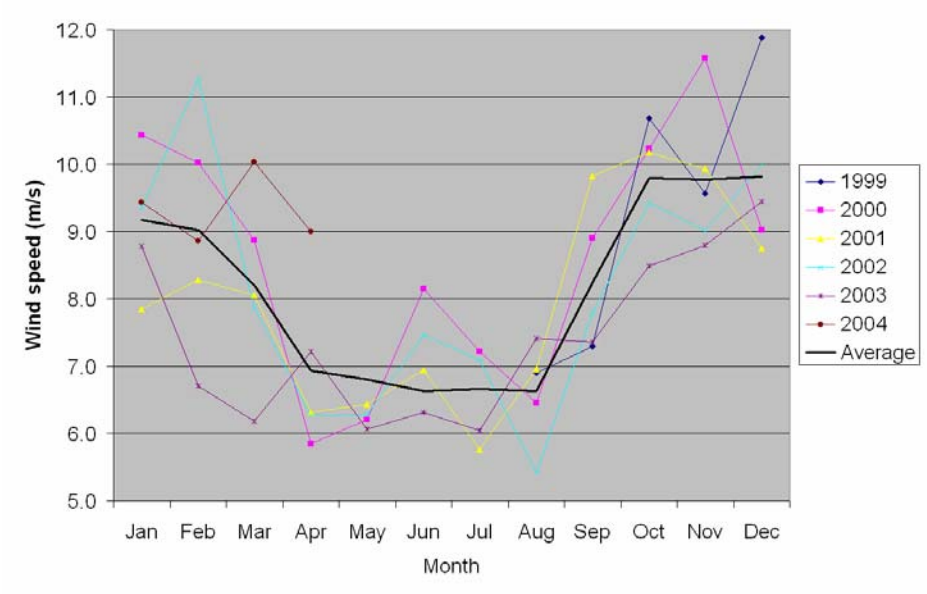

Fig 5.3. Wind speed variation in the North Sea near Horns Rev for a five-year period observed as monthly averages by Quikscat. Data from CERSAT/IFREMER. From (Hasager et al. 2006b).

The data in fig. 5.3 were compared to the meteorological observations and to NCAR/NCEP reanalysis data. This is shown in figure 5.4. The evaluation of the QuikSCAT data was performed by comparing mean monthly wind speeds derived from the QuikSCAT images with 10m wind speeds from the NCEP-NCAR data set for the grid cell centred at 56.189N, 7.5E, and the observed values the Horns Rev mast at 62 m. Each data set was normalized to the mean wind speed over the period 2000-2003 and expressed as a percentage. As shown there was good agreement between the data sets in terms of the month-to-month variability. The observed data had a slightly higher correlation coefficient (r) with NCEP-NCAR (0.96) than they did with the satellite data (0.91) but NCEP-NCAR and the satellite data also had a relatively high correlation coefficient (0.95).

The comparison was good especially keeping in mind that the scatterometer observations were from open ocean and the mast observations were from the coastal zone. For wind resource estimation it would be necessary to transfer the ocean wind data to the coastal zone. This can be done using WAsP (Mortensen *et al.* 2005).

The map of Denmark of the mean wind speed offshore observed from QuikSCAT during 6 years is presented in figure 5.5. The same data set was used to calculate maps of the Weibull A and k parameters (figure 5.6) and the maps of mean winds from the four sectors: North, East, West and South. The result is presented in (figure 5.7).

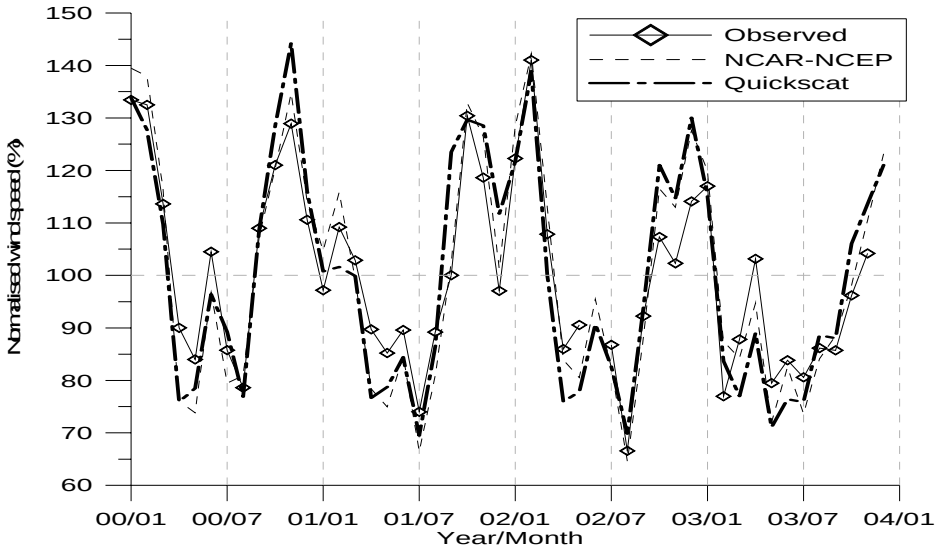

Figure 5.4. Monthly mean wind speeds calculated from observed data at the Horns Rev mast, the NCAR-NCEP data set and QuikSCAT satellite images. Data were normalized by the mean value from each data set for the period 2000-2003 and expressed as a percentage. From(Hasager et al. 2006b).

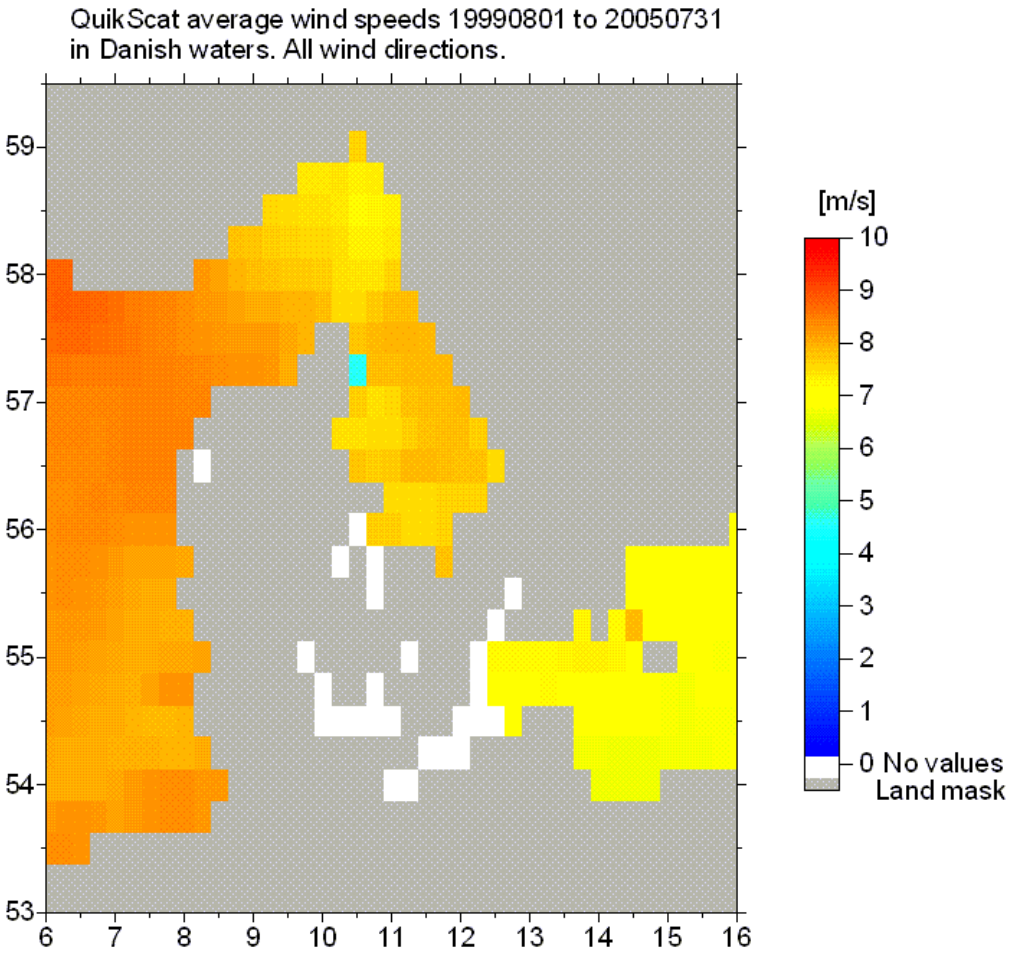

Figure 5.5: Mean wind speeds observed offshore near Denmark from QuikSCAT during 6 years. From (Hasager et al. 2006a).

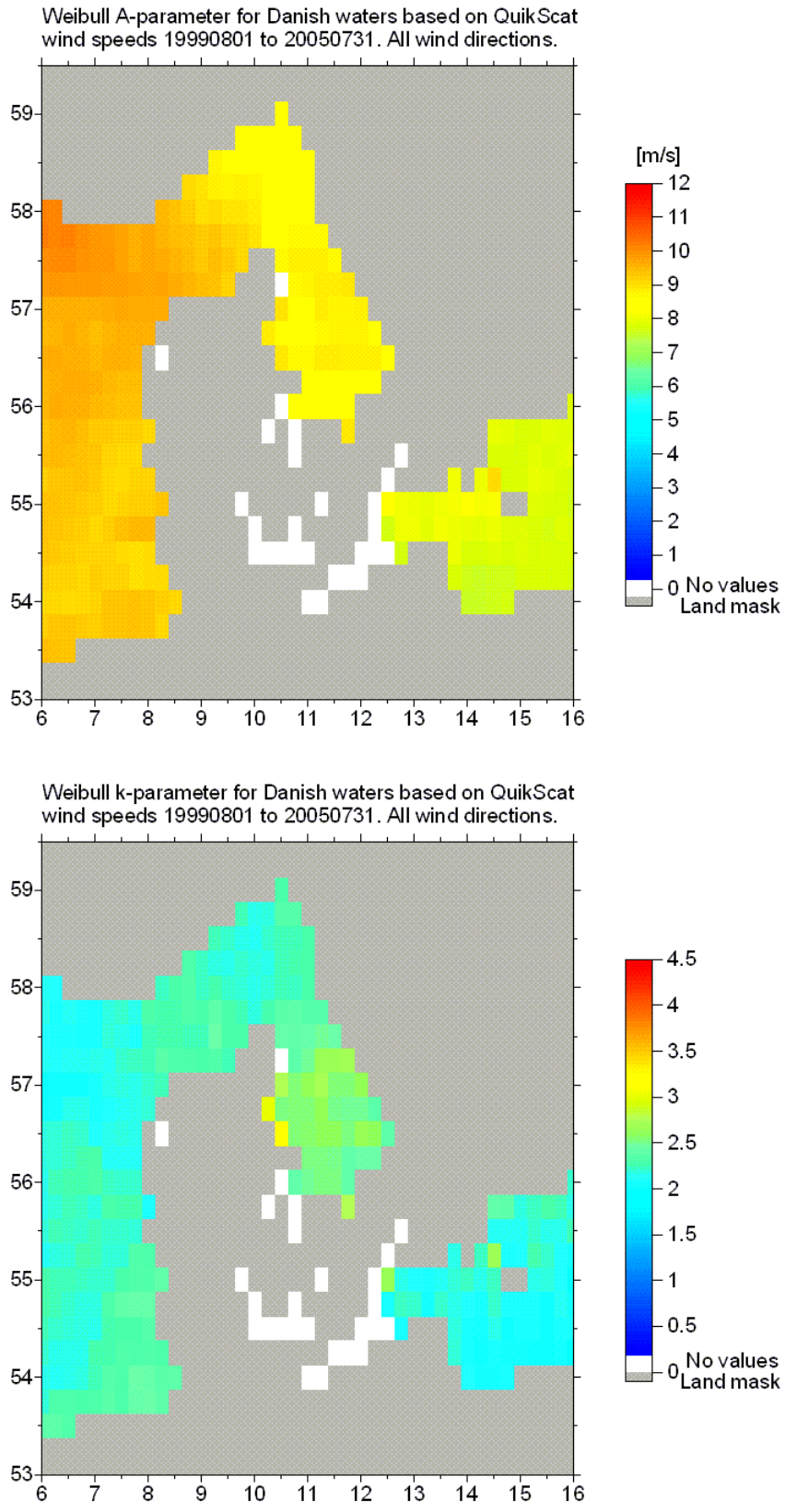

Figure 5.6 Weibull A (above) and Weibull k (below) observed offshore near Denmark from QuikSCAT during 6 years. From (Hasager et al. 2006a).

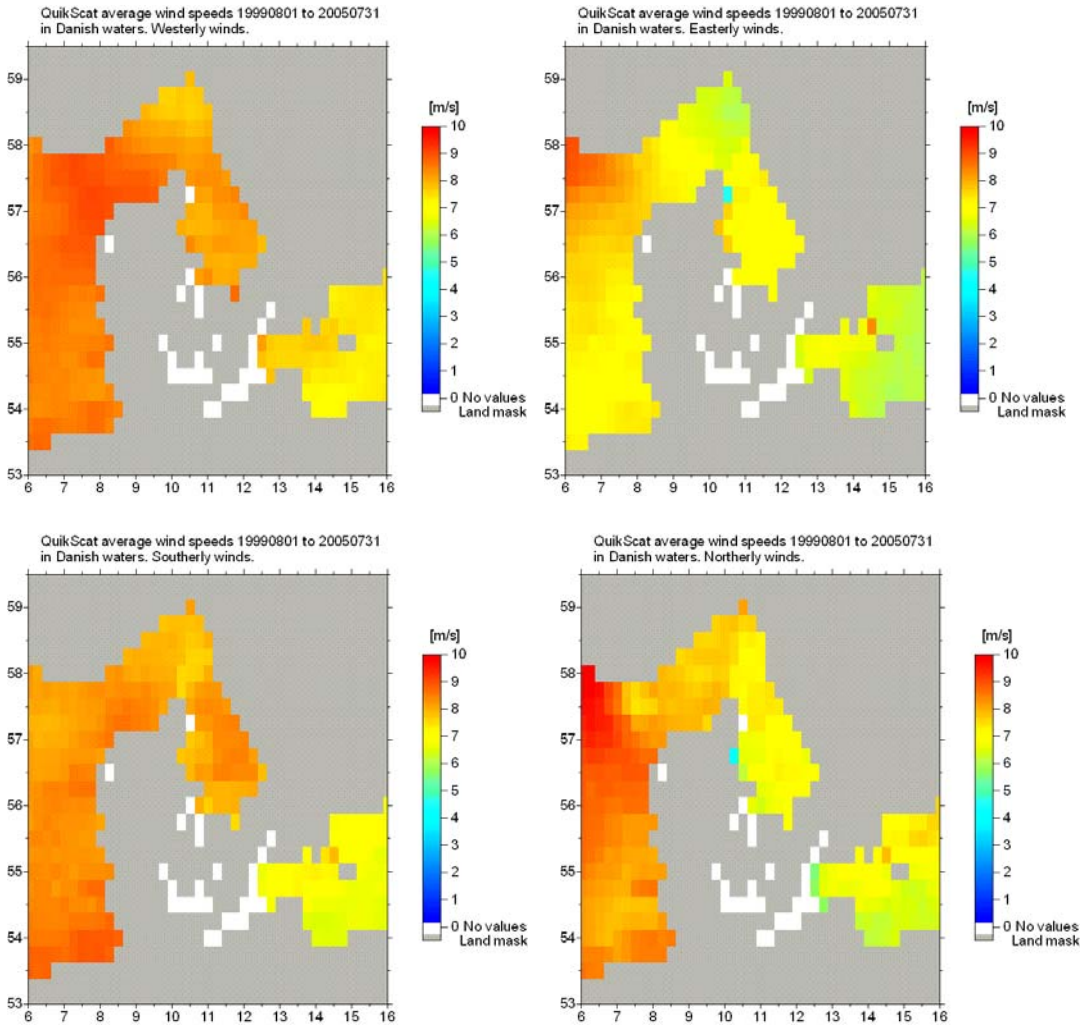

Figure 5.7 Mean wind speed observed offshore near Denmark from four sectors (West, East, South, North) during 6 years from QuikSCAT.

The offshore wind observations from QuikSCAT in figures 5.5, 5.6 and 5.7 covering Denmark show variations in the Danish Seas in mean wind speed and Weibull A and k. Furthermore, the wind sector had a large influence on the winds offshore. E.g. it was noticed that Norway gives lee effect far offshore in Skagerrak for winds from the North. For easterly flow a speed up around Norway was seen. A similar pattern was identified from Envisat ASAR, though with more spatial detail, see figures 5.8 and 5.9.

The advantage of QuikSCAT is the near-global coverage twice daily. A comparison between Horns Rev in the North Sea and a site near Cape Verde located in the trade wind belt is given in figure 5.10 (mean wind maps from 7 years), figure 5.11 (wind roses) and figure 5.12 (monthly variations in wind speed). Further information is available in (Hasager *et al.* 2007) and at

http://galathea3.emu.dk/satelliteeye/casestudies/capeverde/index_uk.html. The web-link is related to the educational material developed in the project Satellite Eye for Galathea 3 (www.satelliteeye.dk).

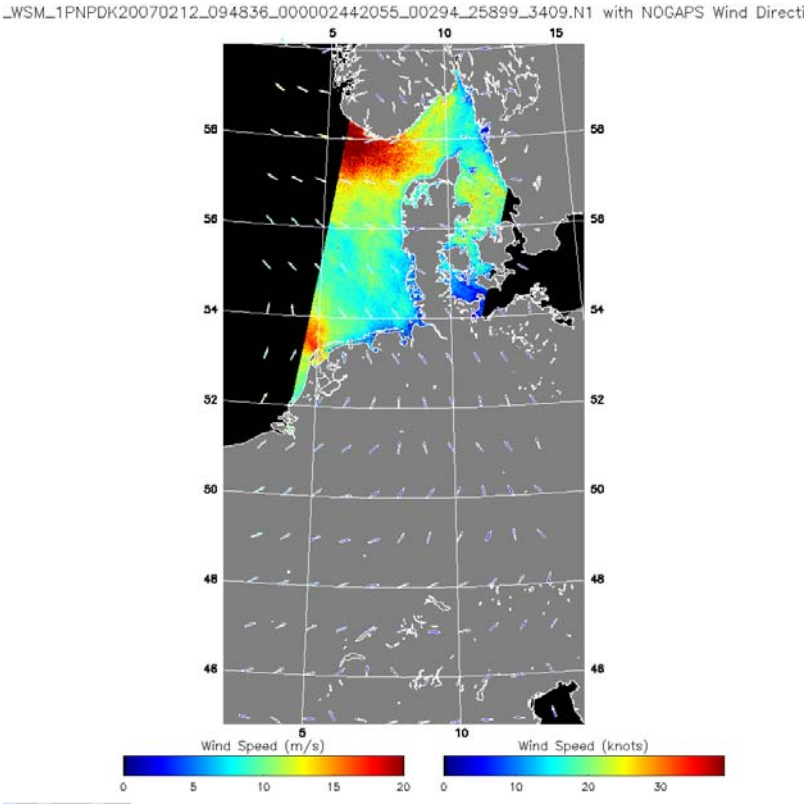

Figure 5.8 Wind speed map for Denmark from Envisat ASAR 12 February 2007 at 09.48 UTC. Arrows indicate the NOGAPS model wind speeds and directions.

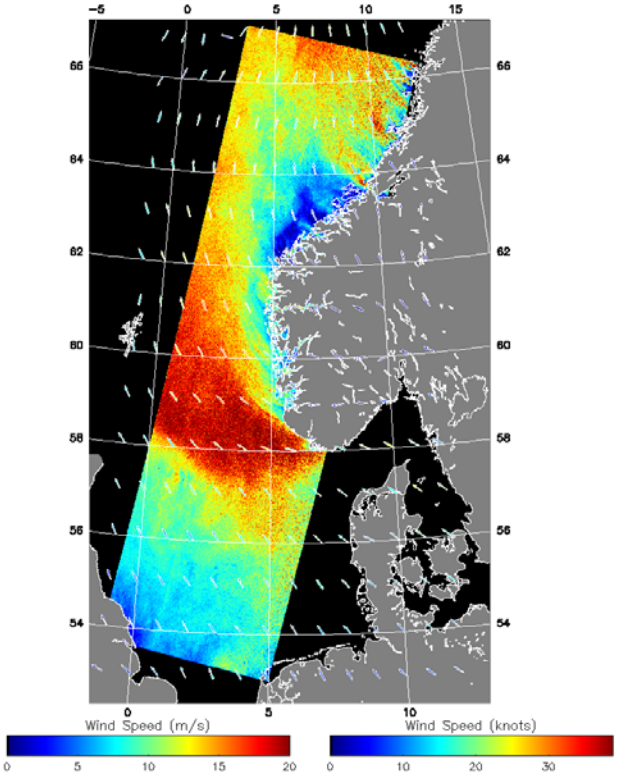

Figure 5.9 Wind speed map for the North Sea from Envisat ASAR 24 February 2007 at 10.09 UTC. Arrows indicate the NOGAPS model wind speeds and directions. From (Hasager et al. 2007).

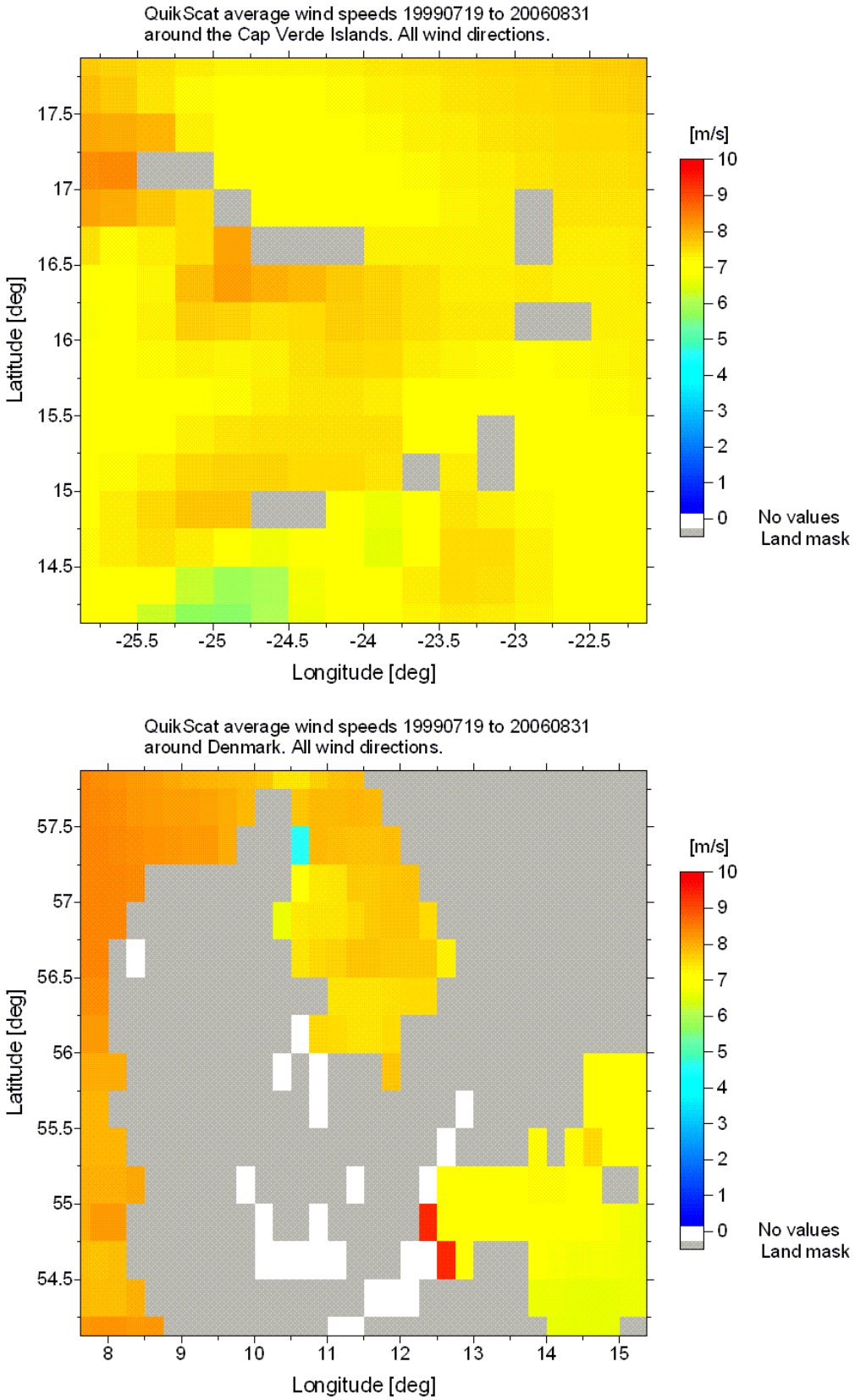

Figure 5.10 Wind speed map for Cape Verde (above) and the North Sea (below) observed from QuikSCAT during 7 years twice daily.

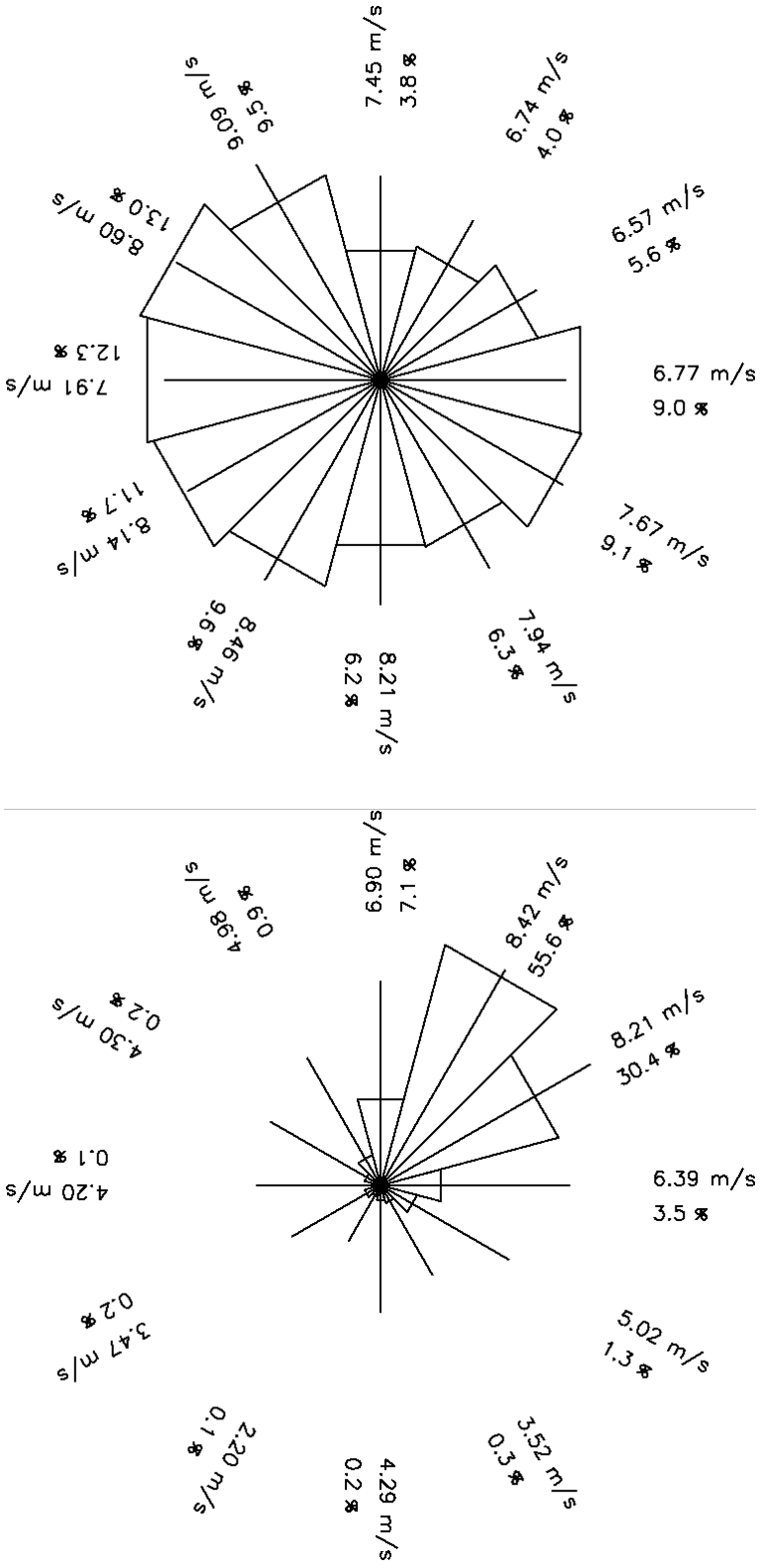

Figure 5.11 Wind-roses near Horns Rev in Denmark (8.0 longitude, 55.4 latitude) (above), and southwest of the island Santo Antão, Cape Verde (25.7 longitude, 16.8 latitude) (below) observed from QuikSCAT during seven years. The mean wind speed in each directional sector and the frequency is shown as occurrence (in %).

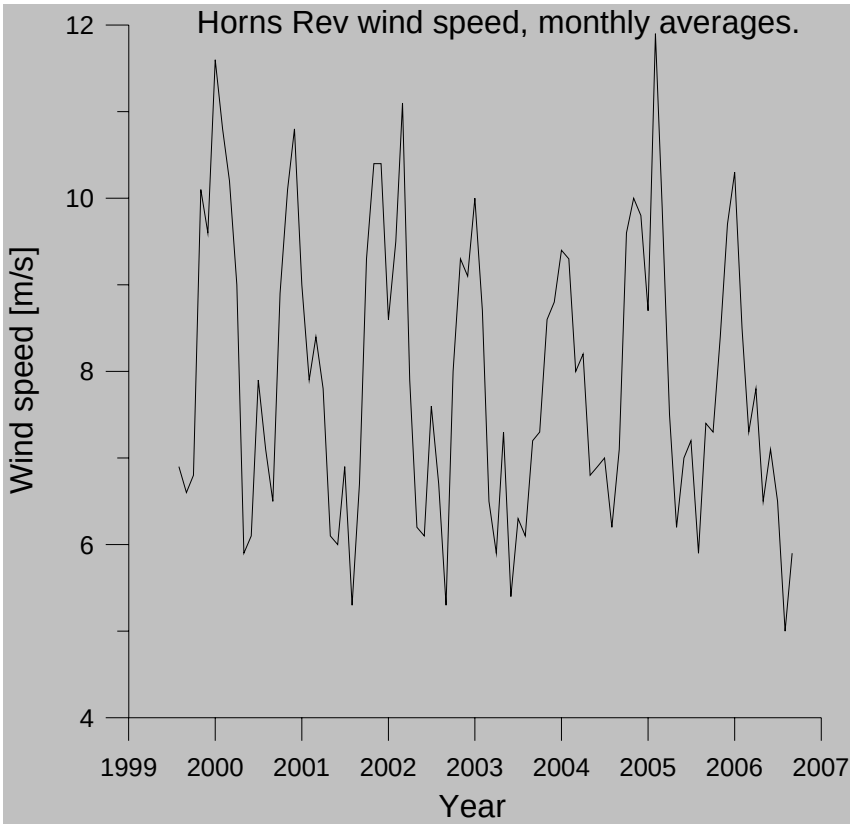

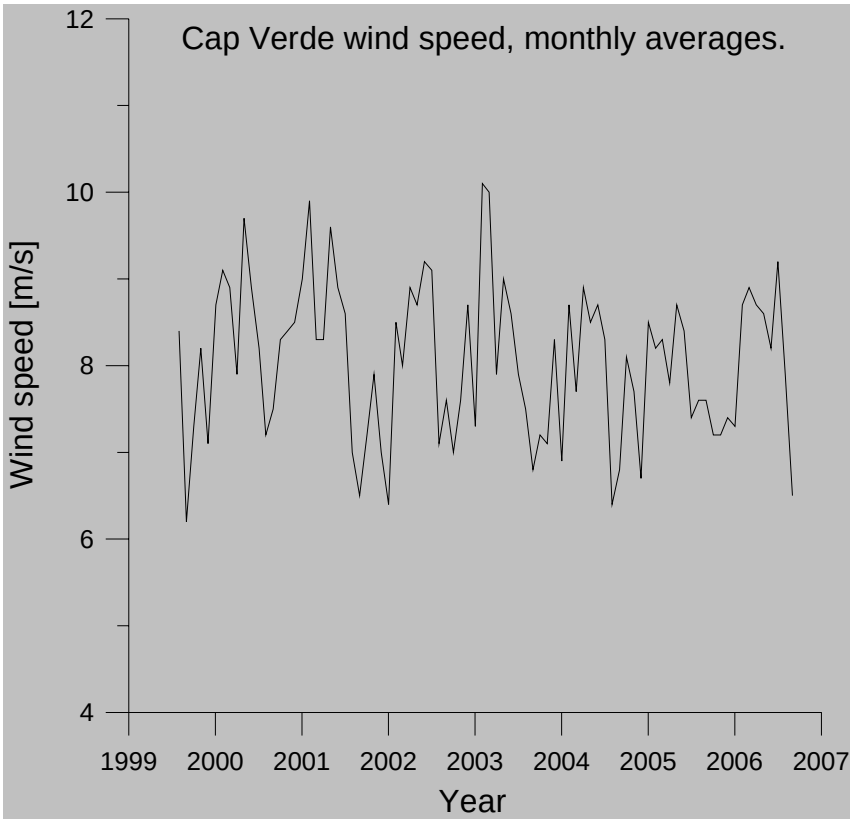

Figure 5.12 Monthly mean wind speed near Horns Rev in Denmark (8.0 longitude, 55.4 latitude) (above), and southwest of the island Santo Antão, Cape Verde (25.7 longitude, 16.8 latitude) (below) observed from QuikSCAT during seven years.

Figure 5.10 shows that the mean wind speed offshore is slightly higher in Denmark than in Cape Verde. Figure 5.11 reveal the many directions of wind occurring at Horns Rev whereas the trade winds in Cape Verde are strongly dominated by north-easterly flow. The mean wind speed is not much different seen from figure 5.12 but the monthly and yearly variations are much larger in Denmark than in Cape Verde.

Comparison results between QuikSCAT wind direction and wind speed with offshore observations at Horns Rev from DONG energy are presented in figures 5.13 and 5.14, respectively. The results are fairly good with slope near 1 and bias of 3° for wind direction and slope near 0.96 and bias of 0.3 ms^{-1} for the hourly mean wind speed from the linear regression results. More scatter is found in the comparison with 10-minute means than for 1-hour means. It is interpreted as follows: the satellite captures a snap-shot wind map in seconds and the spatial scale of the observations is 25 km. This spatial scale apparently corresponds better to hourly observations.

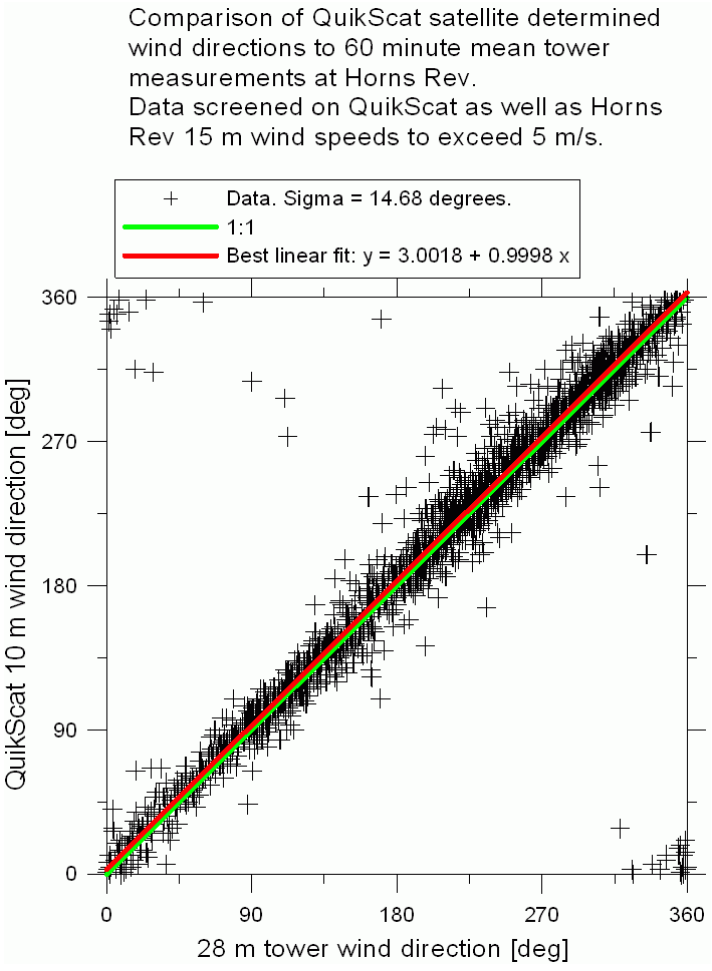

Figure 5.13 Comparison of wind direction near Horns Rev in Denmark (8.0 longitude, 55.4 latitude) from QuikSCAT and hourly values from an offshore meteorological mast (DONG energy data). From (Hasager et al. 2006a).

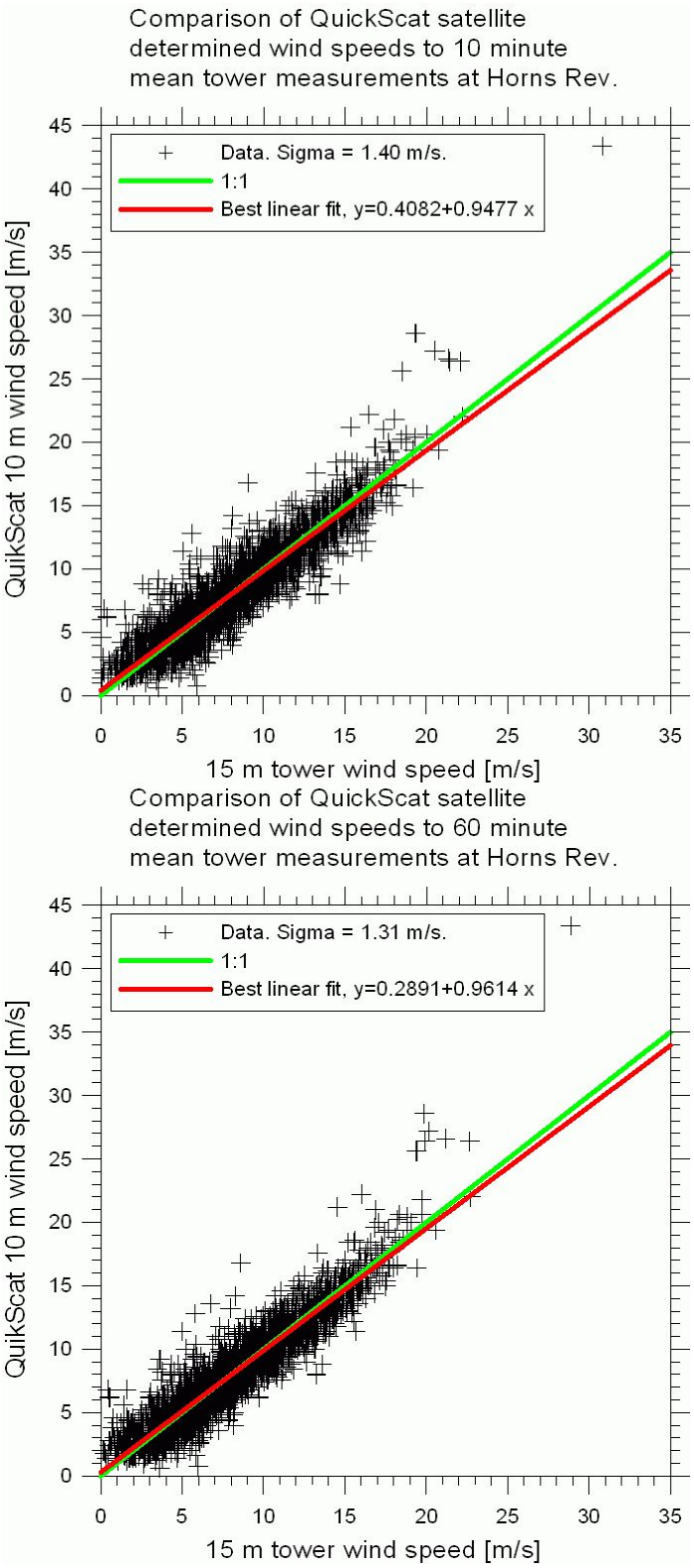

Figure 5.14 Comparison of wind speed near Horns Rev in Denmark (8.0 longitude, 55.4 latitude) from QuikSCAT and 10-minute mean values(above) and hourly mean values(below) from an offshore meteorological mast (DONG energy data). From (Hasager et al. 2006a).

5.1.2 North Sea and Baltic Sea

Observations from the North Sea and Baltic Sea were analyzed from two locations far offshore. The positions are indicated in figure 5.15.

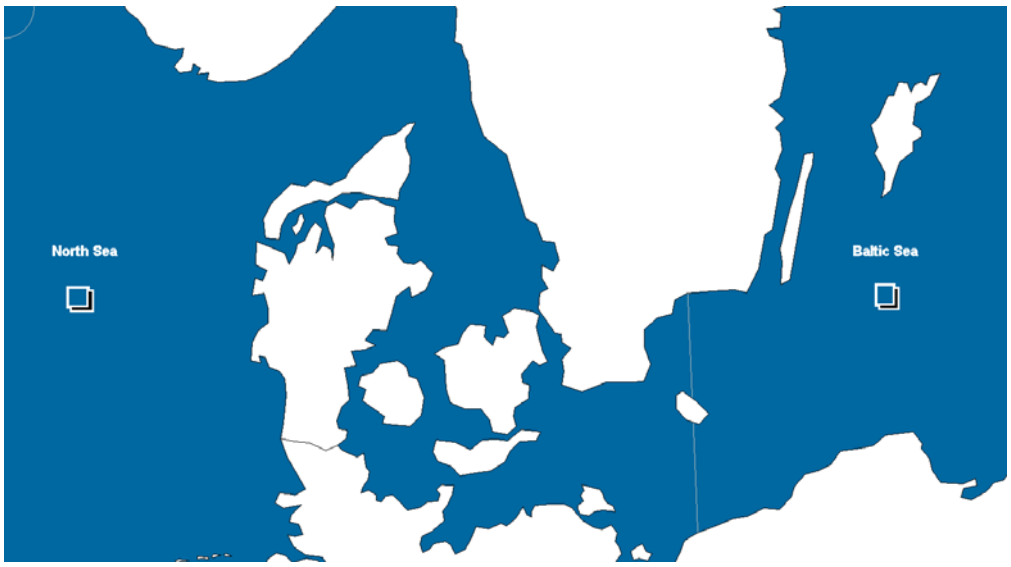

Figure 5.15. Position of two locations investigated.

The wind roses for the sites are presented in figure 5.16. The weekly average values are shown in figure 5.17. Only weeks with 8 or more samples are included in the graph. Large variations appear during years and seasons. In figure 5.18 the monthly mean values are shown. Only months with 30 or more samples are included. The mean wind speed is higher in the North Sea and the difference between winter and summer winds is higher in the Baltic Sea than in the North Sea.

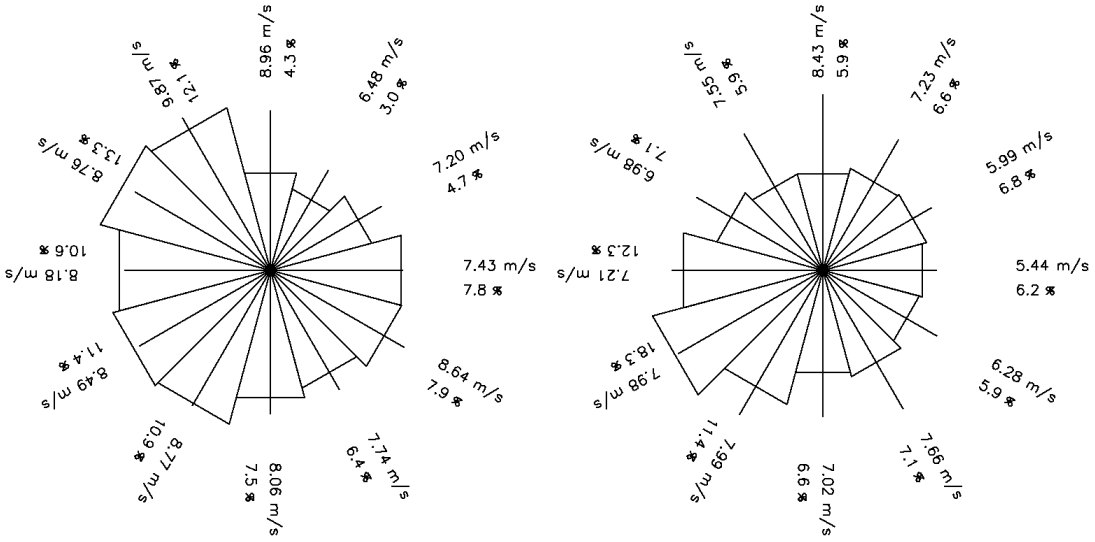

Figure 5.16. Wind roses observed from a site in the North Sea (left) and the Baltic Sea (right) from QuikSCAT in the period June 1999 to February 2007.

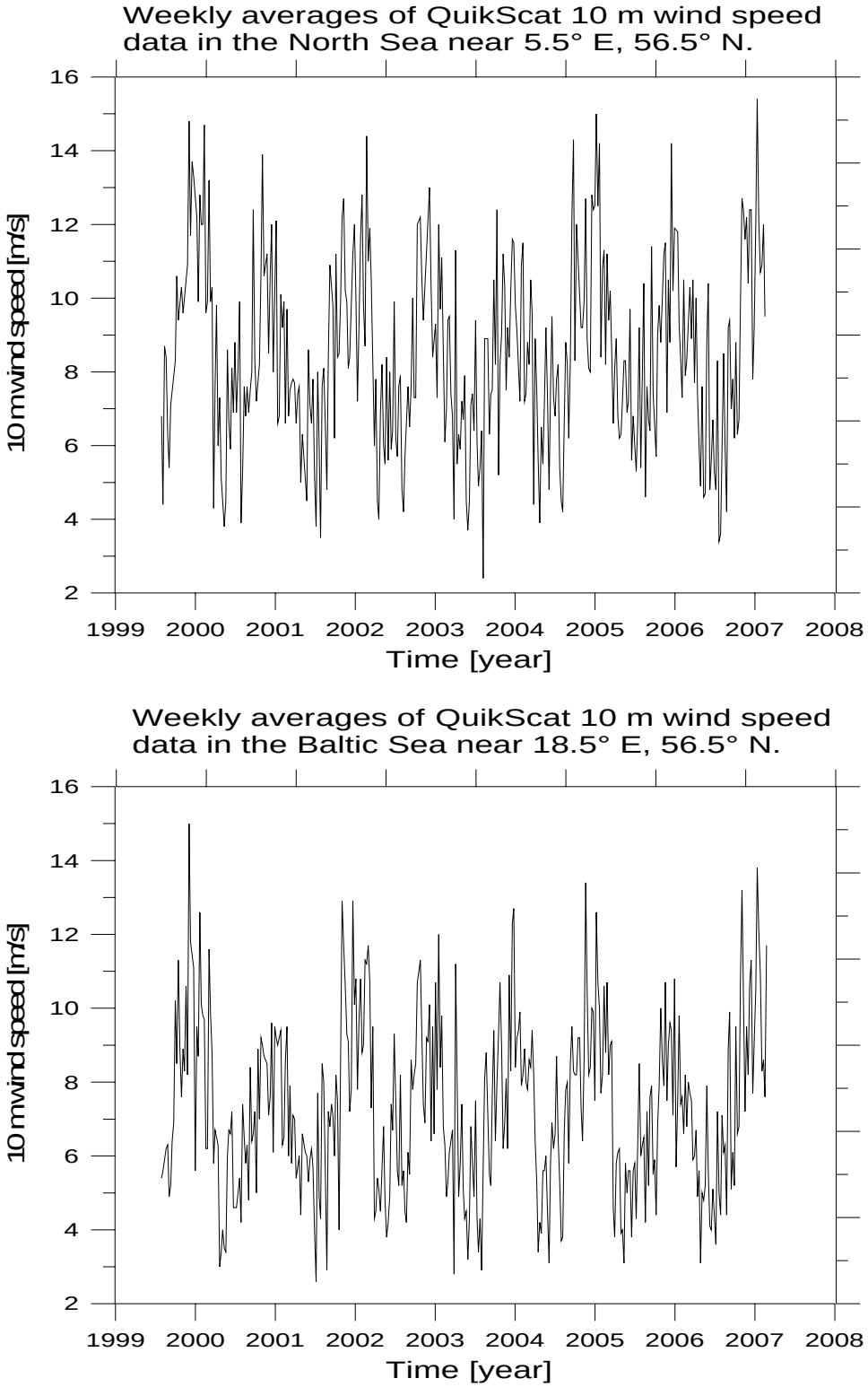

Figure 5.17. Weekly average wind speed observed from QuikSCAT for a site in the North Sea (above) and the Baltic Sea (below).

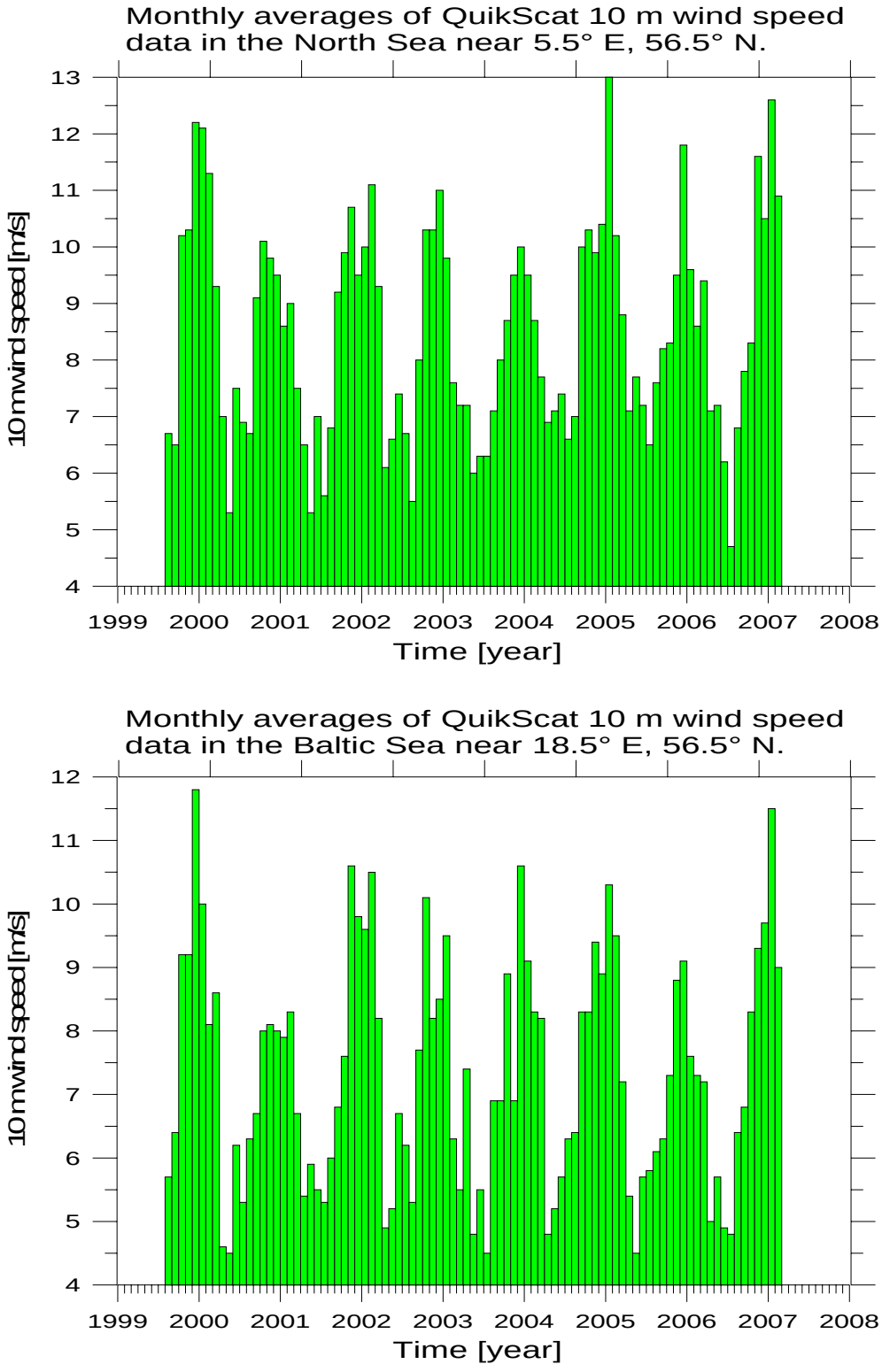

Figure 5.18. Montly average wind speed observed from QuikSCAT for a site in the North Sea (above) and the Baltic Sea (below).

5.1.3 Sweden

QuikSCAT observations from the Baltic Sea are presented. The mean wind speed observed during 8 years is presented in figure 5.19 and the number of observations in figure 5.20. Figure 5.21 include maps of Weibull A and k values. The mean wind speed for four directional bins (east, west, north and south) for the Baltic Sea is presented in figure 5.22.

In the northern part of the maps in figures 5.19 to 5.22 is the island Gotland. At Östergarnsholm (57°25'51"N, 18°59'16"E) near Gotland in the Baltic Sea, Sweden, meteorological observations from May 1995 to July 2002 were collected by Uppsala University. The monthly averages from Östergarnsholm are presented in figure 5.23.

The data were compared to QuikSCAT observations for the times where both the mast was in operation and QuikSCAT had values. The wind speed and wind directions comparisons are presented in figure 5.24. The distance between the mast and the QuikSCAT observations is around 20 km.

For unknown reason(s) the QuikSCAT wind maps do not contain values in the periods 1.12. - 31.5 for the grid cell closest to Östergarnsholm. Therefore the data set was split into a ‘summer’ season including observations from 1.6. - 30.11. and a ‘winter’ season including observations from 1.12. - 31.5. Based on these a wind rose for each season was calculated from the meteorological data and a wind rose for ‘summer’ from QuikSCAT. All data are presented in figure 5.25.

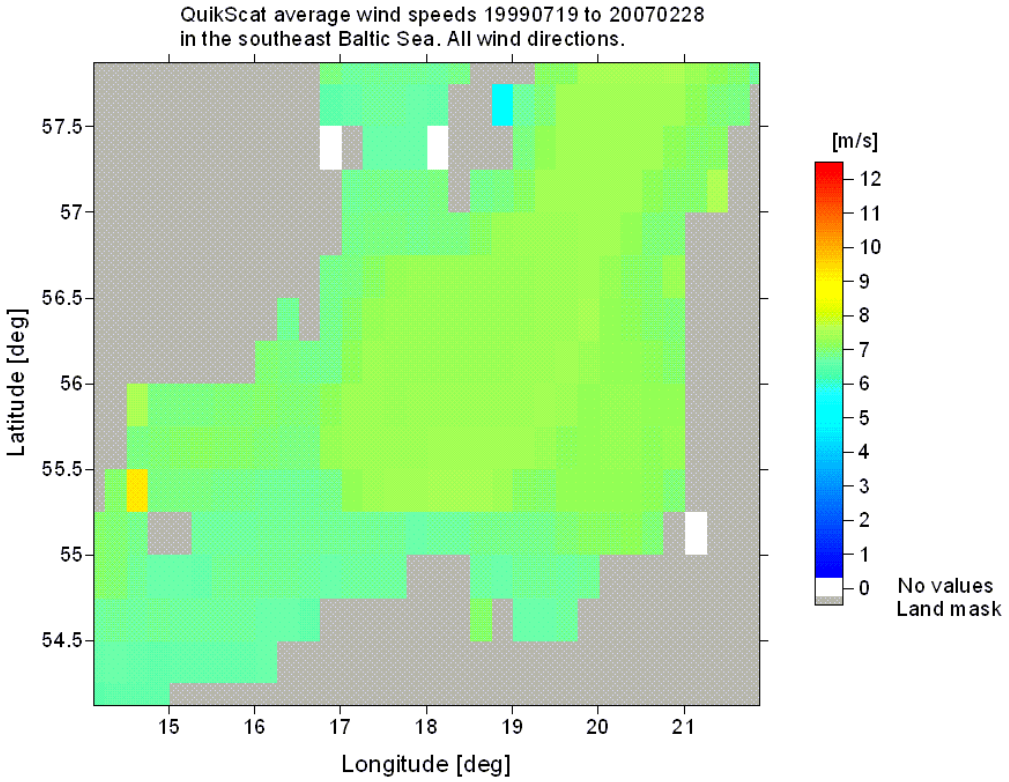

Figure 5.19 Mean wind speeds observed in the Baltic Sea from QuikSCAT during 8 years.

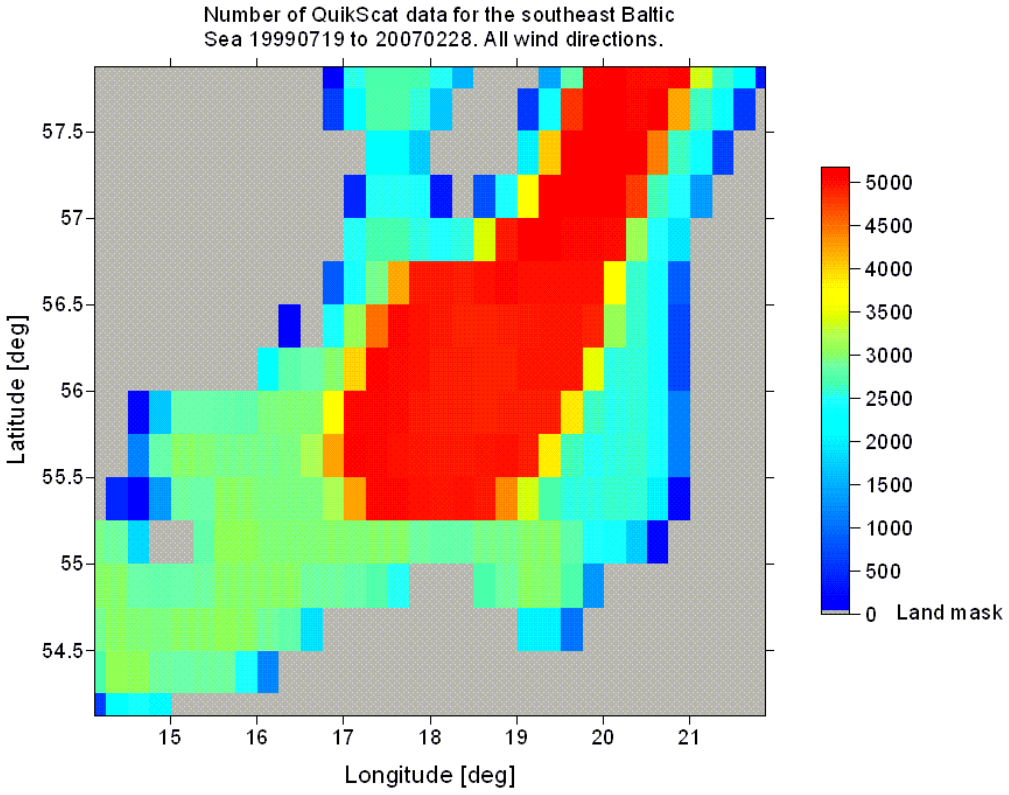

Figure 5.20 Number of observations in the Baltic Sea from QuikSCAT during 8 years.

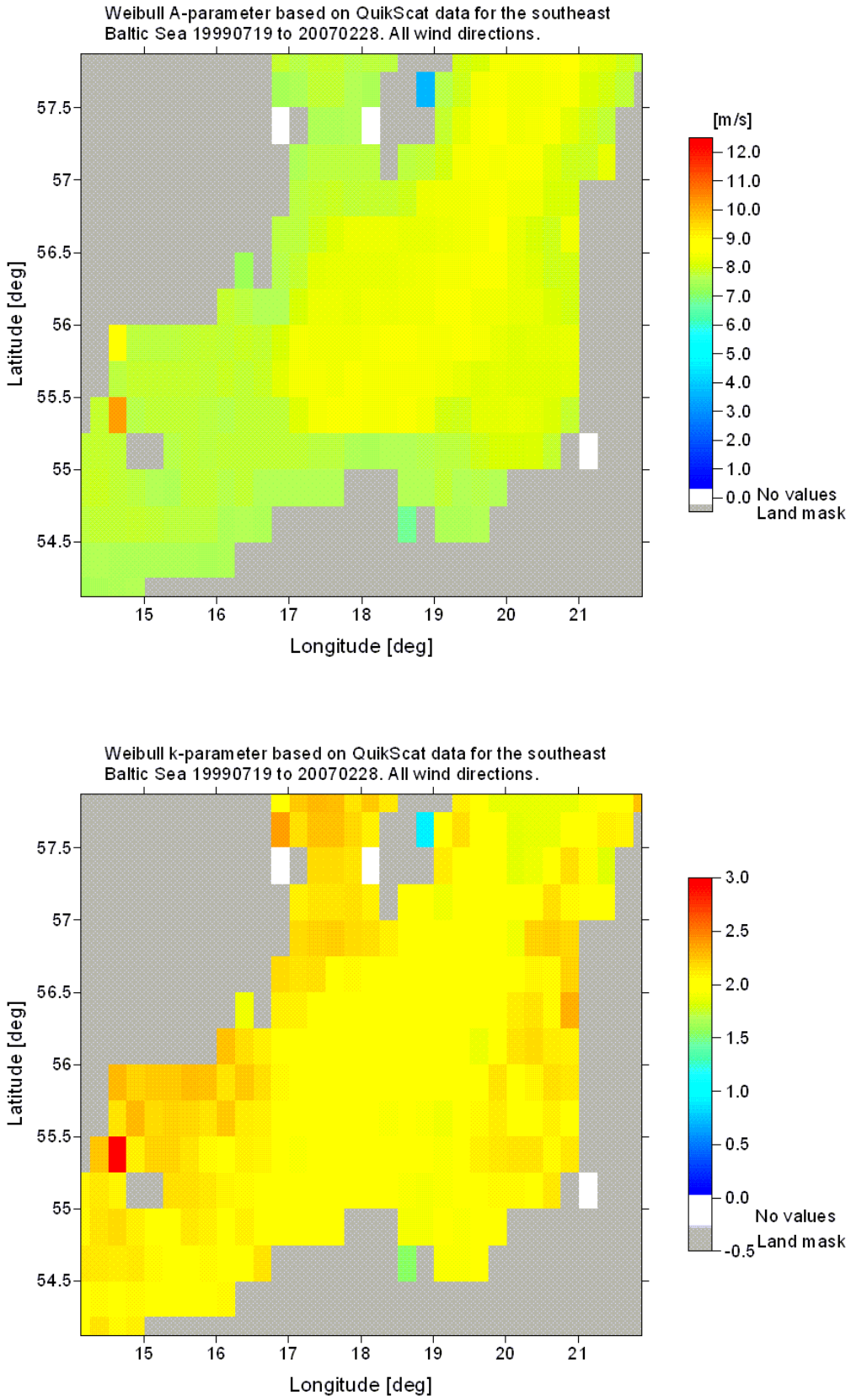

Figure 5.21 Weibull A (above) and Weibull k (below) observed from QuikSCAT during 8 years in the Baltic Sea.

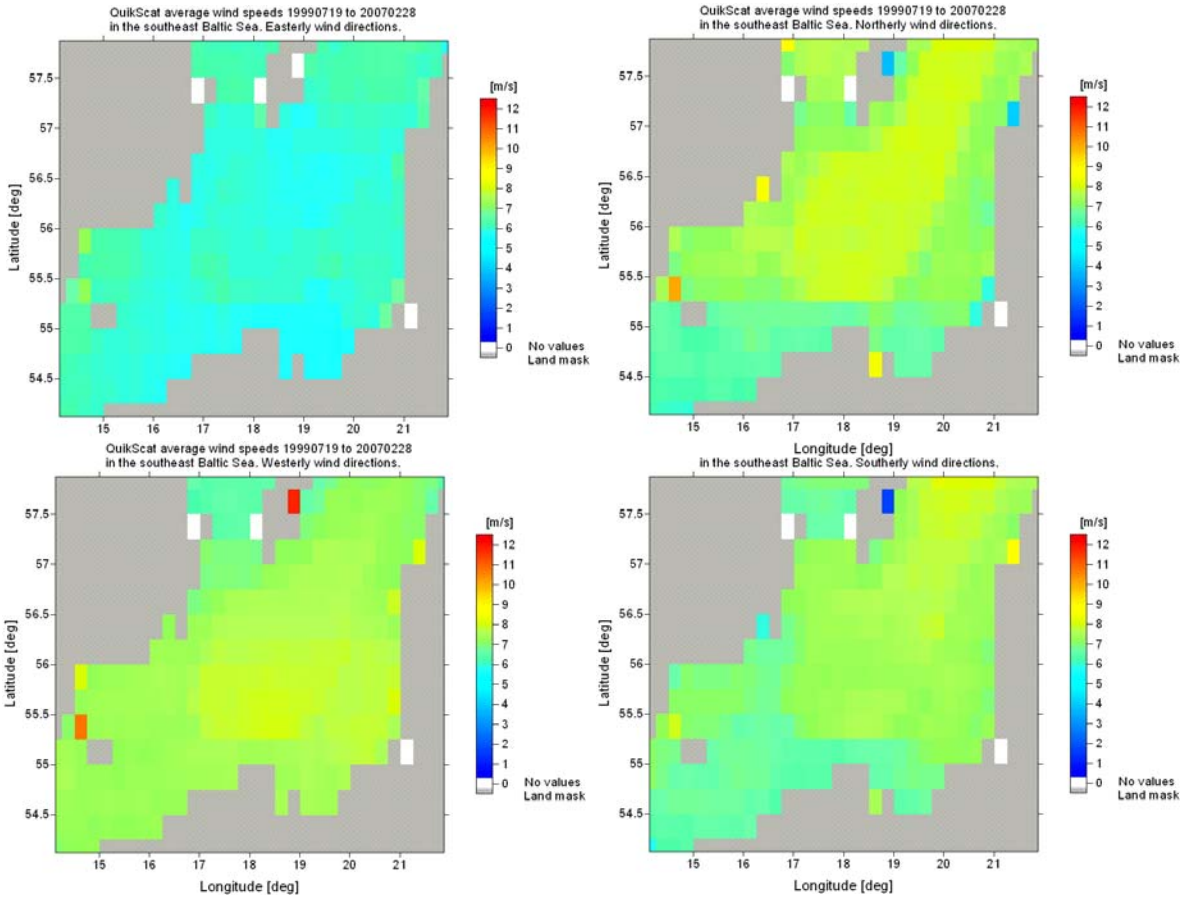

Figure 5.22 Mean wind speed observed from QuikSCAT during 8 years in the Baltic Sea from the four wind direction bins: east (top left), north (top right), west (bottom left) and south (bottom right).

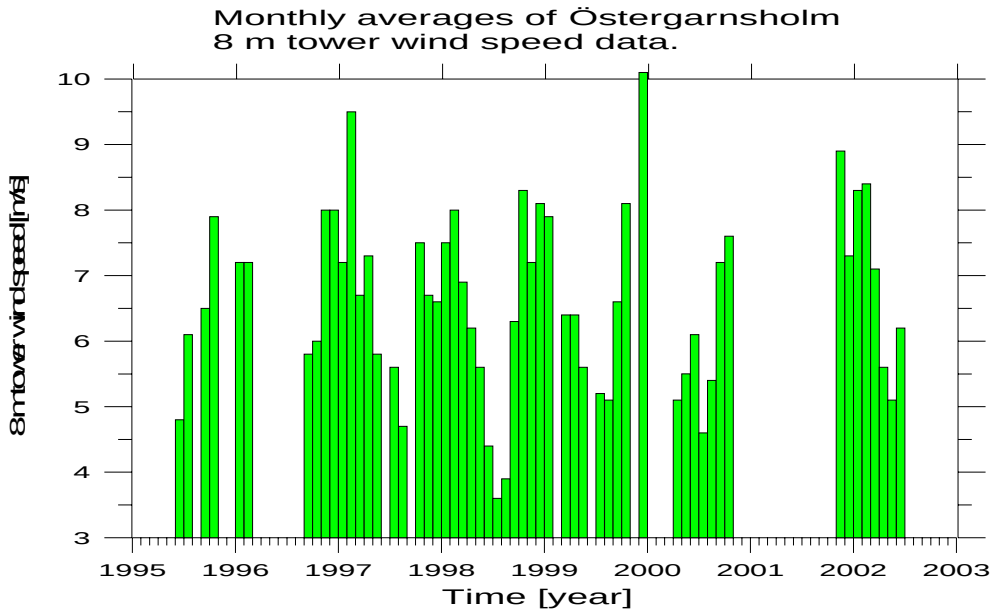

Figure 5.23. Monthly average wind speed at Östergarnsholm, Sweden. Data from Uppsala University.

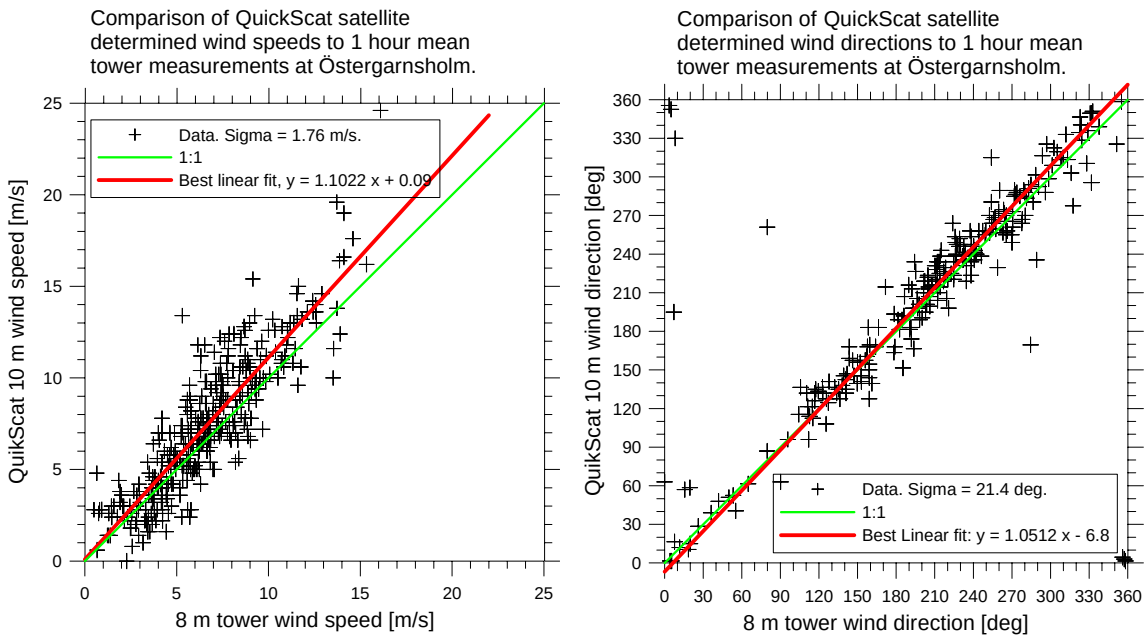

Figure 5.24. Comparing wind speed from Östergarnsholm and QuikSCAT for wind speed (left) and wind direction (right).The observations from Östergarnsholm are from Uppsala University.

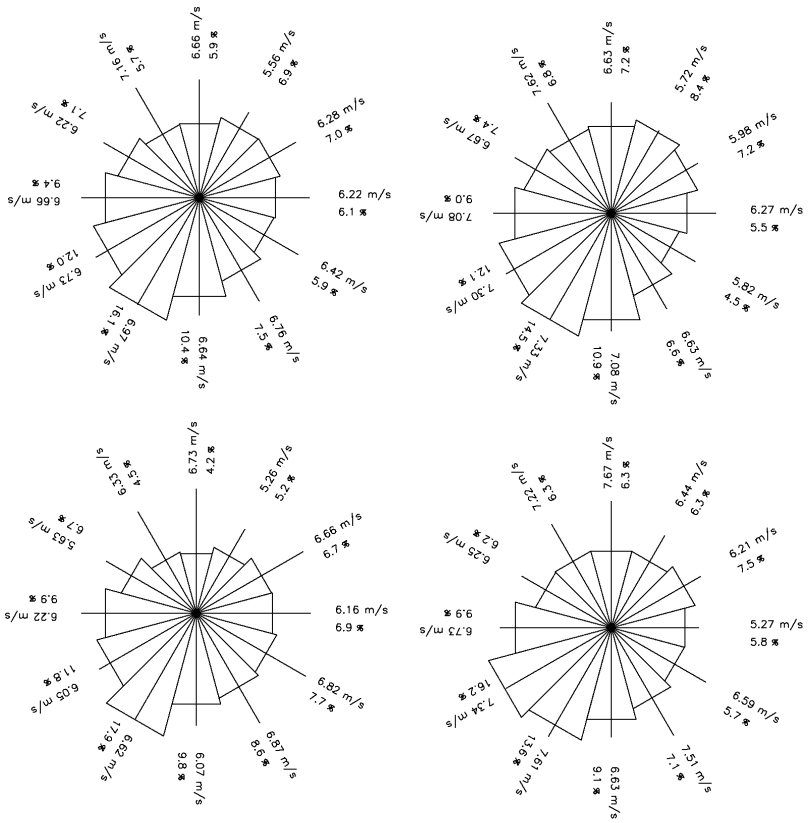

Figure 5.25. Wind roses for Östergarnsholm based on all available data from 7 years (top left), 'winter' seasons only (1.12. – 31.5.) (top right), 'summer' season only (1.6. – 30.11.) (bottom left) and QuikSCAT for 'summer' season only (1.6. – 30.11.) (bottom right).Observations from Östergarnsholm are from Uppsala University.

5.2 Results using Midori-II

From Midori-II wind results from the North Sea and the Baltic Seas are presented. The locations are identical to the sites described in section 5.1.2. Figure 5.26 presents the wind roses. Figure 5.27 presents the monthly averages and figure 5.28 presents the weekly averages. Unfortunately Midori-II was lost after only 7 months of operation.

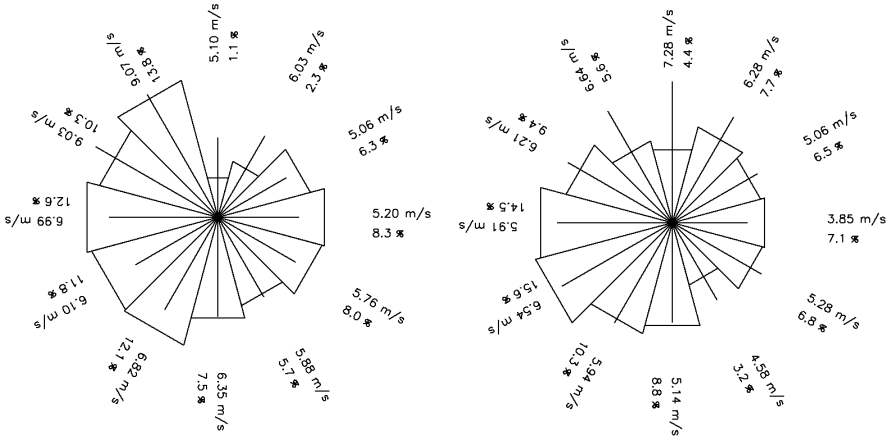

Figure 5.26 Wind roses observed from Midori-II from the North Sea (left) and the Baltic Sea (right).

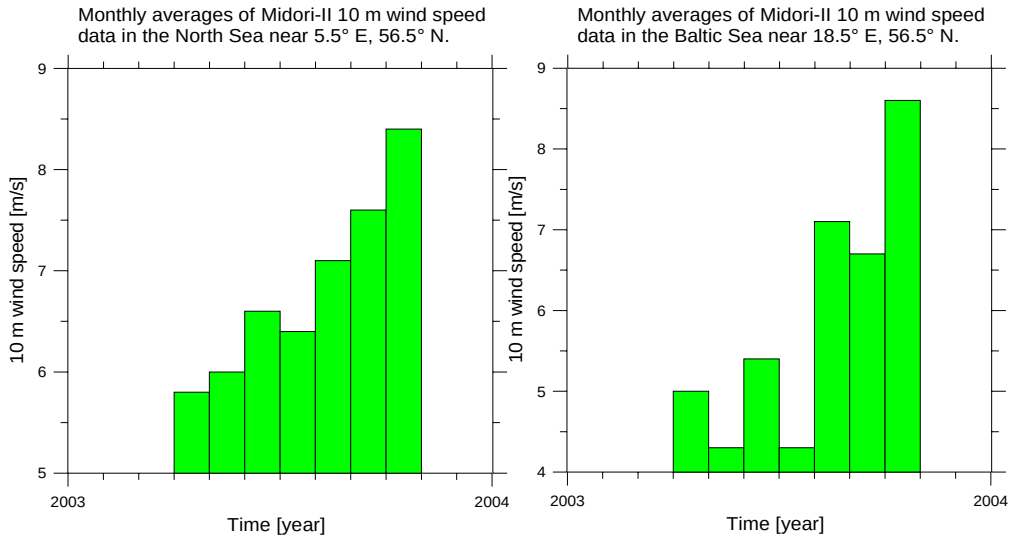

Figure 5.27 Monthly average wind speed observed from Midori-II for a site in the North Sea (above) and the Baltic Sea (below).

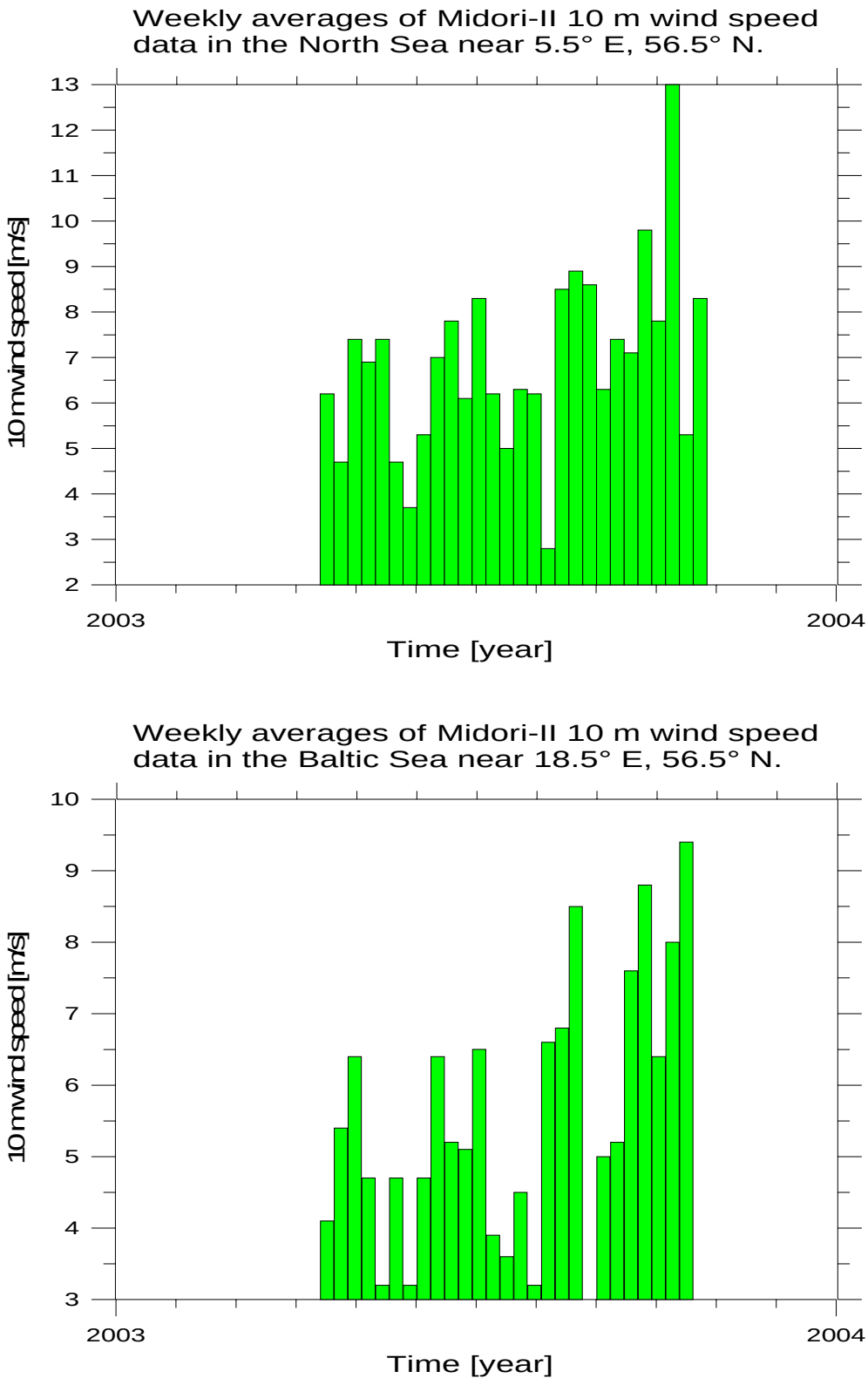

Figure 5.28. Weekly average wind speed observed from Midori-II for a site in the North Sea (above) and the Baltic Sea (below).

5.3 Results using NSCAT

No results are presented. The data source was of poorer quality than QuikSCAT. The swath was narrower and the absolute accuracy on wind speed was poorer than for QuikSCAT. Observations were only available from around one year in 1996-1997.

5.4 Results using ASCAT

No results are presented. The data were not yet available.

5.5 Results using ERS-2 SCAT

Wind speed observations from ERS-1 and -2 SCAT from location 55.52° N, 7.78° E in the period 1991-2003 were provided from ARGOSS http://www.argoss.nl/ by courtesy of Han Wensink. The selected data were within a 1° grid cell. The Weibull A and k were found to be 9.4 ms^{-1} and 2.4, respectively, and the mean wind speed 8.3 ms^{-1}. These values compared reasonably well to the values from (Sommer 2003) observed at Horns Rev in the period April 1999 to November 2002. The wind rose and Weibull fit were calculated and are shown in figure 5.29.

Wind maps from ERS-2 SCAT from the period 6 June 1999 to 28 December 2000 were purchased from ARGOSS and analyzed. Comparison of meteorological observations at Horns Rev and satellite winds are presented in figure 5.30 for wind direction and figure 5.31 for wind speed. The number of observations was low in the grid cell near Horns Rev. Therefore a circle of increasing size was used to capture more satellite wind observations. The circle was changed from 0.25°, to 0.5°, to 1.0° and to 5.0 °.

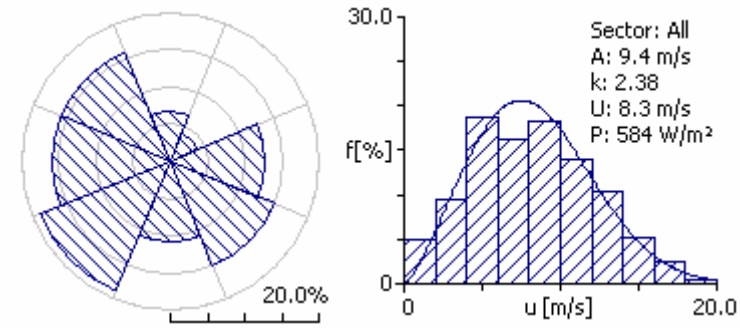

Figure 5.29. Wind speed and direction distribution from the ERS-1 and -2 SCAT data (left) and histogram with wind data and the fitted Weibull distribution (right) near Horns Rev in the North Sea.

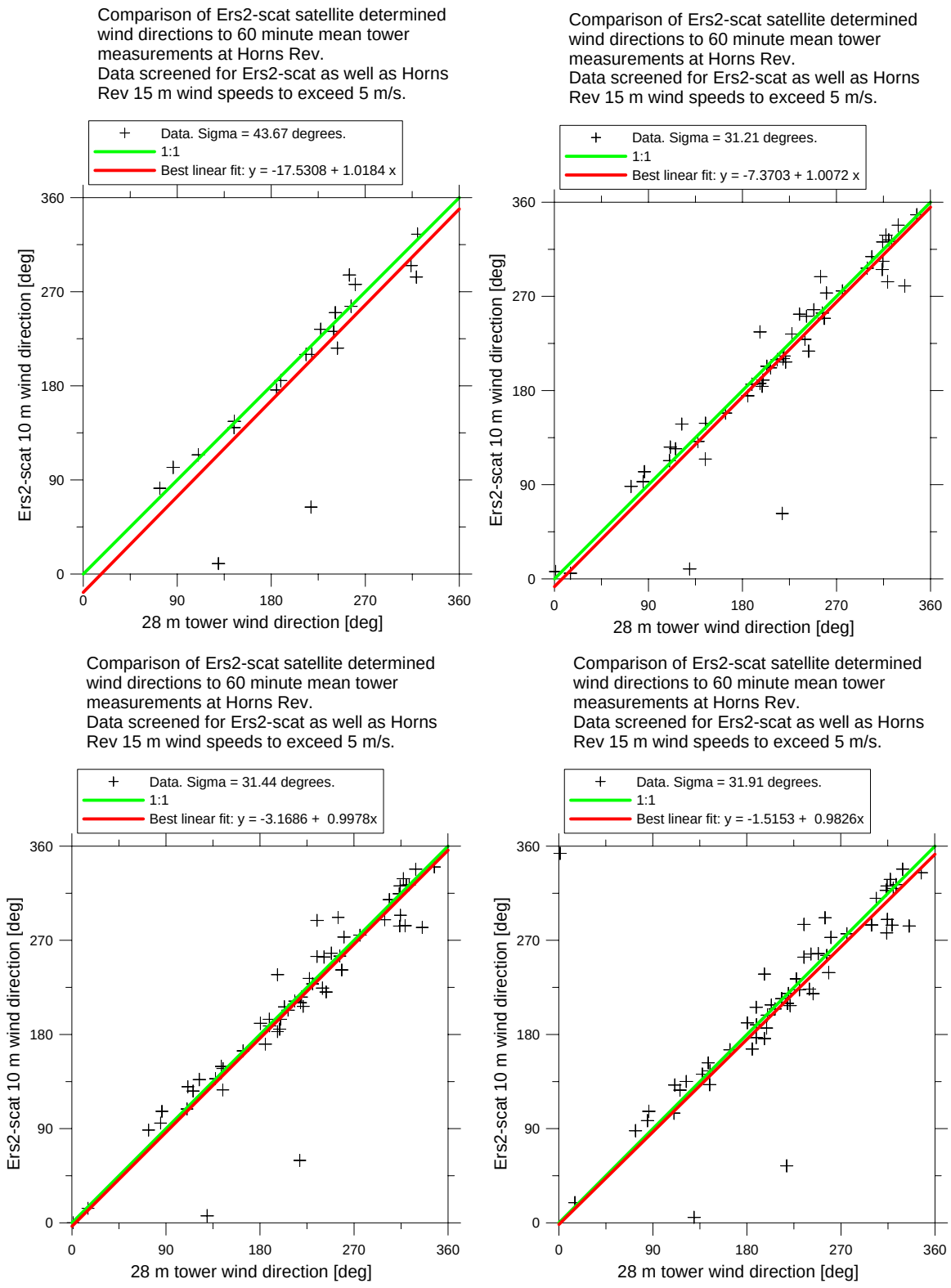

Figure 5.30. Comparison of wind direction near Horns Rev in Denmark (8.0 longitude, 55.4 latitude) from ERS-2 SCAT from ARGOSS and hourly values from an offshore meteorological mast (DONG energy data). The circles used for collection of scattterometer data is 0.25° (top left), 0.25° (top right), 1.0° (bottom left) and 5.0° (bottom right).

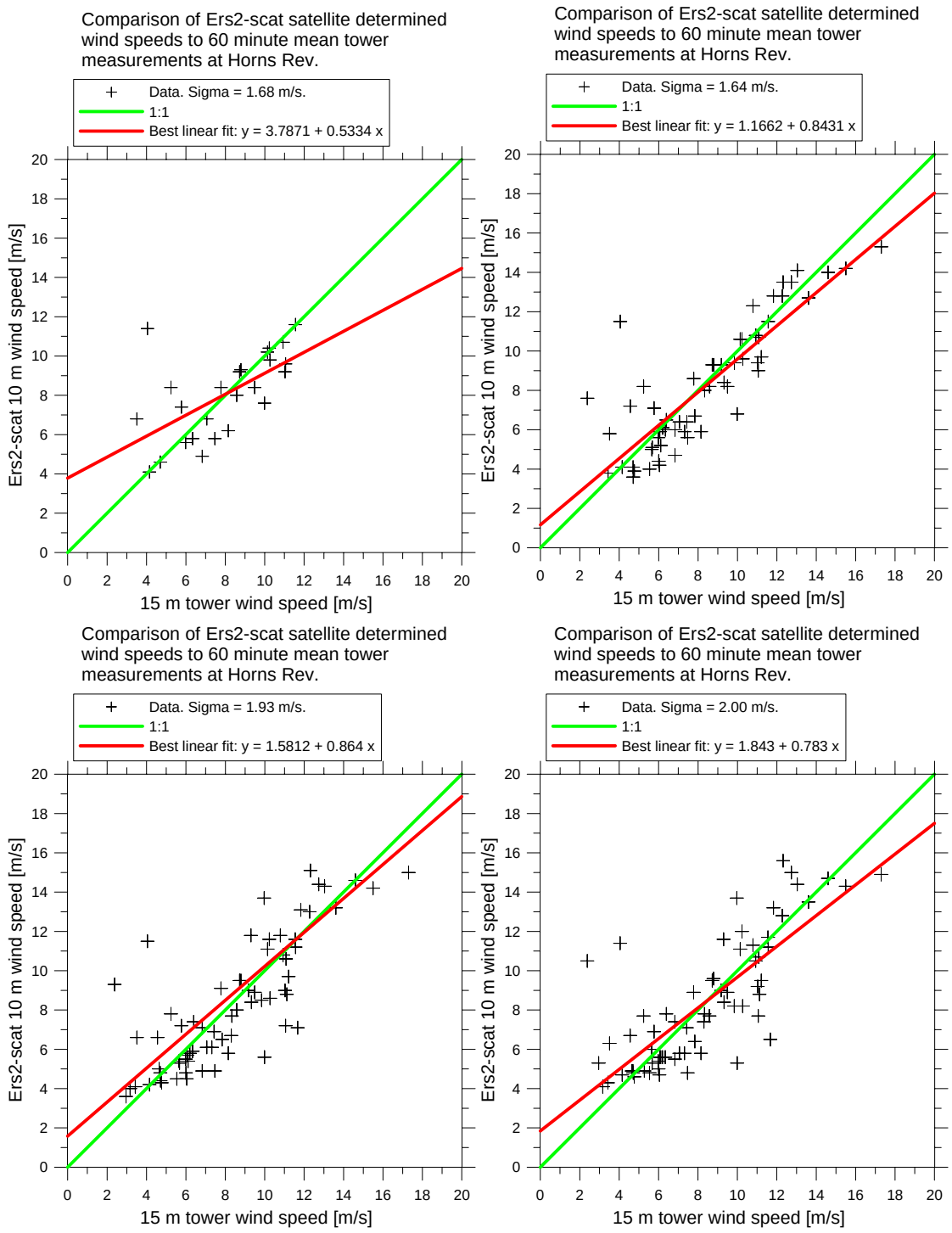

Figure 5.31. Comparison of wind speed near Horns Rev in Denmark (8.0 longitude, 55.4 latitude) from ERS-2 SCAT from ARGOSS and hourly values from an offshore meteorological mast (DONG energy data). The circles used for collection of scattterometer data is 0.25° (top left), 0.25° (top right), 1.0° (bottom left) and 5.0° (bottom right).

5.6 Results using SSM/I

SSM/I wind maps were available several times per day since year 1988. It should be noted, however, that the data were only available far offshore, e.g. in the central part of the Baltic Sea and in the North Sea but not in the inner Danish Seas. See figure 5.32. Wind data from the same two sites as described in section 5.1.2 (figure 5.15) were analyzed from SSM/I. The mean monthly variation during 10 years is presented in figure 5.33 for the North Sea and the Baltic Sea.

The annual mean wind speed values for 17 years are shown in figure 5.34 for a location in the North Sea and a location in the Baltic Sea. Further analysis on the monthly and inter-annual wind speed variation observed by SSM/I is found in chapter 7. Figure 5.34 included QuikSCAT and AMSR-E annual mean wind speed data (available at the time of that analysis). New wind map versions were available later and comparison results are presented in section 5.14. (AMSR-E wind data were upgraded from ver.04 to ver. 05).

Figure5.32. SSM/I wind speed data are only available in the areas in green and yellow.

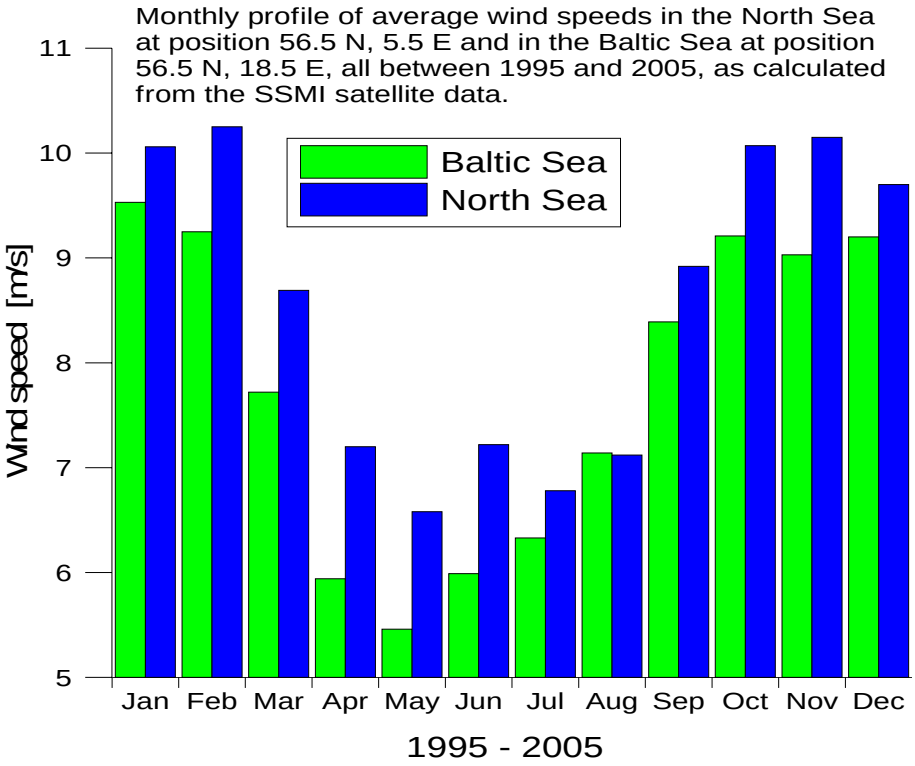

Figure 5.33 SSM/I wind speed data monthly averages from 10 years from an area in the North Sea and an area in the Baltic Sea. From (Hasager et al. 2006a)

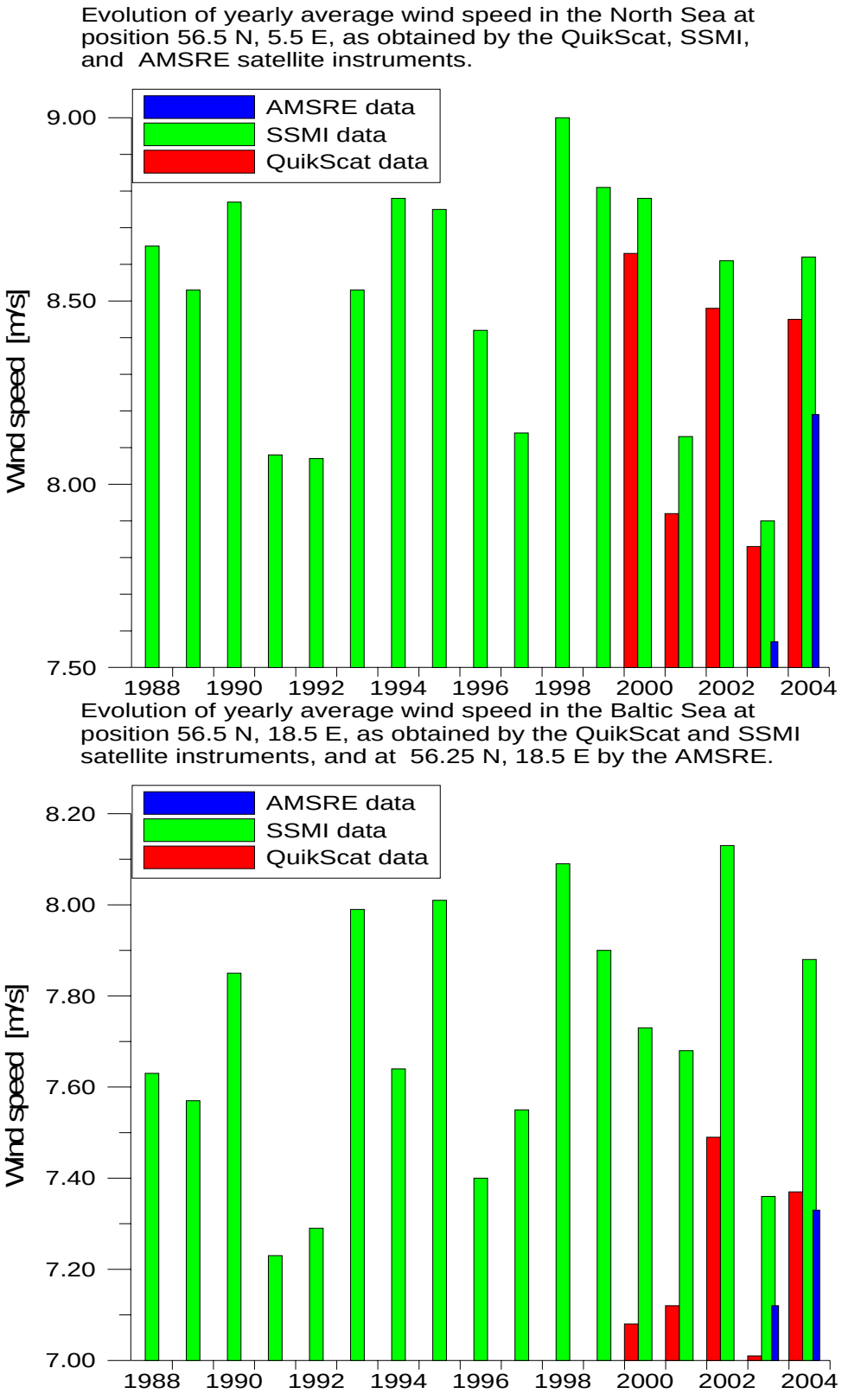

Figure 5.34 SSM/I wind speed data annual averages from 17 years, QuikSCAT wind speed annual averages from 5 years and AMSR-E wind speed annual averages from 2 years for a site in the North Sea (above) and the Baltic Sea (below). From (Hasager et al. 2006a).

5.7 Results using AMSR-E

AMSR-E wind speed observations in an area in the North Sea and in the Baltic Sea similar to section 5.1.2 (figure 5.15) are analyzed. AMSR-E only observes wind speed as SSM/I. The weekly and monthly mean wind speed for the North Sea and Baltic Sea are presented in figure 5.35 and 5.36, respectively.

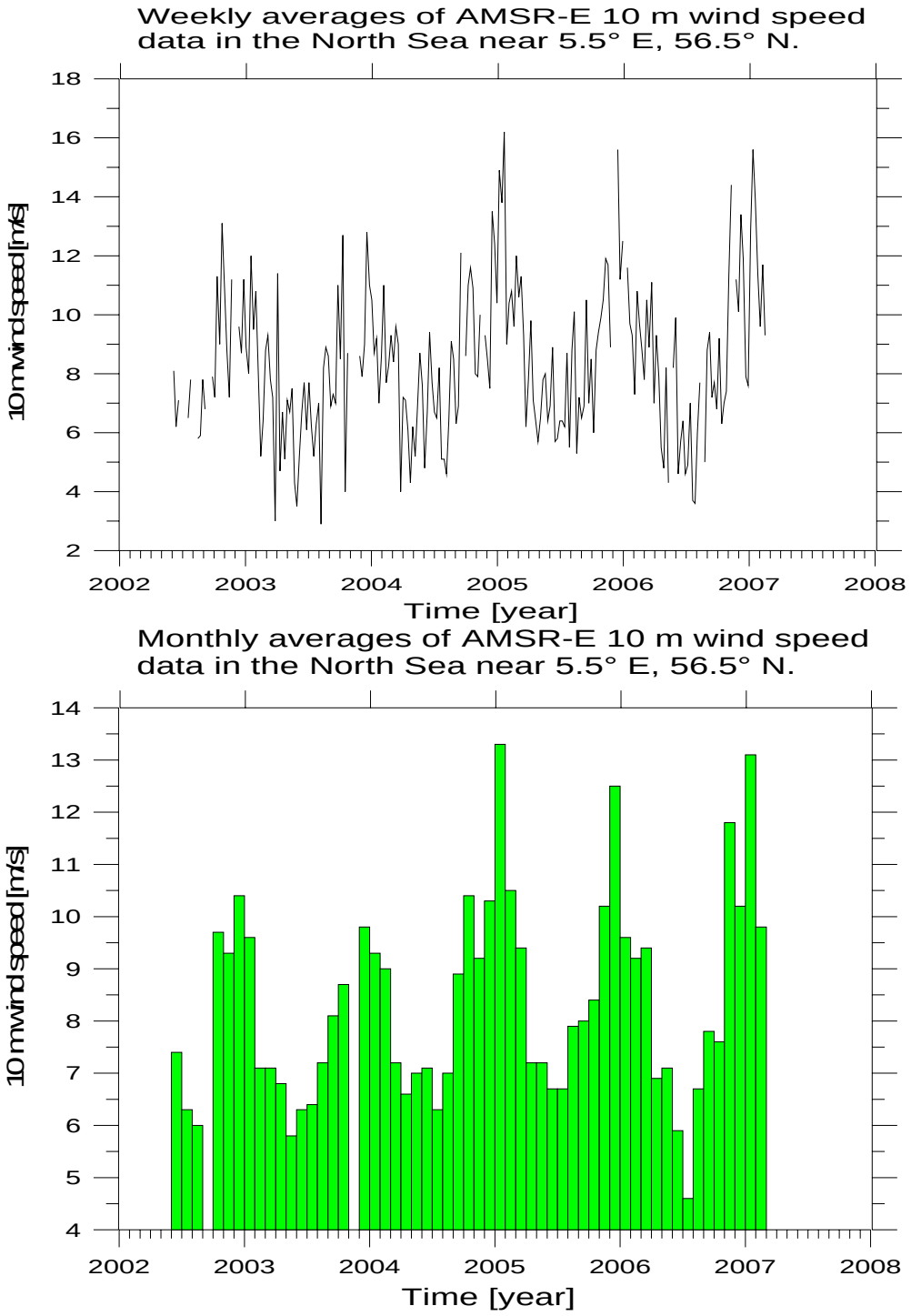

Figure 5.35 Weekly (above) and monthly (below) mean wind speeds from AMSR-E for a site in the North Sea.

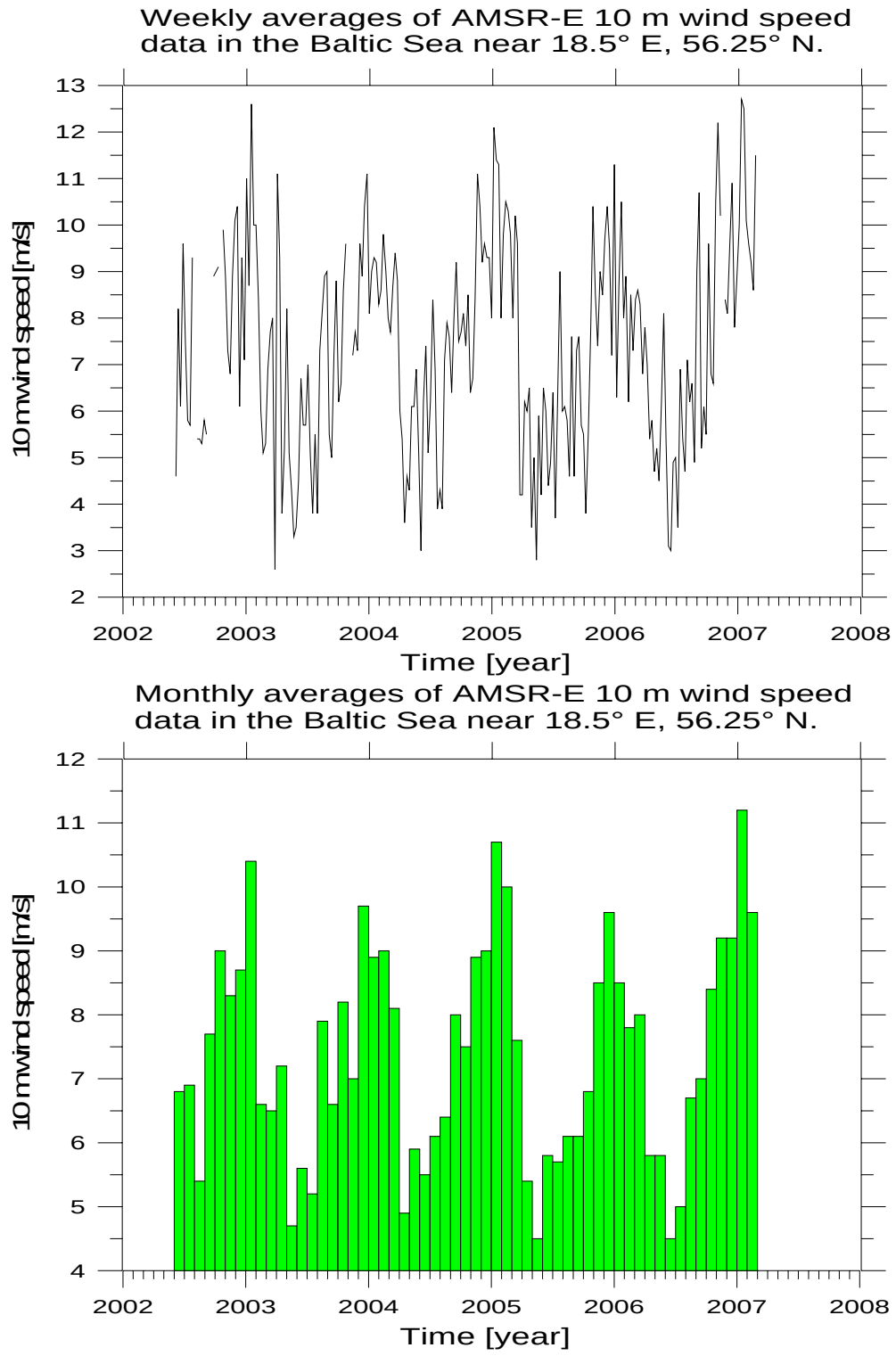

Figure 5.36 Weekly (above) and monthly (below) mean wind speeds from AMSR-E for a site in the Baltic Sea.

5.8 Results using WindSat

Wind maps from WindSat were analyzed and results from a site in the North Sea and the Baltic Sea are presented jointly in figure 5.37. It was from the same location as described in section 5.1.2 (figure 5.15). The weekly and monthly mean wind speeds are presented in figure 5.38. Surprisingly, the wind observations in the Baltic Sea were often higher than in the North Sea. (The wind data are of research quality. An update is expected).

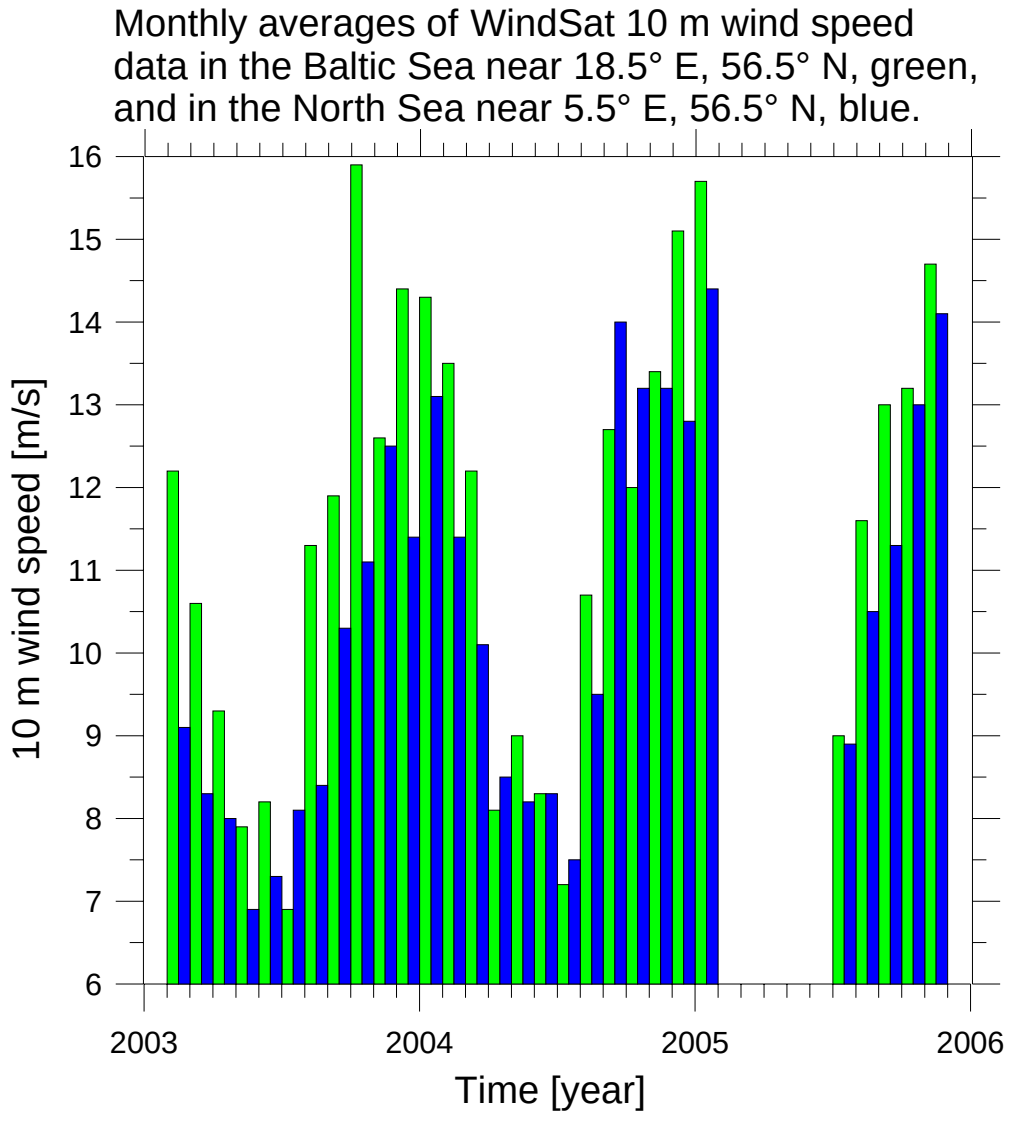

Figure 5.37. Monthly mean wind speed from a site in the North Sea and the Baltic Sea observed from WindSat.

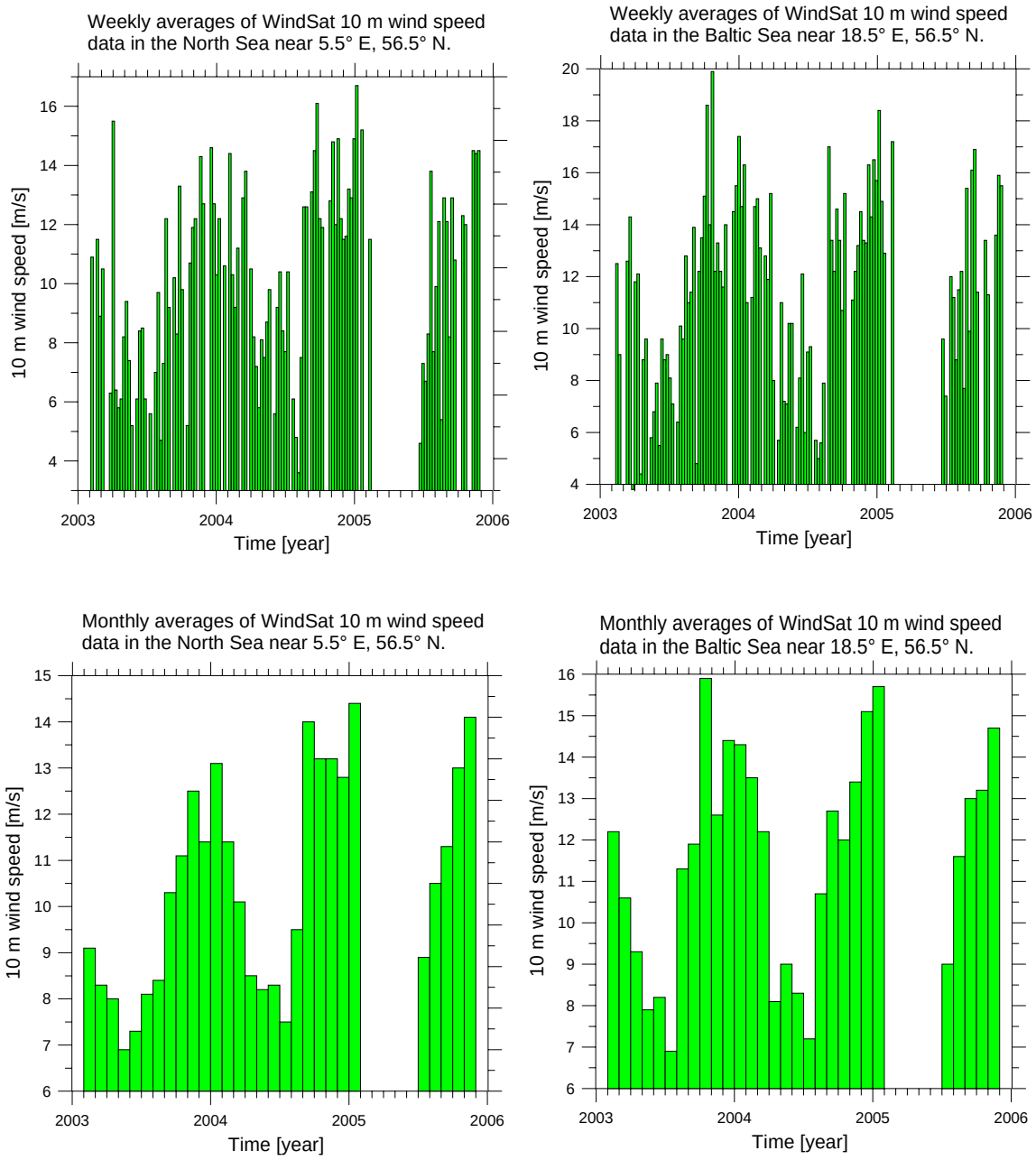

Figure 3.38. Weekly and monthly mean wind speed from a site in the North Sea (left panels) and the Baltic Sea (right panels) observed from WindSat.

5.9 Results using ERS SAR

Research on wind resource estimation based on ERS-SAR started in the EU-WEMSAR project (year 2000 to 2003) covering a small part of the Danish Seas, namely the Horns Rev in the North Sea. The first results included a comparison of the satellite-based wind observations with in-situ data at Horns Rev (Hasager *et al.* 2004b). This was followed by spatial statistics on wind resources using satellite wind observations at Horns Rev reported in (Nielsen *et al.* 2004) and (Hasager *et al.* 2005c). It was clear from figures 5.39, 5.40 and 5.41 that the winds offshore are much higher than near the coast at 10 m above sea level.

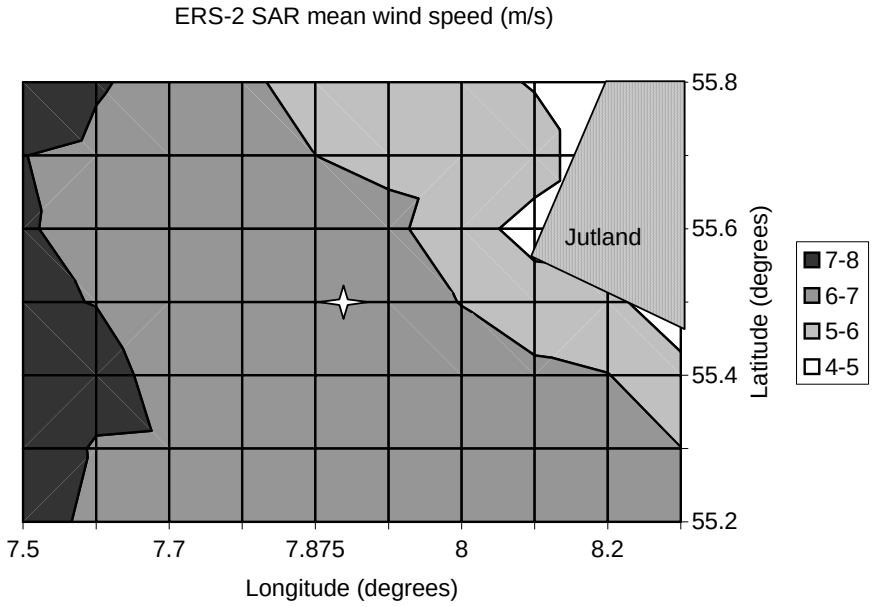

Fig. 5.39 Mean wind speed map at 10 m based on 61 ERS-2 SAR satellite wind maps for the Horns Rev area. The meteorological mast is located at the white star. From (Hasager et al. 2005c).

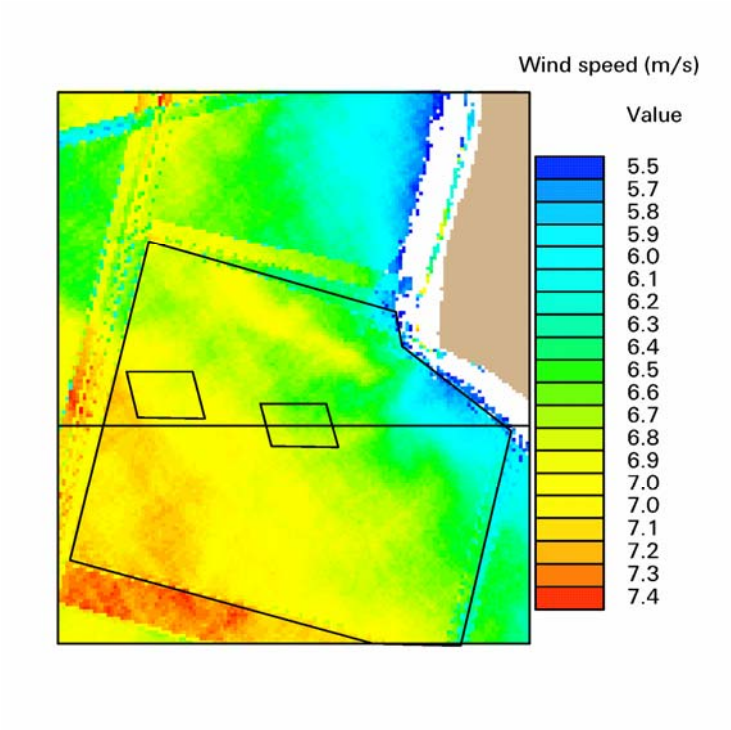

Fig. 5.40 Mean wind speed map based on 30 wind maps. The location of the present (eastern) and prospected (western) wind farm and the horizontal transect line is indicated (see figure 5.7 for the results along the transect-line). The 30 wind maps only cover the area within the black polygon.

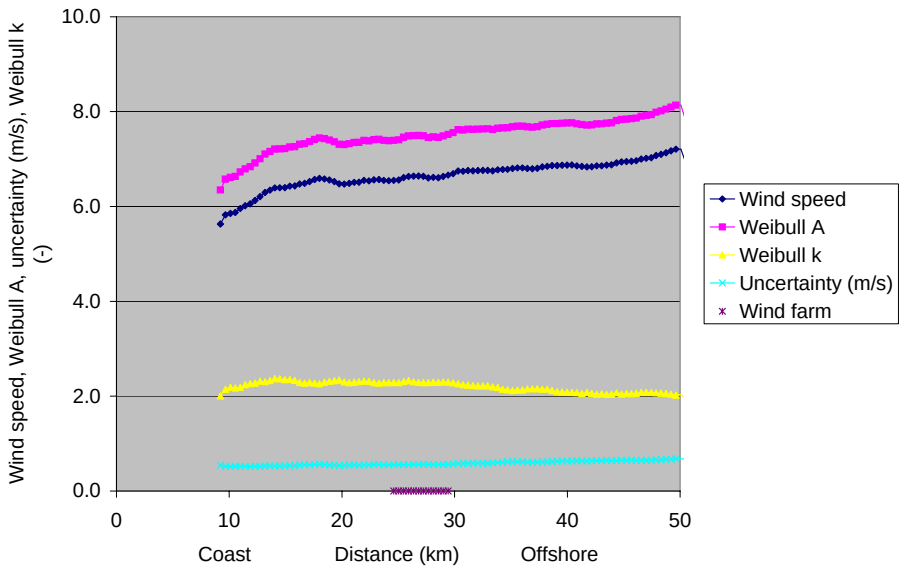

Fig. 5.41 Wind statistics of mean wind speed along a horizontal transect line from the coast and through the Horns Rev wind farm based on 30 wind maps from ERS SAR collected prior to construction of the wind farm. The wind farm is located 25 to 30 km offshore.

5.10 Results using Envisat ASAR

5.10.1 Denmark

The Envisat ASAR instrument allows several modes of operation. One of these is the Wide Swath Mode (WSM) which has the advantage of a wide swath (~ 400 km). At the same time the spatial resolution is less than for image mode of swath (~100 km). From Envisat ASAR it is possible to make analysis from imaging mode with a swath ~ 100 km as described in section 5.8 for ERS SAR. In the present section, however, only results from WSM are presented.

An example of an Envisat ASAR WSM wind map was presented on the cover page. It was from JHU/APL, Risø DTU observed 15 January 2007 at 20.54 UTC. The arrows were from the NOGAPS meteorological model indicating wind speed and direction.

To demonstrate results from S-WAsP (chapter 4) five Envisat ASAR WSM wind maps covering Denmark were used. These were observed at 12.08.2006 20.56 UTC, 22.09.2006 09.42 UTC, 05.01.2007 at 09.42 UTC, 09.02.2007 at 09.42 UTC and 25.02.2007 at 09.40 UTC, i.e. one evening pass and four morning passes. The winds offshore south of Fyn are shown in figure 5.42. The 5 wind maps are shown in figure 5.43.

S-WAsP was run in three ways with input of the 5 wind maps. The results are presented in figure 5.44. The first way was a simple averaging, pixel by pixel; the second way was using the footprint-averaging and filtering for 10 m; the third way was using the footprint-averaging and filtering for 70 m. The overall result is similar, yet it can be seen that the non-filtered result is more ‘speckled’ than the filtered results that have a smoother appearance. The large footprint associated with 70 m compared to 10 m gave a type of ‘striping’ in the dominant wind direction. It is recommended to use the 10 m footprint-averaging and filtering.

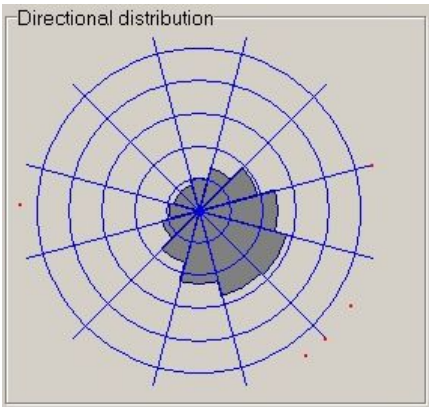

Figure 5.42 Wind rose from 5 Envisat ASAR wind maps for a site south of the island Fyn.

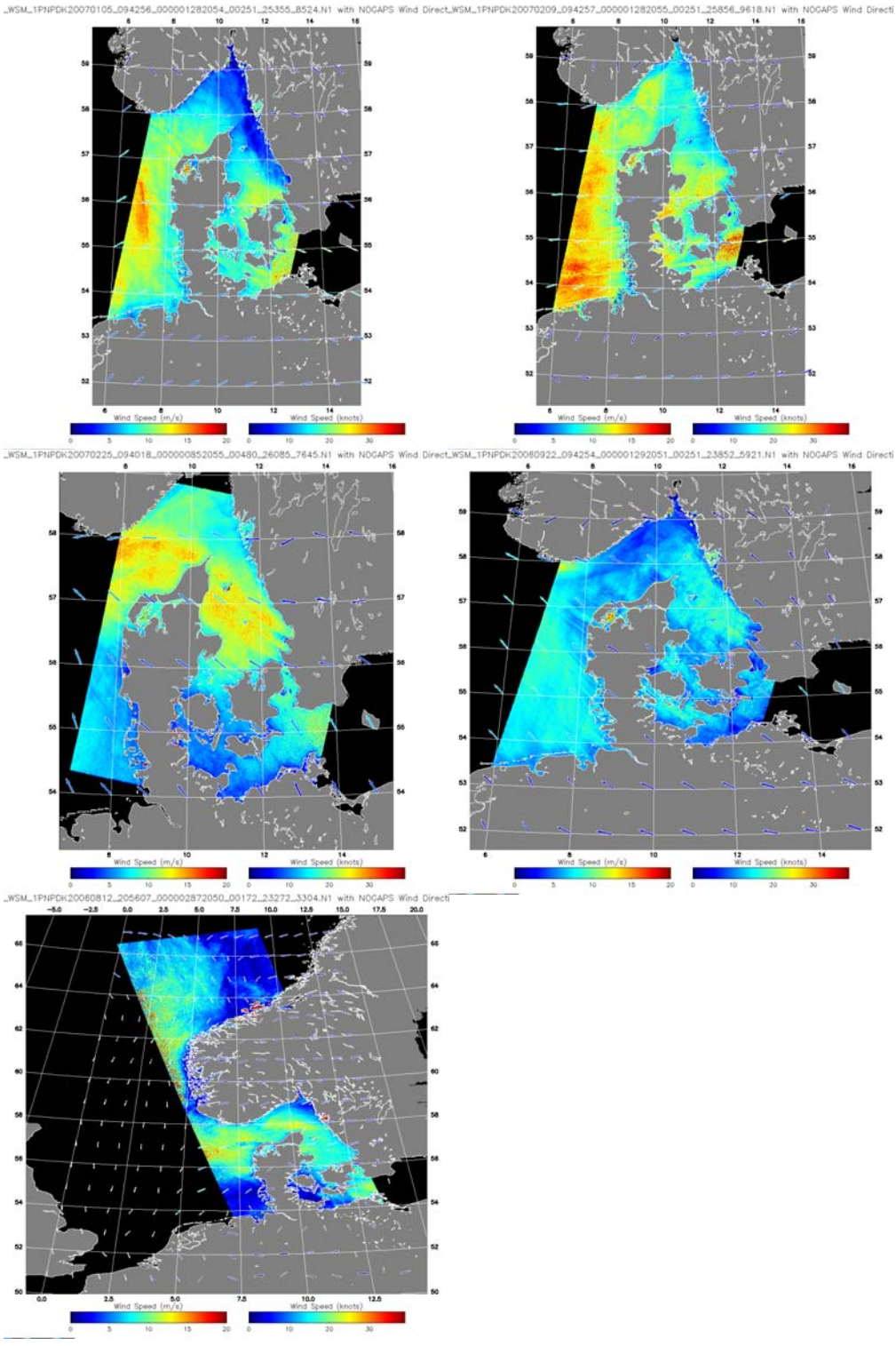

Figure 5.43 Wind maps from Envisat ASAR WSM covering Denmark. Processed by JHU/APL, Risø DTU. The arrows are from the NOGAPS meteorological model indicating wind speed and direction. The date and hour of observation are included in the wind maps.

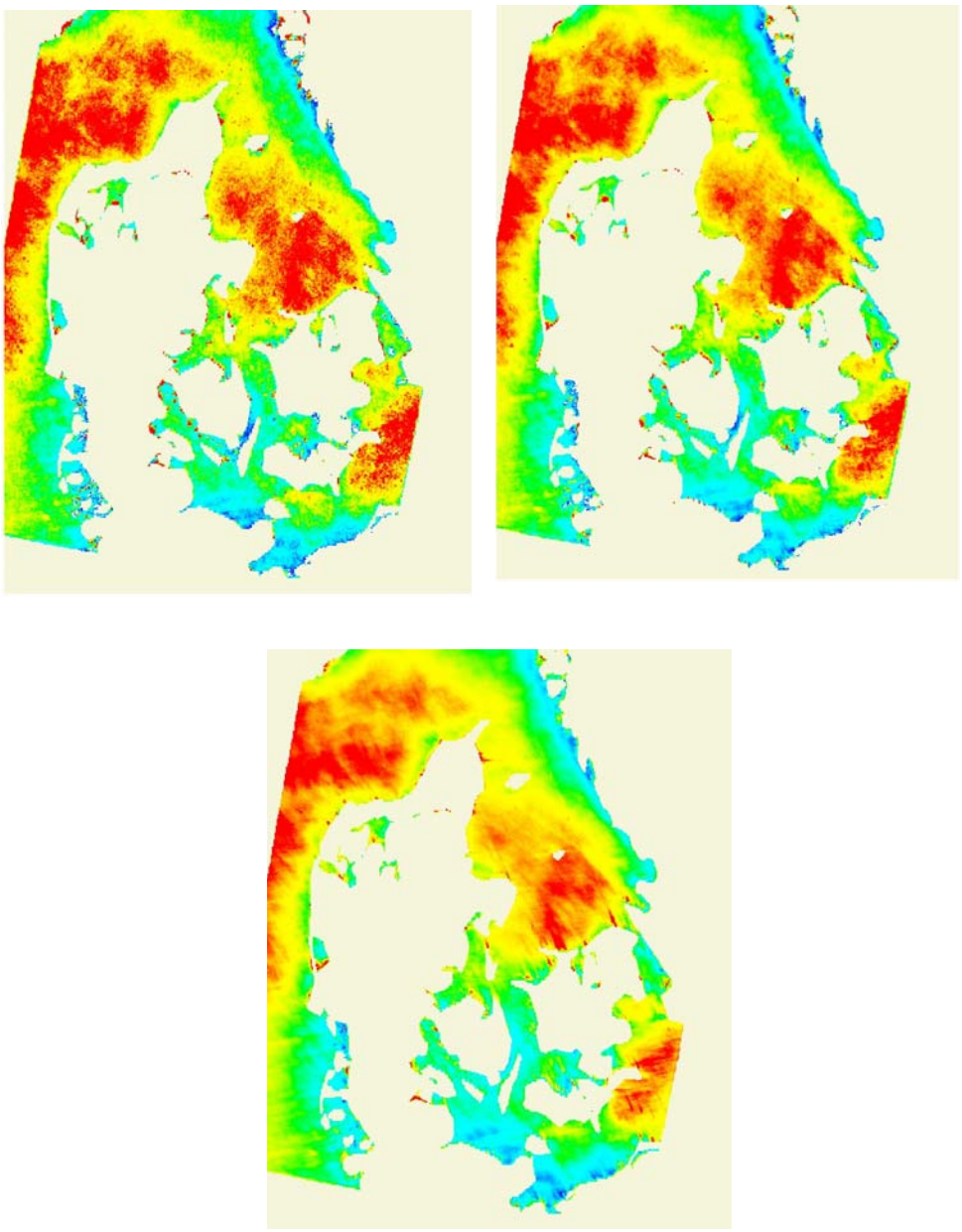

Figure 5.44 Mean wind speed from 5 Envisat ASAR wind maps from S-WAsP for (top left) non-filtered; (top right) footprint-averaged and filtered for 10 m; (bottom) footprint-averaged and filtered for 70 m.

It is also recommended to find a series of wind maps with a large spatial overlap. As an example three wind maps are shown in figure 5.45 in Google Earth. It is clear that only a minor part was viewed from all three satellite scenes. Figure 5.46 shows the mean wind speed in central Denmark seen from 20 overlapping Envisat ASAR WSM wind maps. Figure 5.47 shows the mean wind speed in eastern Denmark from 26 overlapping wind speed maps and figure 5.48 shows the mean wind speed in central Denmark from 41 overlapping wind speed maps.

Spatial variations in mean wind speed were found in all cases. In figure 5.48 two parallel horizontal transect lines were drawn from North to South and the mean wind speed is shown in figure 5.49. The mean wind speeds were similar in the two transects in the northern part along 150 km of transects but deviating in the southern part along 100 km

of transect. Transects were located 11 km apart. At around 175 km on the x-axis scale was an exceptionally high value. This was artifact from backscatter of C-band radiation from the 80 wind turbines in the Horns Rev offshore wind farm. The satellite scenes showed high values due to large backscatter, and this was calculated falsely as high wind.

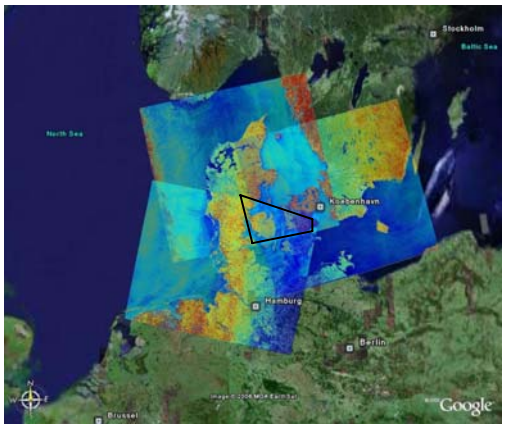

Figure 5.45 Three wind maps shown in Google Earth. Only in the black polygon is there an overlap.

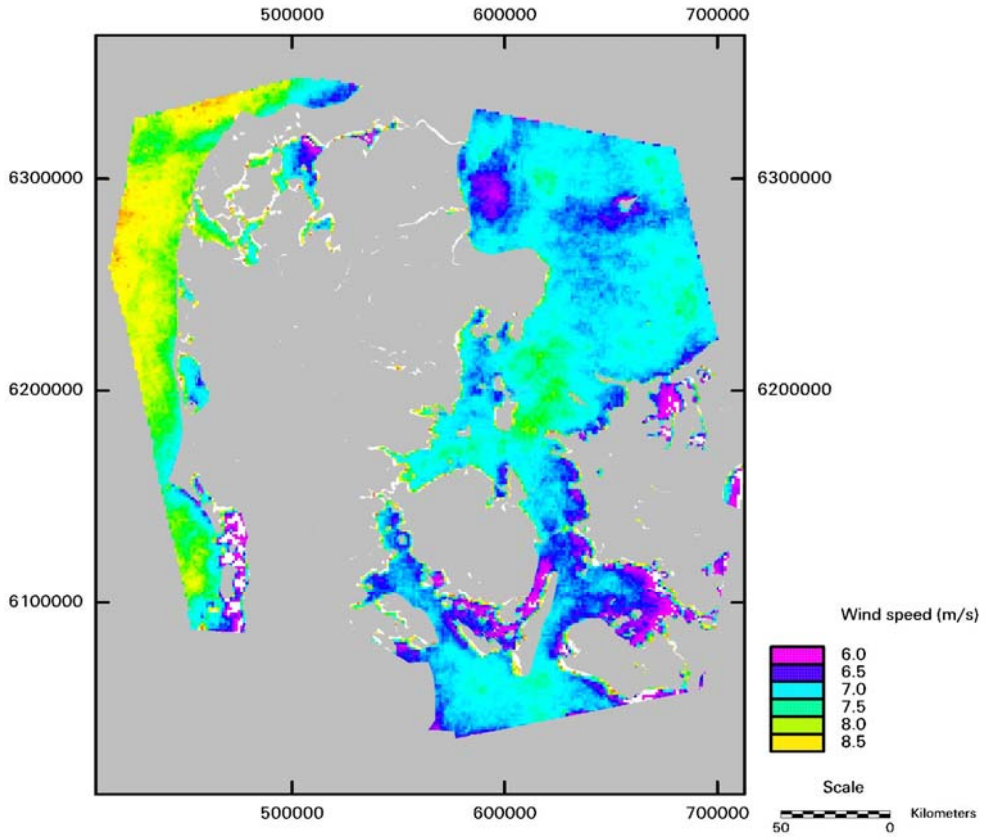

Figure 5.46 Mean wind speed observed from 20 Envisat ASAR wind maps. From (Hasager et al. 2006a).

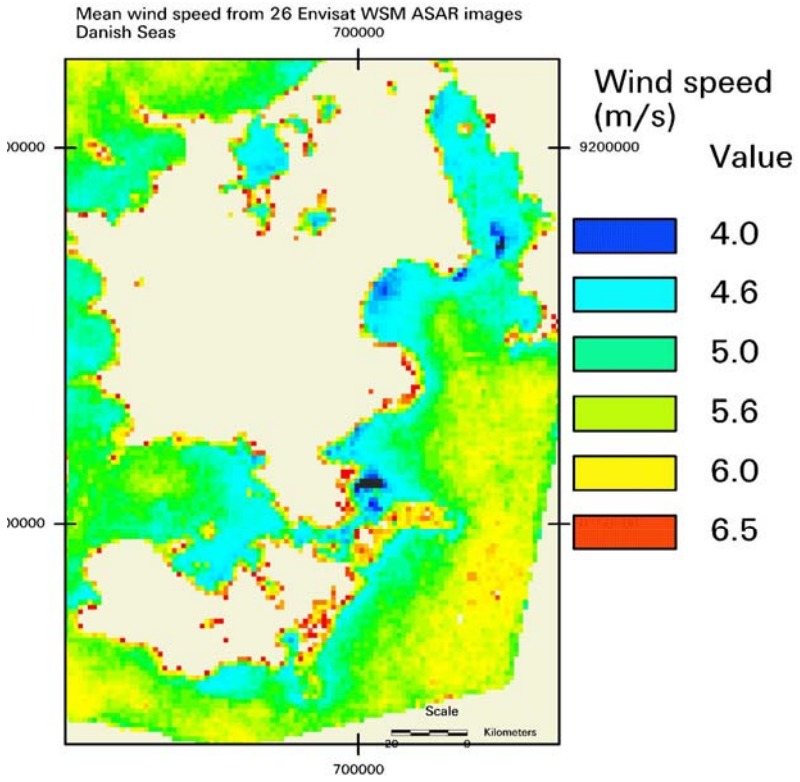

Figure 5.47 Mean wind speed from 26 Envisat ASAR wind maps (Hasager et al. 2006c).

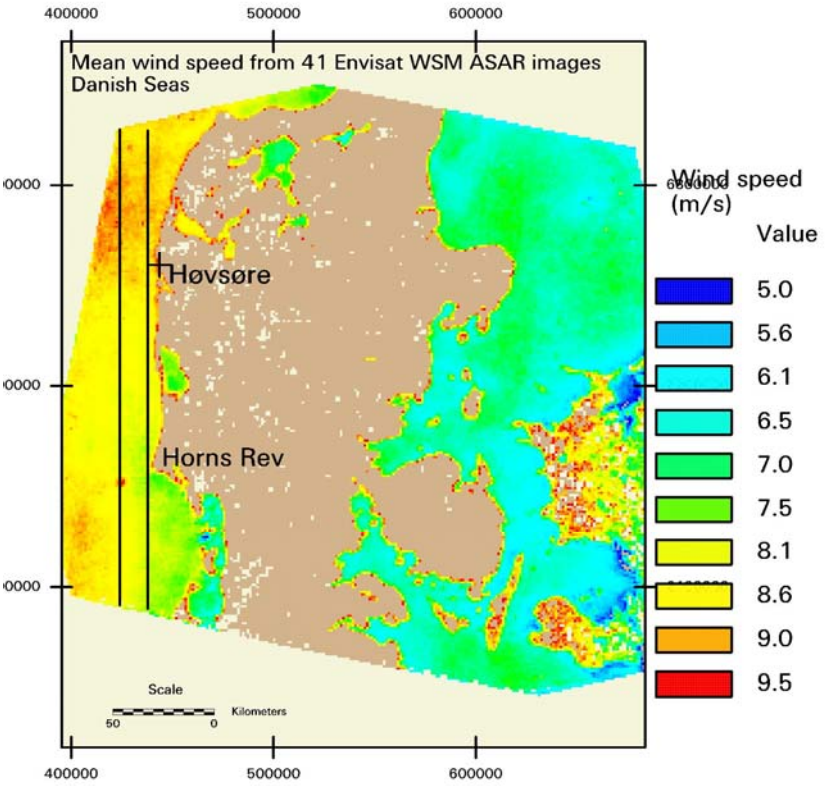

Figure 5.48 Mean wind speed from 41 Envisat ASAR wind maps (Hasager et al. 2006c).

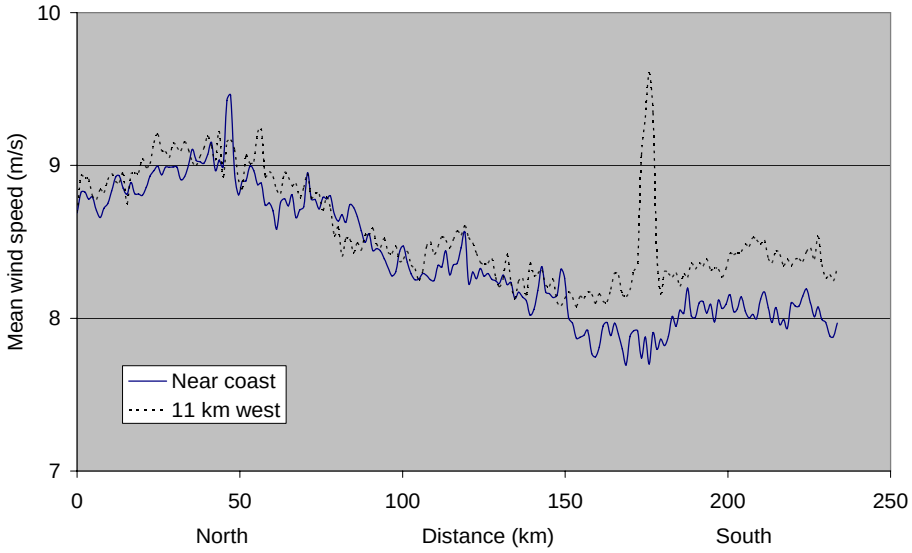

Figure 5.49: Mean wind speed along two horizontal transect lines in the North Sea (cf. Fig.5.14). From (Hasager et al. 2006c).

(Christiansen *et al.* 2006b) presented a detailed analysis of wind observed from satellite SAR compared to offshore meteorological observations. A series of 91 collocated SAR wind observations were analyzed. The Weibull fit for the satellite winds and the meteorological mast data are presented in figure 5.50 along with the mean wind speed and energy. The results were compared to the Horns Rev Fyrskib, 1962-80 (European Wind Atlas) of mean wind speed 7.3 m/s and energy 456 W/m2.

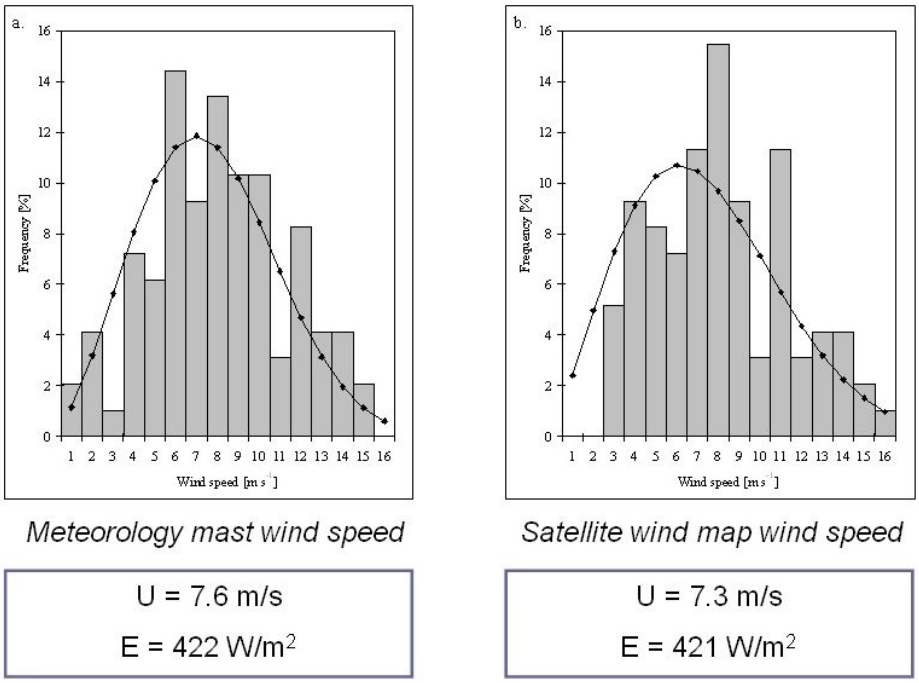

Figure 5.50. Weibull fit based on 91 meteorological observations (left) and 91 satellite SAR wind observations (right). Partly from (Christiansen et al. 2006b).

At the meteorological mast observations of air temperature were collected at two heights and from analysis of the observations it was possible to identify cases of stable, neutral and unstable flow conditions at the time of satellite observations. Based on this information the data set was divided into different categories. Linear regression results between mast observations of wind speed and satellite wind speed is presented in table 5.1. The best fit was (as expected) found for near-neutral conditions and for onshore winds. These conditions are most similar to open ocean conditions for which the CMOD geophysical model functions were developed. It is comforting, however, that reasonable results were obtained in all categories. This supports further use of the method for offshore wind resource estimation.

Table 5.1 Linear regression results from a total of 91 satellite wind maps and meteorological observations for various categories. From (Christiansen et al. 2006b).

	SD [m s^{-1}]	Bias [m s^{-1}]	R^2	N
Onshore winds	1.10	-0.06	0.89	49
Offshore winds	1.08	-0.52	0.88	42

	SD [m s^{-1}]	Bias [m s^{-1}]	R^2	N
Stable	1.47	-0.86	0.88	11
Near-neutral	0.95	-0.13	0.93	22
Unstable	1.06	-0.26	0.85	52

	SD [m s^{-1}]	Bias [m s^{-1}]	R^2	N
No wind farm	0.93	-0.57	0.90	46
Wind farm	1.20	0.04	0.87	45

5.10.2 Sweden

Envisat ASAR wind maps for the entire length of the Baltic Sea were occasionally observed. Six cases from 2006 were used for a preliminary study. The six individual wind maps are presented in figure 5.51. The S-WAsP result of mean wind speed in figure 5.52 and the wind rose for the six samples is graphed. The wind rose is from latitude 57.25° N and longitude 19.00° E near Östergarnsholm. The wind speed and wind direction was listed in table 5.2. The wind direction was from the NOGAPS atmospheric model and the wind speed from CMOD-5. The mean wind speed was 5.5 ms^{-1}.

Table 5.2. Wind speed and wind direction from six Envisat ASAR wind maps for a site near Gotland, Sweden.

Yyyymmdd_hhmmss	wind speed (ms^{-1})	wind direction (°)
20060607_090121	3.1	348
20060819_090708	4.7	78
20060822_091250	2.4	243
20061119_091553	5.2	315
20061205_091259	10.8	199
20061218_090423	6.8	315

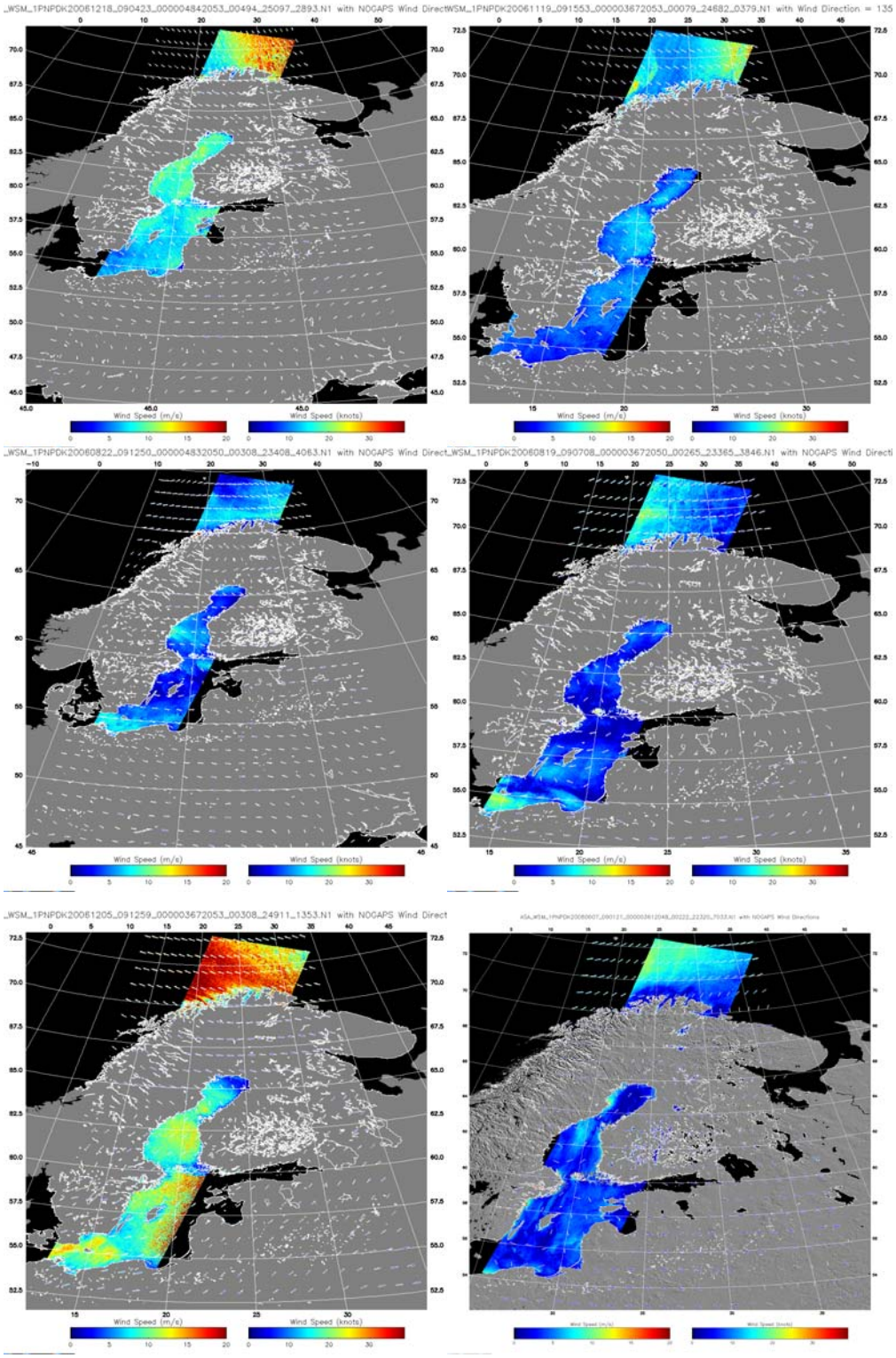

Figure 5.51 Wind maps from Envisat ASAR WSM covering the Baltic Sea. Processed by JHU/APL, Risø DTU. The arrows were from the NOGAPS meteorological model indicating wind speed and direction. The date and hour of observation were included in the wind maps.

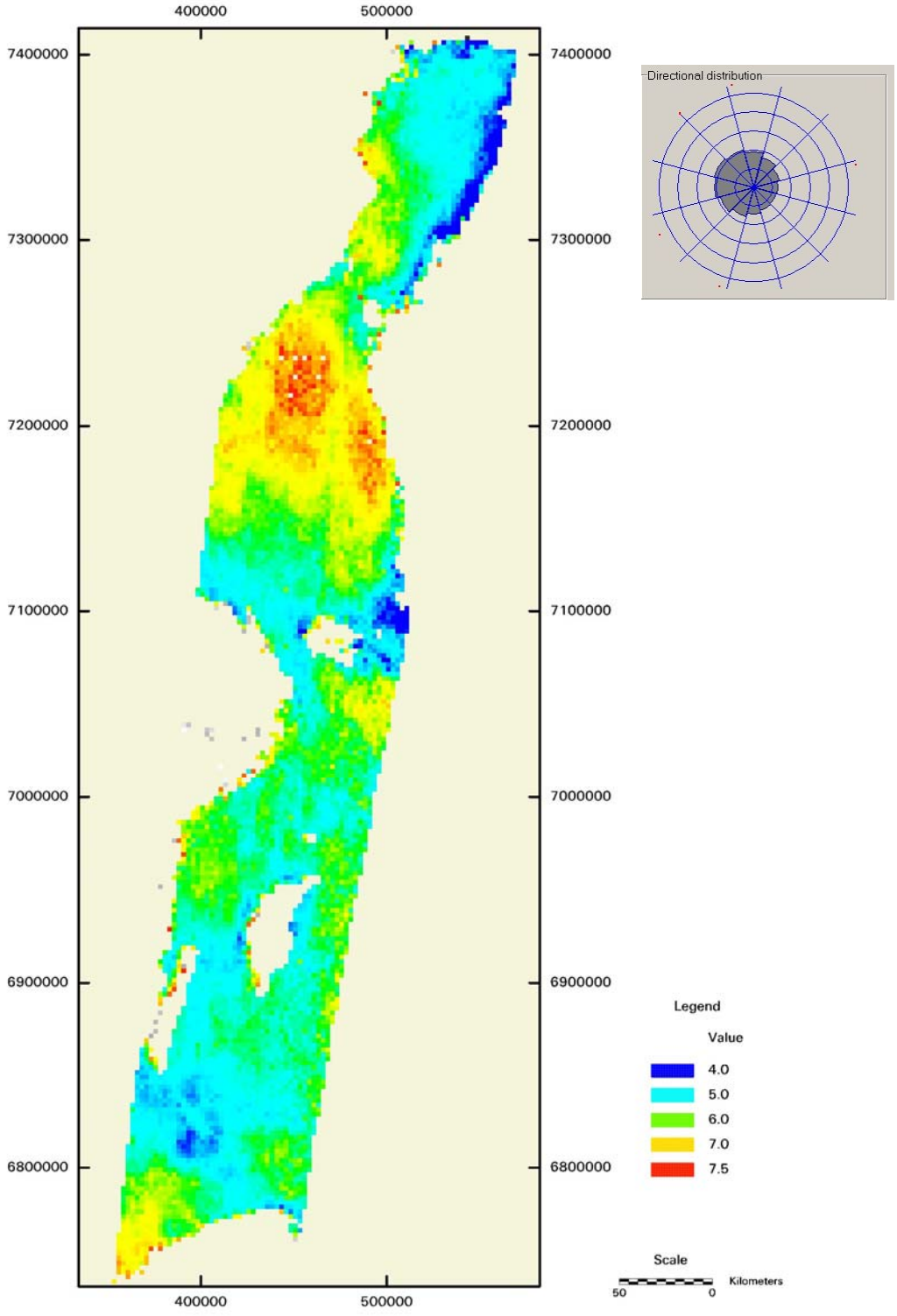

Figure 5.52 Mean wind speed from 6 Envisat ASAR wind maps of the Baltic Sea. The wind rose is from near Gotland showing wind speed and direction of the 6 wind maps.

5.11 Results using ERS altimeter

Wind speed maps from ERS radar altimeter (RA) purchased from ARGOSS were compared to meteorological observations at Horns Rev for the period 12 May 1999 to 27 December 2000. The comparison results are presented in figure 5.53. The number of observations was low in the grid cell near Horns Rev. Therefore a circle of increasing size was used to capture more satellite wind observations. The circle was changed from 0.25°, to 0.5°, to 1.0° and to 5.0 °. Altimeters only observe wind speed, not direction.

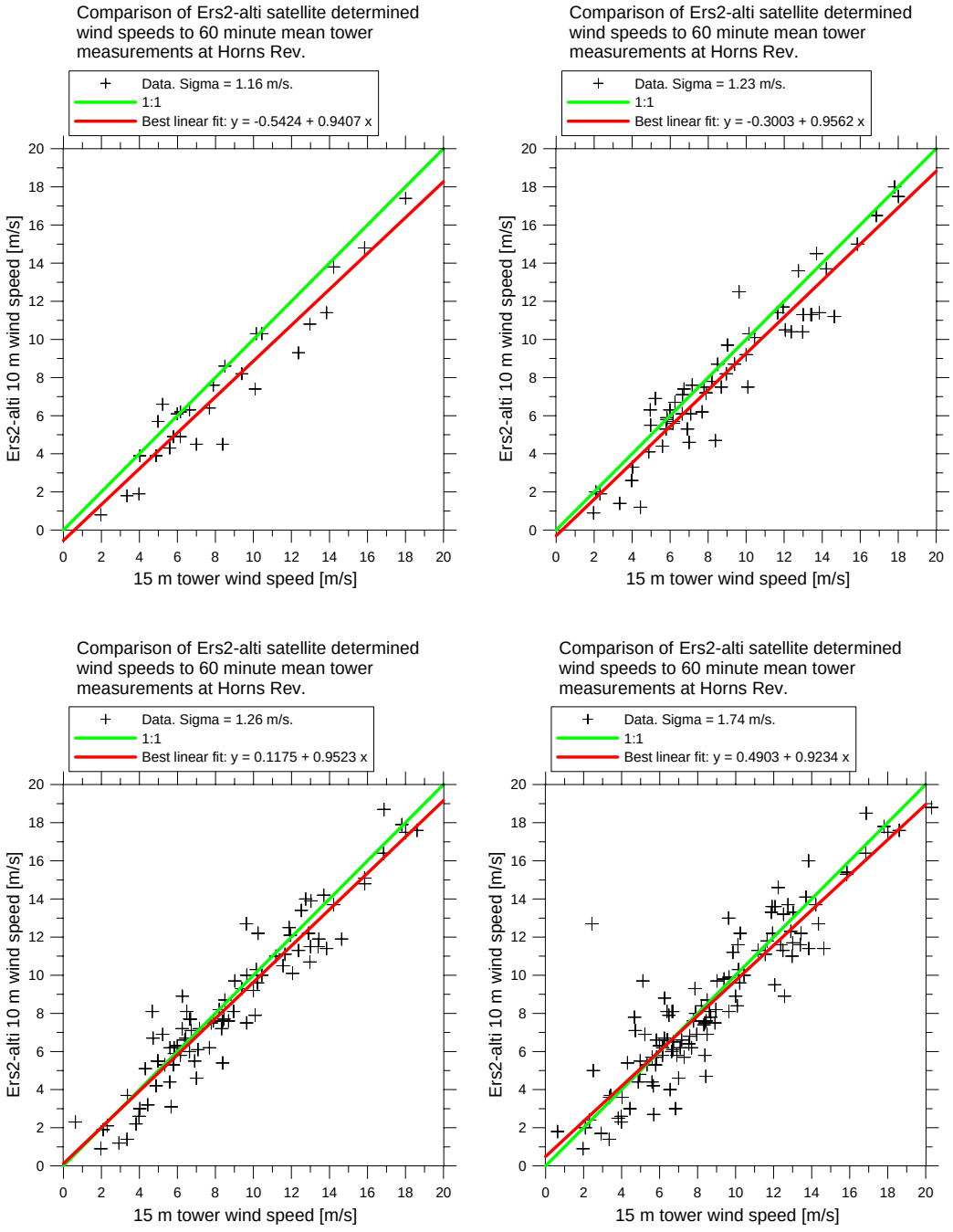

Figure 5.53 Comparison of wind speed near Horns Rev in Denmark (8.0 longitude, 55.4 latitude) from ERS-2 altimeter (RA) from ARGOSS and hourly values from an offshore meteorological mast (DONG energy data). The circles used for collection of altimeter data was 0.25° (top left), 0.5° (top right), 1.0° (bottom left) and 5.0° (bottom right).

5.12 Results using Topex altimeter

Wind speed maps from Topex radar altimeter purchased from ARGOSS were compared to meteorological observations at Horns Rev for the period 2 June 1999 to 31 December 2000. The comparison results are presented in figure 5.54. The number of observations was low in the grid cell near Horns Rev. Therefore a circle of increasing size was used to capture more satellite wind observations. The circle was changed from 0.25°, to 0.5°, to 1.0° and to 5.0 °.

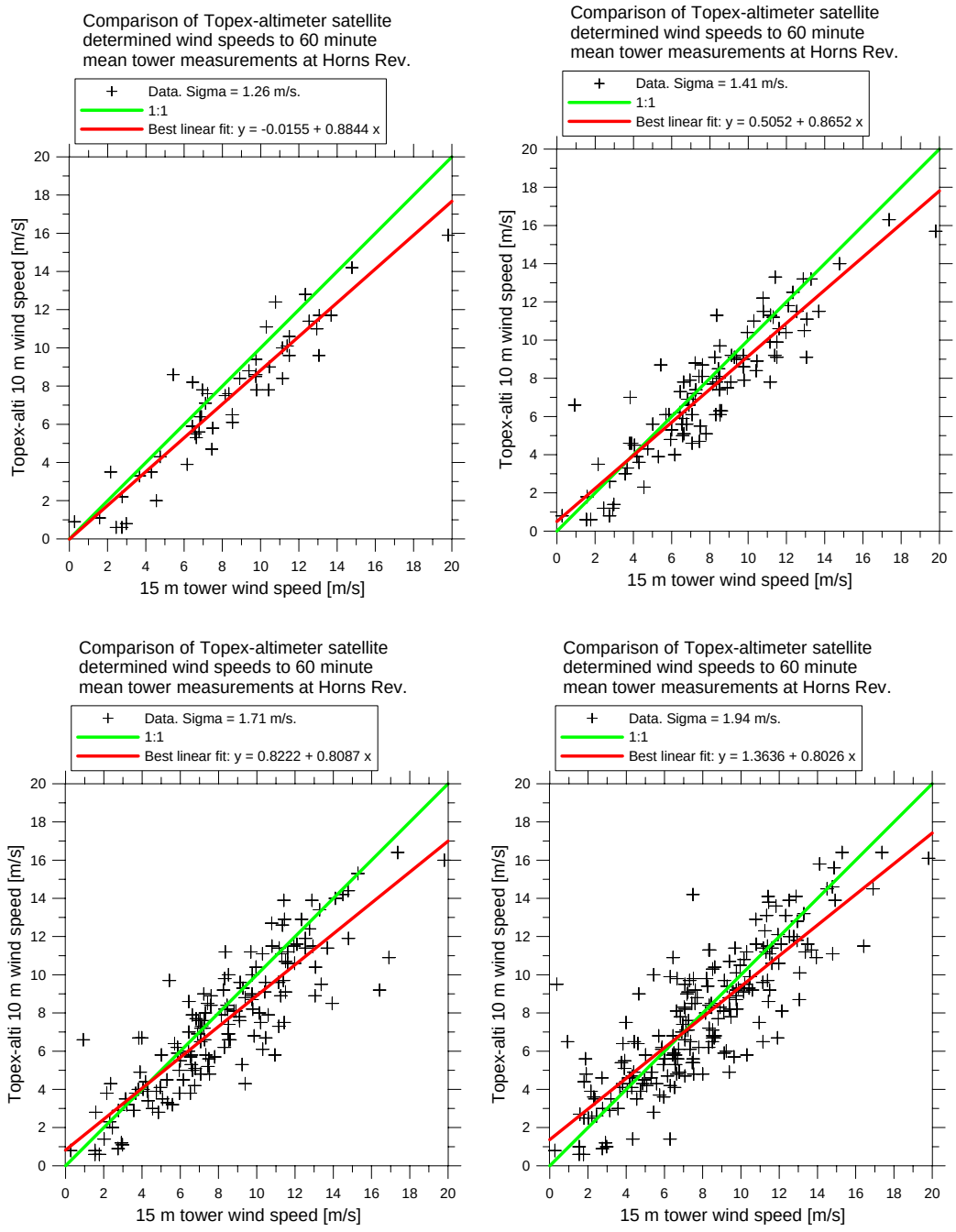

Figure 5.54 Comparison of wind speed near Horns Rev in Denmark (8.0 longitude, 55.4 latitude) from Topex altimeter from ARGOSS and hourly values from an offshore meteorological mast (DONG energy data). The circles used for collection of altimeter data was 0.25° (top left), 0.5° (top right), 1.0° (bottom left) and 5.0° (bottom right).

5.13 Results using Poseidon altimeter

Wind speed maps from Poseidon radar altimeter purchased from ARGOSS were compared to meteorological observations at Horns Rev for the period 29 August 1999 to 1 November 2000. The comparison results are presented in figure 5.55. The number of observations was low in the grid cell near Horns Rev. Therefore a circle of increasing size was used to capture more satellite wind observations. The circle was changed from 0.25°, to 0.5°, to 1.0° and to 5.0 °.

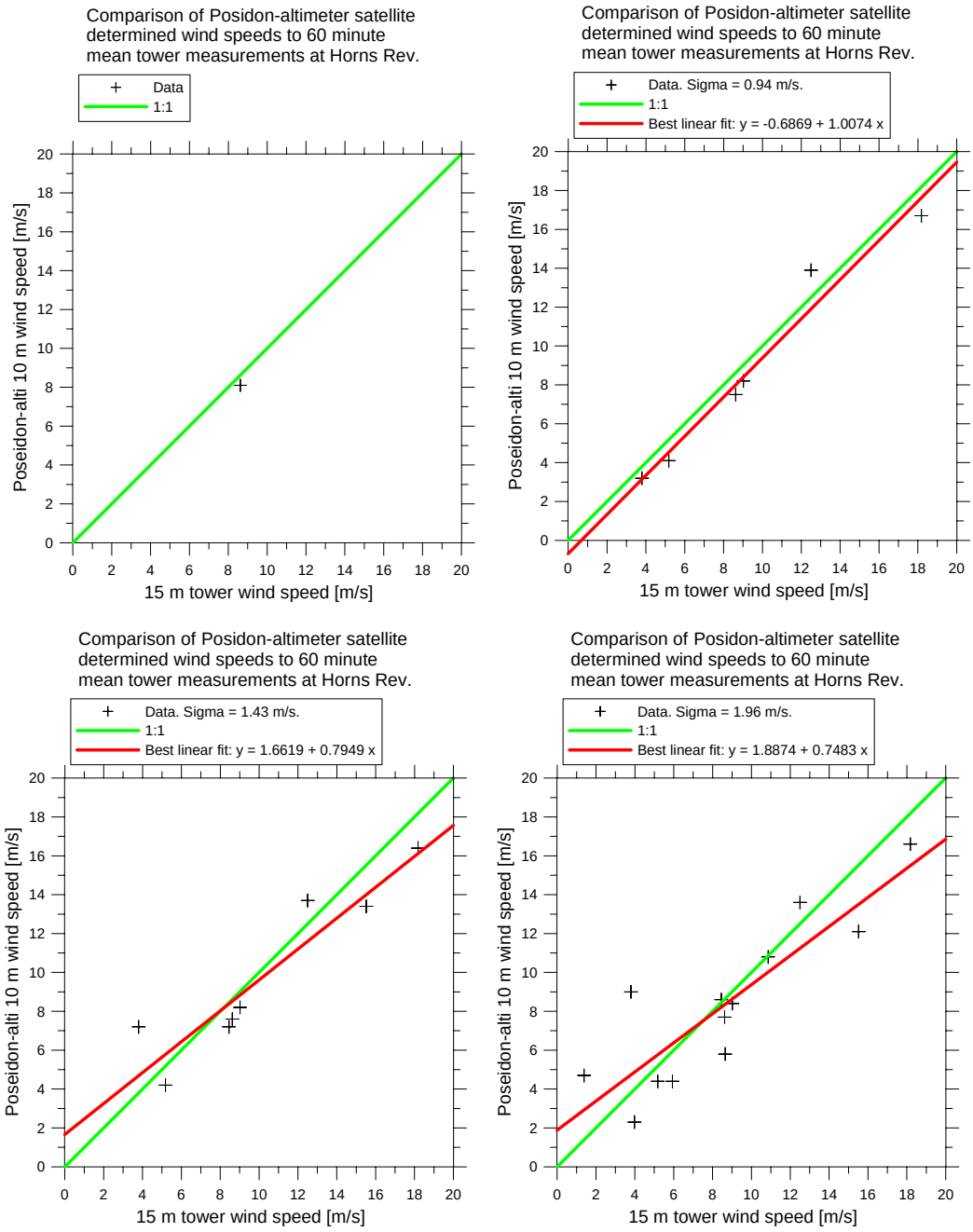

Figure 5.55 Comparison of wind speed near Horns Rev in Denmark (8.0 longitude, 55.4 latitude) from Poseidon altimeter from ARGOSS and hourly values from an offshore meteorological mast (DONG energy data). The circles used for collection of altimeter data was 0.25° (top left), 0.5° (top right), 1.0° (bottom left) and 5.0° (bottom right).

5.14 Results using several satellites

Wind maps from several satellite sensors have been inter-compared. In figure 5.34 wind speed data annual averages from SSM/I, QuikSCAT and AMSR-E were compared for a site in the North Sea (above) and the Baltic Sea (below) from (Hasager et al. 2006a). The results were not very convincing. It was noted that the AMSR-E wind data were of research quality. Since then a new version of AMSR-E wind maps (version 5 compared to the previous version 4) have become available. Also QuikSCAT have been released as ver. 4 (since 30.8.2006) and SSM/I (as ver. 6). The new wind map versions were used in the following analysis.

A study was made based on SSM/I, QuikSCAT, AMSR-E and WindSat. The three instruments have operated in parallel since 2003. The wind speed maps from years 2003, 2004 and 2005 were compared as monthly means for a site in the North Sea and a site in the Baltic Sea in figure 5.56. It was comforting to notice that only WindSat winds deviate strongly from the other three. WindSat is a research version, and future update may be expected. It was clear that all sensors capture the relative differences between the months. At the same time, it was clear that WindSat showed too high winds at both sites but in particular in the Baltic Sea.

A comparison analysis of wind speed observed from altimeter provided by ARGOSS (H. Wensink, personal communication), QuikSCAT, NCAR/NCEP re-analysis data and offshore meteorological observations at Horns Rev (from DONG energy) from different time periods was made. The result is shown in figure 5.57. Table 5.3 lists the data. In making these comparisons it is important to note that NCEP-NCAR assimilate some QuikSCAT data over the oceans so the data sets (NCEP-NCAR versus QuikSCAT) are not entirely independent.

Table 5.3 Details of data sources

Type	Area	Central location	Height (m)	Data period
Cup anemometer	Mast	55.52°N, 7.78°E	62 15	June 1999- December 2003 April 1999 to November 2002
QuikSCAT	0.5° by 0.5°	55.5°N, 7.5°E	10	August 1999 – December 2003
NCEP-NCAR model results	1.875°by 1.875°	56.19°N, 7.5°E	10	June 1999- December 2003
Altimeter (Topex, Poseidon GFO-1, Jason-1)	100 km by 100 km	55.52° N, 7.78° E	10	1991- 2003

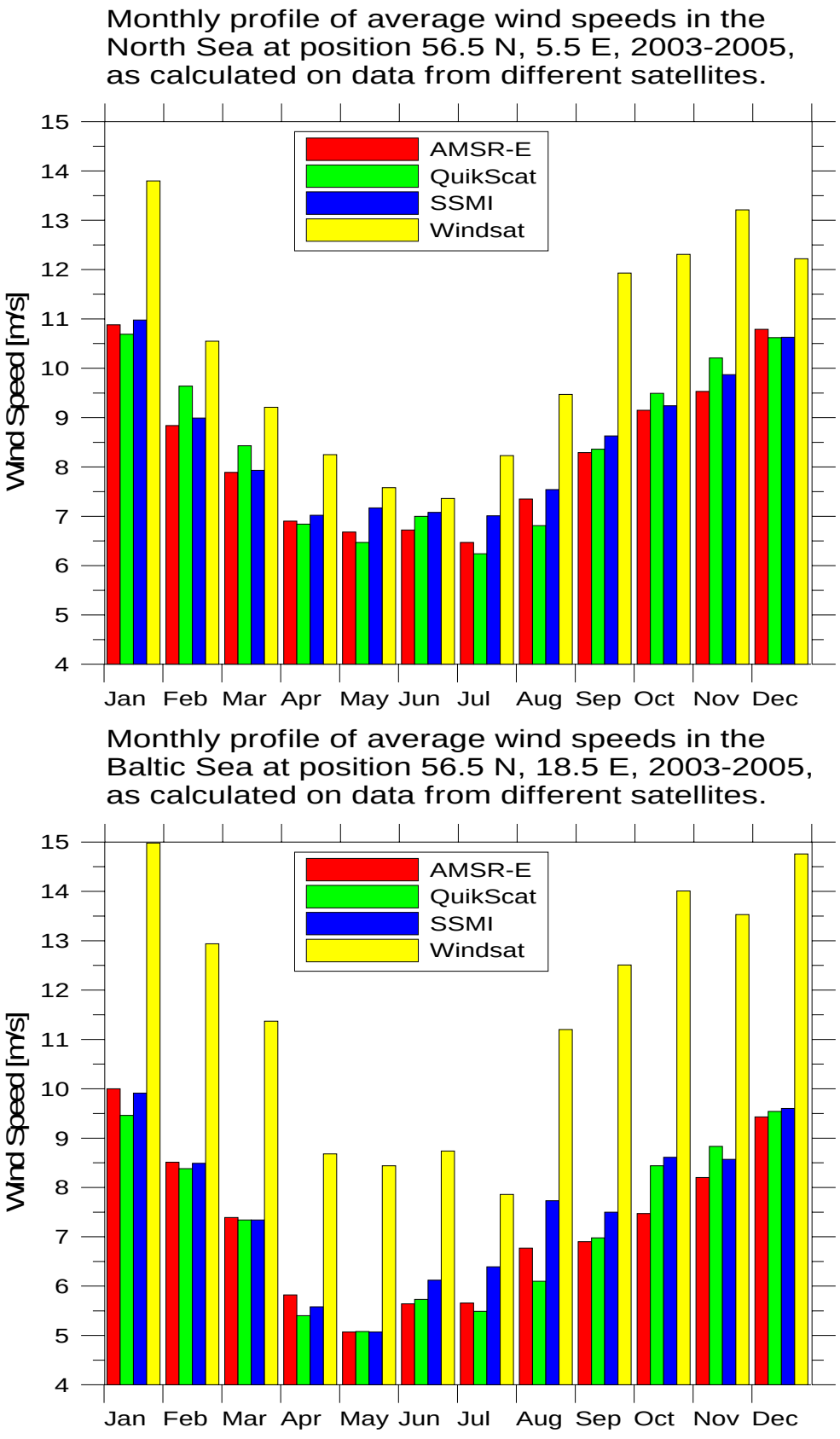

Figure 5.56. Monthly mean wind speed from SSM/I, QuikSCAT, AMSR-E and WindSat from 3 years, 2003-2005 from a site in the North Sea (top) and the Baltic Sea (bottom panel).

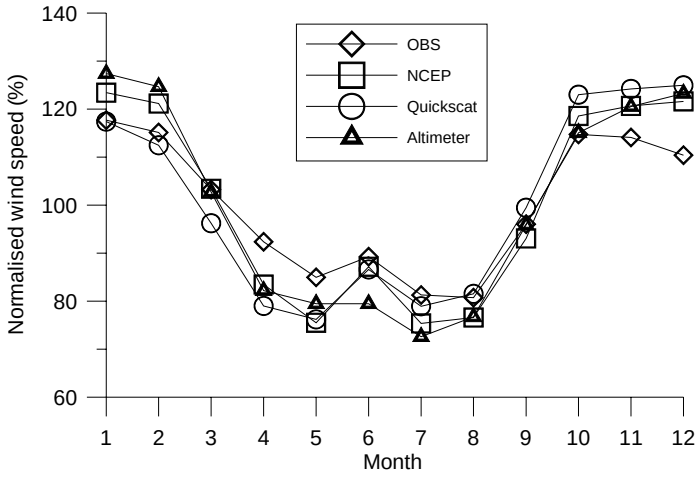

Figure 5.57 Normalized mean monthly wind speeds from mast observations (OBS), NCEP-NCAR model results,, QuikSCAT and altimeter data (%). In this graph each data set was normalized to the mean wind speed from that data and expressed as a percentage of the mean.

As shown in figure 5.57 there was good agreement between the data sets in terms of the seasonal variability. However, the mast data showed rather less month-to-month variability than the other data sets. While the absolute range between the maximum and minimum normalized monthly averages from the observed data was 37%, it was 48% for both NCEP-NCAR and QuikSCAT and 55% for the altimeter data. The altimeter data included observations from 343 Topex/Poseidon passes and 1516 Jason-1 passes. NCAR/NCEP model results were from 4 times per day and from QuikSCAT winds were observed twice daily.

5.15 Summary on satellite results

Wind mapping from satellites were compared in various ways. For some sensors it was possible to make comparison to meteorological observations in the North Sea near Horns Rev in Denmark and Östergarnsholm near Gotland in Sweden. The meteorological observations were kindly provided by DONG energy and Uppsala University, respectively.

The individual wind map comparisons with meteorological observations typically were compared to one-hour average winds. The satellite wind data were extracted from the closest available grid point of 0.25° (QuikSCAT), from various areas varying from 0.25° to 5.0° (ERS-2 SCAT, ERS altimeter, Topex and Poseidon altimeter). For ERS-2 and Envisat ASAR values from the footprint areas were always used in the comparison analysis. The linear regressions are summarized in table 5.3.

At Horns Rev in the North Sea the results from QuikSCAT and ERS SAR were observed around 30 km from the offshore meteorological mast (for 0.25° grid cells). The mast was located around 14 km offshore. As winds were observed further offshore than the offshore mast, a negative bias was expected. For ERS and altimeter with larger grid cells, up to 5.0° the effective area would be located even further offshore.

For Östergarnsholm QuikSCAT winds were observed only 20 km away from the mast. The mast was located on the coast, not offshore.

SAR winds were observed directly upwind of the offshore mast (with a footprint) and this is likely to explain the good general fit on wind speed. Wind direction from SAR has been discussed in various studies, see (Christiansen *et al.* 2006b) for a review.

*Table 5.4 Linear regression results between mast observations and satellite wind data. *For SAR (Christiansen et al. 2006b) have presented a detailed analysis, so the numbers are just indicative.*

Wind speed	**Site**	**Bias (ms^{-1})**	**Slope (ms^{-1})**	**Rms. (ms^{-1})**
QuikSCAT	Horns Rev	0.29	0.96	1.31
QuikSCAT	Östergarnsholm	0.09	1.10	1.76
ERS Scat	Horns Rev	0.84	1.16	1.64
SAR ERS and Envisat	Horns Rev	-0.27*	1.00*	1.11*
Altimeter ERS	Horns Rev	-0.30	0.96	1.23
Altimeter Topex	Horns Rev	0.51	0.86	1.41
Altimeter Poseidon	Horns Rev	-0.96	1.01	0.94
Wind direction	**Site**	**Bias (°)**	**Slope (°)**	**Rms. (°)**
QuikSCAT	Horns Rev	3.00	1.00	14.7
QuikSCAT	Östergarnsholm	-6.8	1.05	21.4
ERS Scat	Horns Rev	-7.3	1.01	31.2
SAR ERS and Envisat	Horns Rev	8.00*	1.00*	21.0*

Wind mapping during time was possible from several satellites. The more frequent the observation rate, the more reliable (in general) was the monthly averaged values expected to be. The results of monthly comparison between SSM/I, QuikSCAT and AMSR-E from a site in the North Sea and the Baltic Sea were good (for the newest versions of wind data, March 2007). There was found very similar behaviour between months and sites during the three years. For WindSat the data quality was not yet adequate. A new version of data is expected.

Similarly the comparison result of monthly wind speed variations between QuikSCAT and altimeter winds were good despite the different years of the data sets.

SSM/I wind maps constitute a unique long-term time-series on offshore winds. Further analysis is presented in chapter 7.

SAR comparison between months would not make sense due to the low sampling rate. The results from SAR are presented as averages for specific data sets, and the low number of samples should always be kept in mind. It is surprising how well the SAR-based results compared to general knowledge on wind resource e.g. in the North Sea near Horns Rev.

However, satellite SAR has its greatest potential for spatial mapping of winds. Much spatial detail is identified in each SAR wind map. Also a series of overlapping wind maps can be used to estimate the offshore wind resource though with relatively low accuracy. The spatial maps were compared to QuikSCAT wind maps and mesoscale wind maps. The results are presented in chapter 6.

6 Mesoscale modeling and comparison

6.1 KAMM/WAsP method

The text from here: *(start) to ….* (finish) is a copy of work submitted to (Hasager *et al.* 2007).

*(start)

The atmospheric flow over coastal regions is complicated. This is because the coastal region represents a transition of two distinct surface types, land and sea. For homogeneous surface conditions there is a much better understanding of, for example, the wind velocity profiles within the boundary layer, compared to profiles for the coastal regions. The distinction between the two surface types in the coastal region may be described using at least three different properties, namely surface aerodynamic roughness length, surface temperature, and surface elevation.

The surface aerodynamic roughness length describes a property that determines how, according to the logarithmic wind profile, the wind speed increases with increasing height above the surface. However the logarithmic wind profile is only a good approximation for homogeneous roughness and neutral conditions. For a hypothetical simple coastal zone where the only distinction between land and sea is the surface aerodynamic roughness length (i.e. flat, level, land at same temperature and approximate height temperature as sea), there will be a region where the wind profile will be transition, where the upwind there is a combination of land and sea roughness lengths. This transition behaviour is described by roughness induced internal boundary layer development, e.g. (Sempreviva *et al.* 1990).

Now imagine a slightly more complicated coastal zone where land and sea have different temperature, as well as different roughness. This new complication introduces a change in the surface heat flux into the atmosphere when air flows from land to sea or vice versa. The impact of the surface heat flux on surface profiles for homogeneous conditions is described by Monin-Obukhov similarity theory (Dyer 1974), however for heterogeneous conditions the transition of the wind profile is less well understood. (Owinoh *et al.* 2005) describe the investigations of the response of wind profile to abrupt changes in surface heat fluxes using analytical, numerical simulation and tank experiments in the laboratory.

The next complication to introduce to the hypothetical coastal zone is heterogeneous surface elevation (orography) of the land surface. Orography has a large impact on the surface winds, not just at the location of the orographic feature itself (for instance, strong winds at a hill top) but also some distance from the feature. This is strongly related to the stability of the atmosphere. For more stably stratified conditions, flow tends to be steered more laterally around orography obstacles such as hills and mountains. The range at which the flow can be modified by orography can be in the order of hundreds of kilometers (see figure 8). Therefore onshore orography can impact offshore wind properties. High orography along the coast can lead to flow damming, or the creation of barrier jets enhancing flow parallel to the coast. Where islands with high orography are present, the deflection of flow around the island can increase winds on the flanks of the island, including offshore areas, similarly, flow can be enhanced in the gaps between

islands. For examples of these phenomena as seen from SAR satellite imagery, see (Beal *et al.* 2004).

There are further distinctions that can be made between land and sea surfaces in a coastal region that were not covered here, such as moisture fluxes. However, considering just dry processes between surface and atmosphere alone has created challenging problems to be addressed.

Mesoscale models can be used to model the wind flow in coastal regions and are able, to some extent, model the influence of the heterogeneous surface aerodynamic roughness, surface heat fluxes, and orography. (Smedman *et al.* 1996) discuss the phenomena of low level jets in relation to siting of offshore wind energy in the Baltic Sea, and (Bergström 2002) has used mesoscale modelling to calculate wind climates in the same region. As an example of an offshore mesoscale study a summary of an mesoscale investigation for the Nysted Wind Farm in Denmark is given. More details of the study can be found in (Badger *et al.* 2006). The motivation was to determine the variation of wind conditions over the extent of the offshore wind farm. The wind farm is large and there for horizontal gradient of wind speed found in coastal zones can have a big impact.

The mesoscale model used was Karlsruhe Atmospheric Mesoscale Model (KAMM), (Adrian & Fiedler 1991). The model has been used extensively in wind energy applications, mostly in the calculation of numerical wind atlases in the KAMM/WAsP methodology, (Frank & Landberg 1997; Mortensen *et al.* 2005).

In this study KAMM was run with a uniform 2 km horizontal resolution in a domain of 200 x 200 km. In the vertical 25 model levels using a terrain following coordinate were used from the surface to 5500 m. The spacing between vertical levels is not uniform; levels close to the surface have the smallest interval.

The mesoscale requires a description of the surface elevation (orography), surface aerodynamic roughness, and profiles of geostrophic wind speed, direction, and potential temperature. The orography for computational domain was derived from the Shuttle Radar Topography Mission (SRTM), dataset available for download at 30 arc second resolution. A similar gridded dataset is created for the surface roughness in the computation domain, derived from the Global Land Cover Classification (GLCC) dataset from the United States Geological Survey.

The atmospheric profiles were based on the means derived from NCEP/NCAR reanalysis temperature and geo-potential height gradient data determined for years 1965 to 1998 for the heights 0 m, 1500 m, 3000 m and 5500 m above sea level. Based on the mean wind speeds at these heights, in this idealized study a set of 12 wind directions was used from 0^o to 330^o with a constant 30^o interval, with no variation of direction with height.

In KAMM the land and sea surface temperatures can be set by a constant offset relative to the lowest model level air temperature at initialization. In the first set of integrations, set A, the offset temperature is set to 0K for both land and sea surfaces. That is to say that the surface temperature is set to the lowest model level air temperature at initialization everywhere in the domain. The surface temperatures do not change during the model integration.

In the second set of integrations, set B, the surface temperature offset relative to the lowest model level air temperature is +5K for sea surfaces and –5K for land surfaces. That is to say the sea surface is warm and the land surface is cold. In the third set of

integrations, set C, the surface temperature offset is –5K for sea surfaces and +5K for land surfaces, meaning a cold sea surface and a warm land surface.

Figure 6.1 shows ones the modeled winds at 70 m above surface level for the 150 degree wind forcing in case C (the cool sea, warm land configuration), next to a SAR image derived winds for a similar large-scale forcing situation. A similar spatial variation of the wind speed is seen in the modeled winds and those derived from the SAR image. Especially in the streaky form of the higher wind regions formed in the gaps between islands.

Figure 6.2 shows the winds at 70 m above surface level for the three surface configurations using the 60 degree wind forcing. It is from this direction that there is a large range of wind speeds experienced over the wind farm extent (shown in the figure by the red box and blue corner markers). It can also be seen that the wind field at 70 m above surface level is sensitive to the different surface temperature configurations. For the warm sea cases there is a tendency for the winds blowing offshore to increase speed over a shorter distance, and then remain rather uniform. For the cool sea cases there is a tendency for the wind blowing offshore to increase speed over a longer distance and to create more elongated narrow jet features, with higher wind.

This mesoscale study demonstrates the complexity of offshore winds, and there sensitivity of the winds to the surface heat flux conditions that influence the stability of the boundary layer. The consequences of this complexity and sensitivity can have been impacts on the wind characteristics over the extent of wind farm site. Mesoscale modeling provides a valuable tool for investigating the flow behaviour in coastal regions.

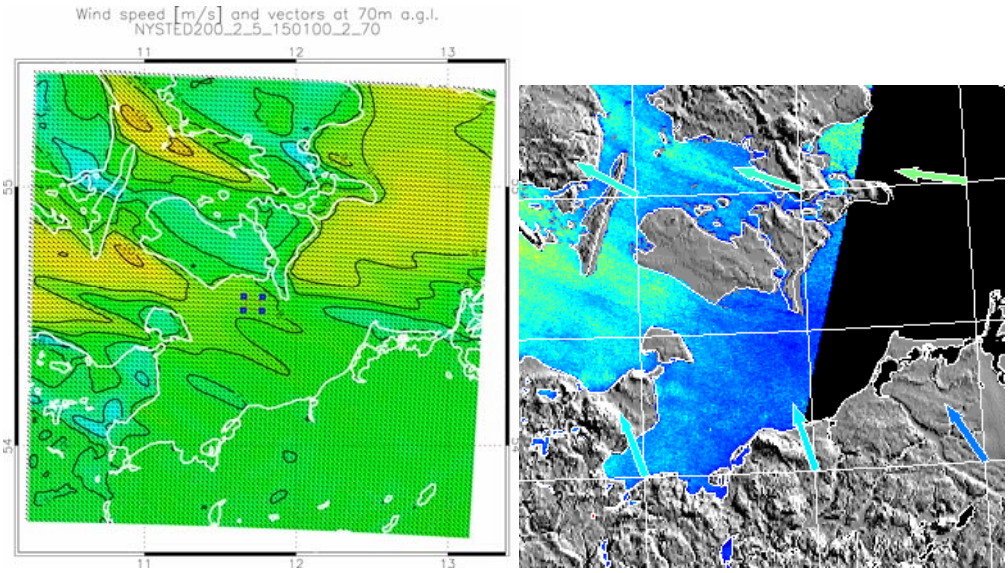

Figure 6.1 Comparison of mesoscale model winds at 70 m above surface level using a large-scale wind forcing from 150 degree (left) and wind derived from a SAR image during similar large-scale wind conditions (right).

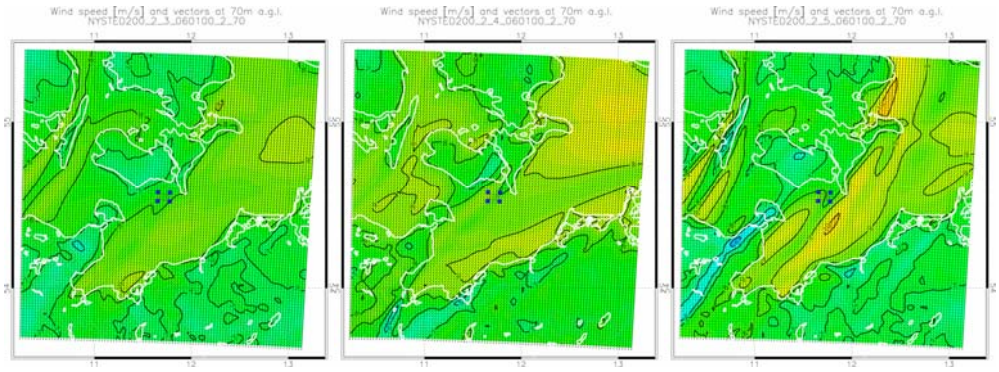

(a) (b) (c)

Figure 6.2 The winds at 70 m above surface level for a large-scale forcing from 60 degrees, using three different surface temperature configurations (see main text); (a) configuration A: land and sea same temperature, (b) configuration :, warm sea, cool land, (c) configuration :, cool sea, warm land.

*(finish).

6.1.1 Results – wind climate in Denmark

The KAMM/WAsP method was applied for Denmark (Frank *et al.* 2001). Results from this work are presented. The mean wind at 100 m above ground is presented in figure 6.3. For comparison figure 5.10 is re-printed as figure 6.4. QuikSCAT maps 10m winds whereas the KAMM/WAsP map is for 100m winds. Therefore it was expected that QuikSCAT show lower winds. This was true.

Part of the Danish Seas was mapped from 57 overlapping Envisat ASAR WSM wind maps, and this result is presented in figure 6.5. Envisat maps winds 10m above sea level. As expected Envisat also show lower mean wind speeds than the KAMM/WAsP. The level of mean wind speed from QuikSCAT and Envisat are of the same order but because QuikSCAT was based on more than 5000 observations it is assumed statistically more reliable.

Most striking though is the many fine details revealed by Envisat, e.g. the lee effect of the island Anholt in the Kattegat Sea. A high-wind area in the Baltic Sea is seen south of the island Langeland and Lolland from both Envisat and KAMM/WAsP. Unfortunately QuikSCAT did not map this area.

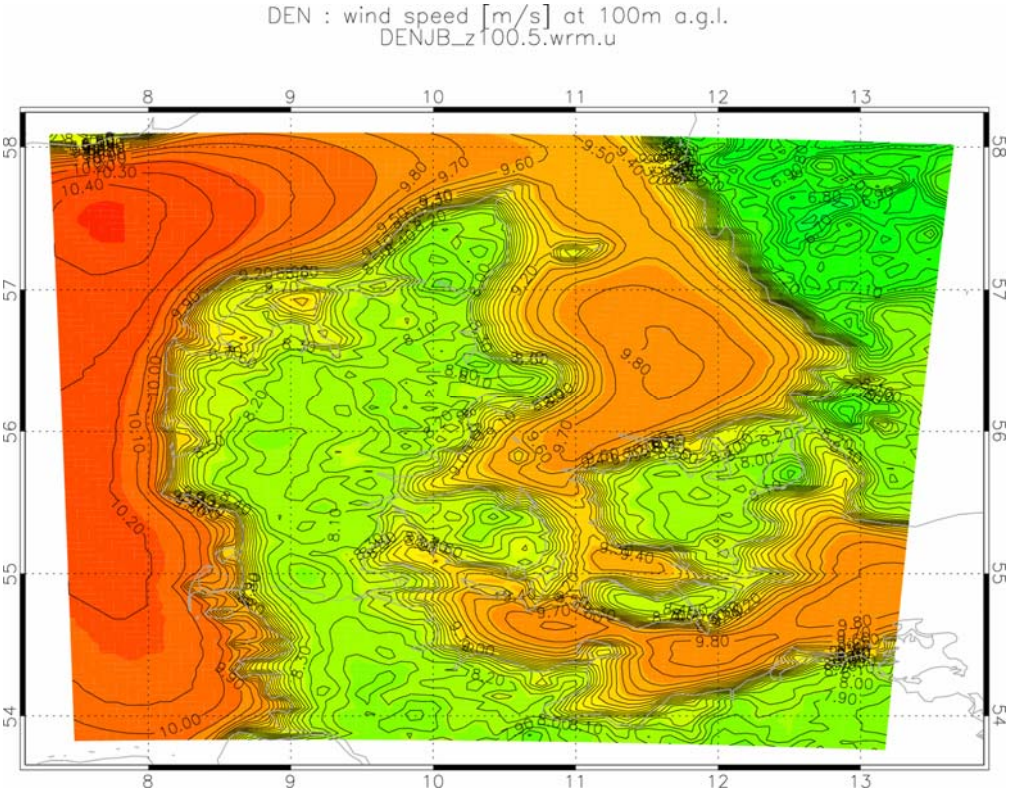

Figure 6.3 The calculated annual mean wind speed [m/s] at 100m for Denmark using the KAMM/WAsP method developed at Risø National Laboratory. The mesoscale modeling study was validated against land measurements (Frank et al. 2001)

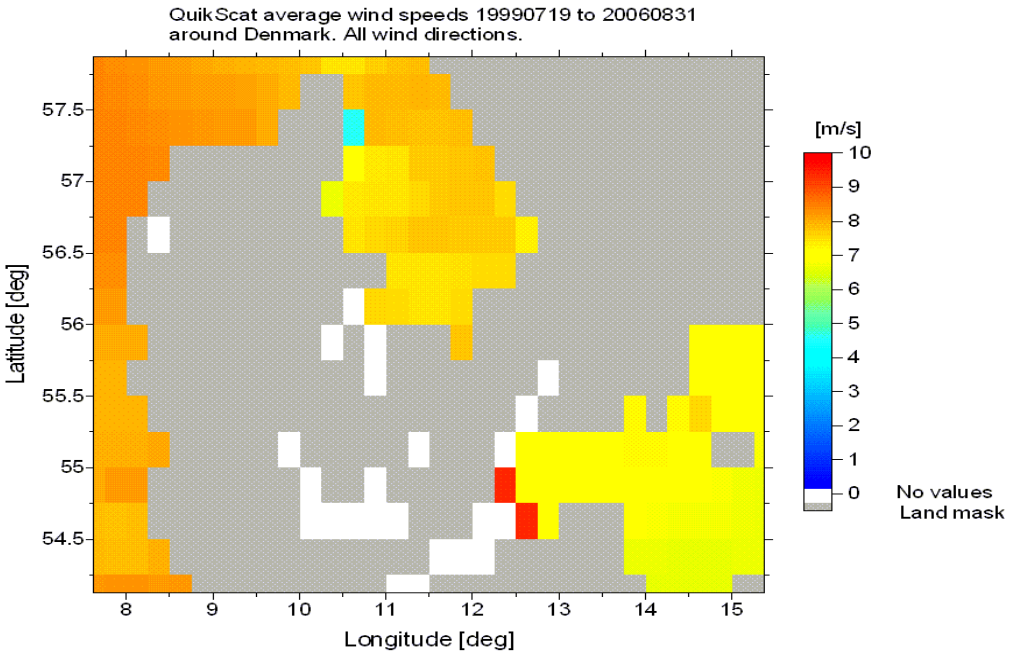

Figure 6.4 Wind speed map for Denmark observed from QuikSCAT during 7 years twice daily for 10 m above sea level. The pale blue and two red grid cells are unrealistic outliers.

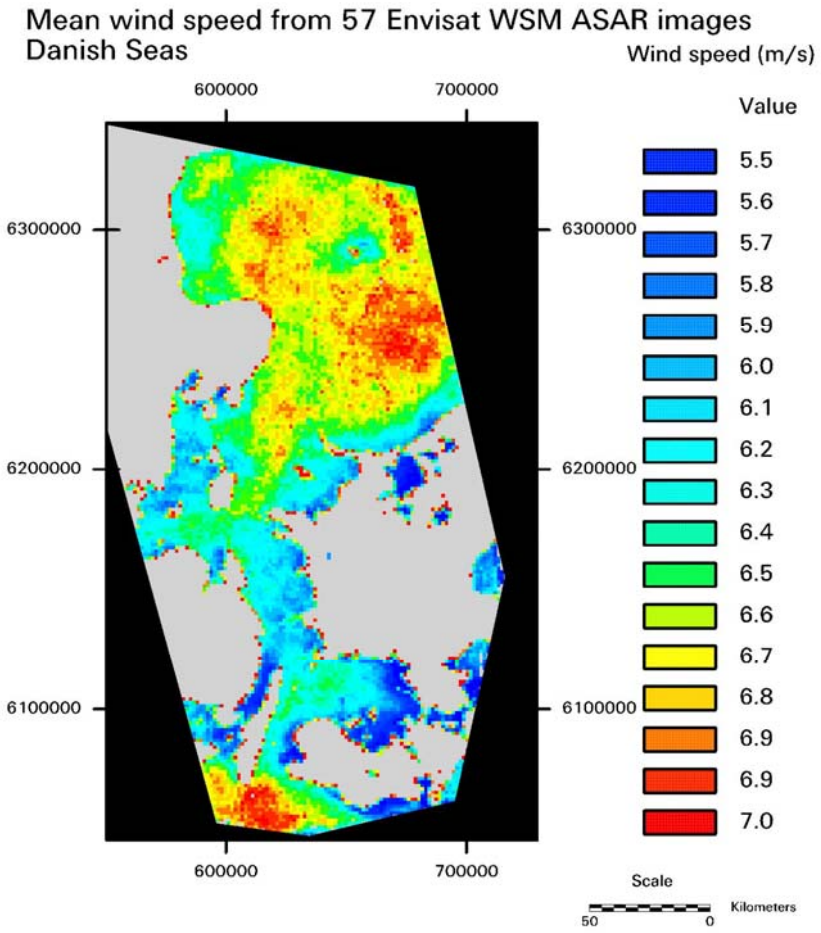

Figure 6.5 Wind speed map for part of Denmark observed from57 Envisat ASAR wide-swath-mode wind maps at 10 m above sea level. Along the coastline there are several red grid cells as unrealistic outliers.

The color scale in figure 6.5 is chosen to demonstrate the variations in mean wind speed in the inner Danish Seas observed from 57 overlapping wind maps from Envisat ASAR. Figure 6.6 is showing the mean wind speed variations for a larger region including part of the North Sea with significantly higher winds. This means that the spatial variations in mean wind speed in e.g. the Kattegat Sea are less clearly visualized in figure 6.6 than in figure 6.5. The wind maps in figure 6.6 are not overlapping. This makes the relative spatial comparison more uncertain but the number of samples is above 100 in all grid cells. The wind rose shows that all wind directions are represented in the data set.

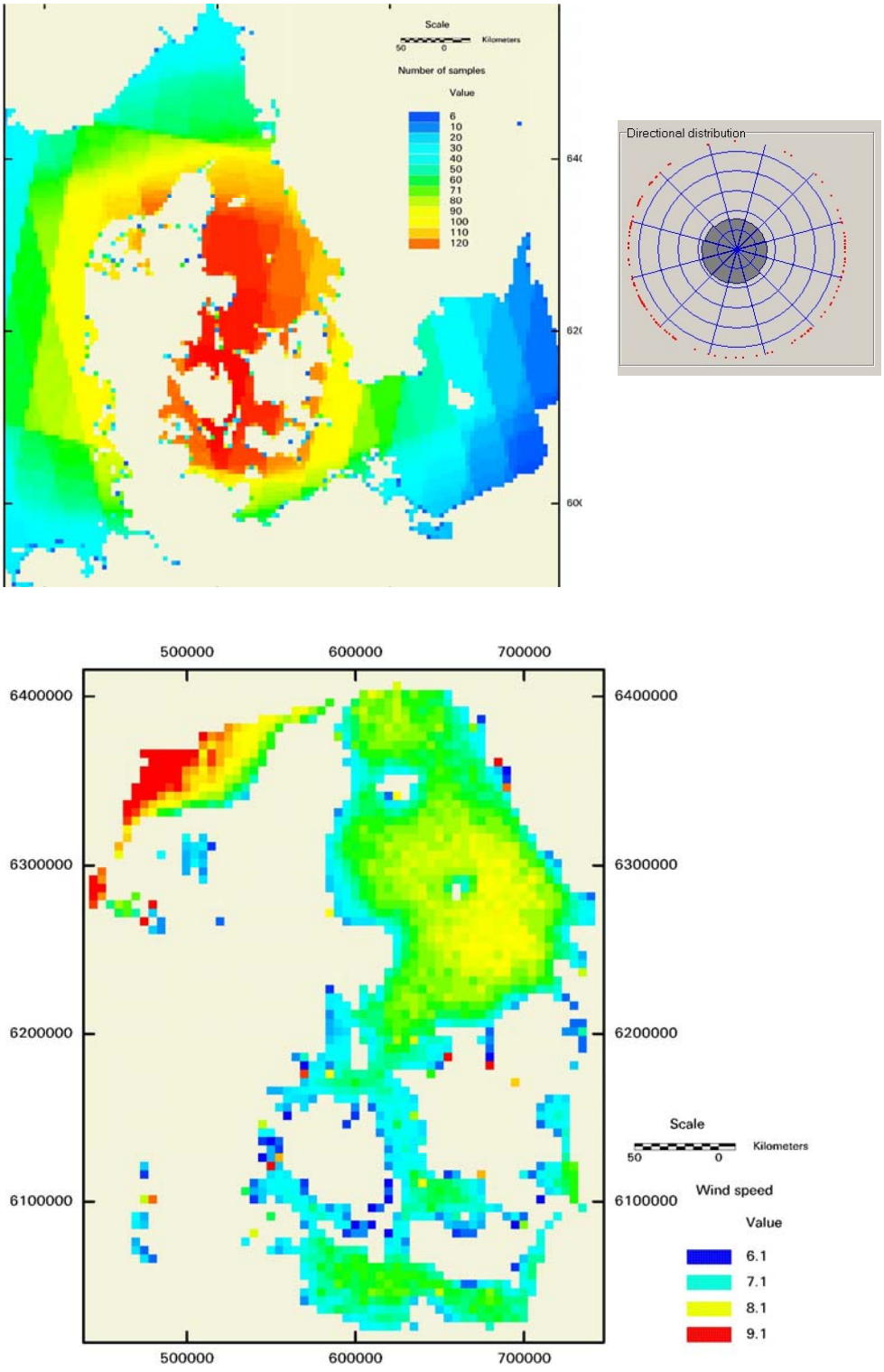

Figure 6.6 Denmark observed from Envisat ASAR above) number of samples; below) mean wind speed map for part of Denmark observed from more than 100 Envisat ASAR wide-swath-mode wind maps at 10 m above sea level. Along the coastline there are a few red grid cells as unrealistic outliers. The wind-rose shows the directions and wind speed. Each red dot corresponds to one wind map.

The spatial variations in mean wind speed observed in both QuikSCAT and Envisat may indicate a more complicated offshore wind resource than given by the KAMM/WAsP map. Even minor differences in the spatial domain have a large effect for the predicted offshore wind resource. The KAMM/WAsP method for wind power density at 100 m above ground is presented in figure 6.7 (Frank *et al.* 2001). In order to produce a wind resource estimate at 100 m from QuikSCAT and Envisat it would be necessary to extrapolate the winds to 100 m and use the third power on wind speed.

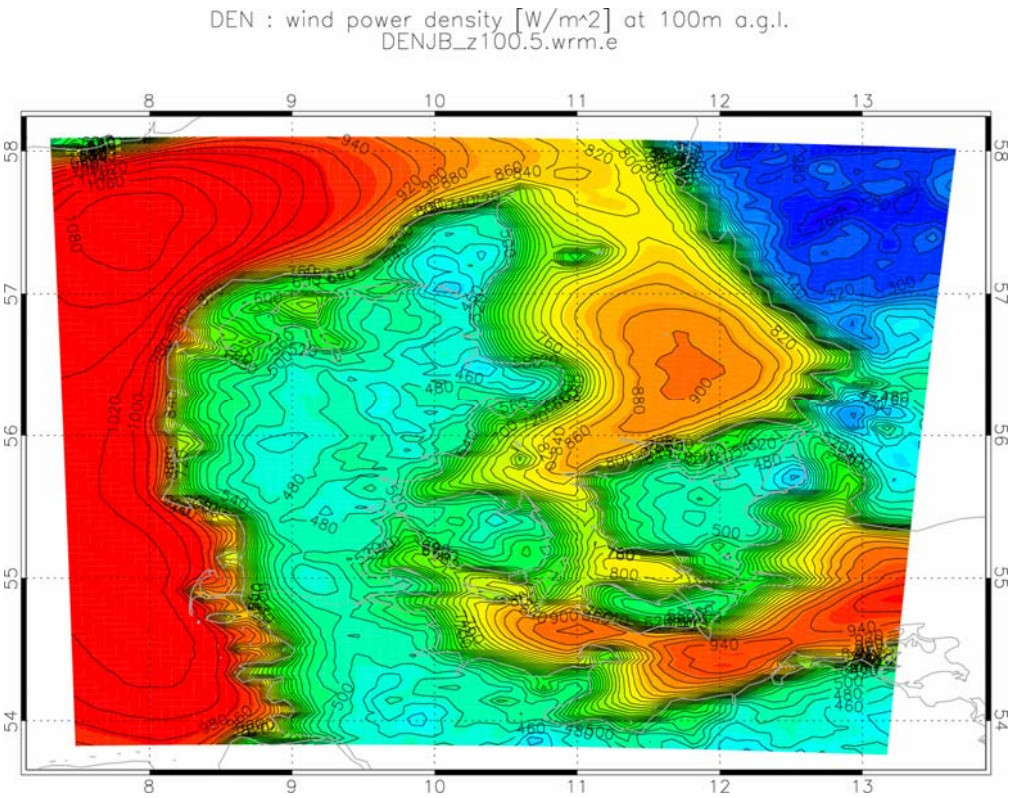

Figure 6.7 The calculated annual mean wind power density [W/m^2] at 100m for Denmark using the KAMM/WAsP method developed at Risø National Laboratory. The mesoscale modelling study was validated against land measurements (Frank et al. 2001).

6.2 MIUU model

The use of meso-scale models for wind resource assessments has increased during recent years. Especially in complex terrain the need for better models than has earlier been used is often obvious. Also offshore observations over the Baltic Sea show complexity and inhomogeneity of the wind field to a much larger extent than is often expected regarding offshore winds. Results with a higher-order closure meso-scale model, (the MIUU-model developed at the Department of Meteorology, Uppsala University), show that with this type of model the complex and inhomogeneous wind fields also turn up in the model results.

A higher-order closure model is, however, computer-time consuming to run. A method to simulate the climatological wind field using the MIUU model has been developed at Uppsala University, reducing the total number of simulations needed, (Bergström 2002; Bergström 1996; Sandström 1997). With this method a limited number of climatologically relevant simulations are performed, and a weighting based on climatological data for the horizontal pressure gradient (geostrophic wind) is made in order to finally estimate the wind resource. The method is applicable for mapping the wind potential with a resolution of 0.5-10 km. To use this method geostrophic wind (strength and direction), sea and land temperatures, topography, roughness, and land-use are needed. Comparisons between model results and measurements show good agreement.

6.2.1 The MIUU meso-scale model

The MIUU-model is a 3-dimensional numerical, hydrostatic, higher-order closure meso-scale model (Enger 1990). The model has prognostic equations for wind, temperature, humidity and turbulent kinetic energy. The MIUU-model has a terrain-influenced coordinate system, roughly following the terrain close to the surface and gradually transforming to horizontal at model top. To reduce influences from the boundaries, the modelled area is chosen to be much larger than the area of interest. This also makes it possible to account for effects of, for instance, mountains and water areas that are outside the investigated area, but which may anyhow be of importance to the wind field within the area of interest. To limit the number of horizontal grid points, a telescopic grid is often used, with the highest resolution only in the area of interest. In the vertical, the lower levels are log spaced while the higher levels are linearly spaced. The lowest grid point is at height z_0 = the roughness length, and the model top is typically at 10000 m. Commonly 8 levels are used in the model up to 100 m height.

At the lower boundary, roughness length and terrain height have to be specified at each grid point. The roughness over land is divided into classes according to land use. Topography and land use are taken from digitised maps, with a resolution of 1 km or 30” (the U.S. Geological Survey, the University of Nebraska-Lincoln, and the European Commission's Joint Research Centre 1-km resolution global land cover characteristics database, 1999, version 2.0). For water, z_0 is either assumed constant, equal to 0.00025 m, or estimated from the Charnock relation. During winter, the roughness length is set to 0.001 m over open terrain to represent snow-covered land areas. Also temperature has to be given or estimated at the lower boundary for each grid point. The land surface temperature, and its daily and monthly variation, is estimated with a surface energy

balance routine using as input solar radiation and land use. Over sea the observed monthly average sea-surface temperatures have been used.

The MIUU model has been used earlier in many case studies in different types of landscapes, showing good agreement with observations. In (Källstrand *et al.* 2000)the Baltic Sea offshore wind field is investigated. Simulations with the MIUU model in mountainous terrain have been done, for example over areas of the mountain range in Northern Sweden (Bergström & Källstrand 2001; Bergström & Källstrand 2000), around Lake Mohave in the Colorado River Valley (Koracin & Enger 1994; Enger *et al.* 1993), and at the Adriatic coast (Enger & Grisogono 1998). In (Bergström 1996) and (Sandström 1997) the MIUU-model has been used to simulate the climatological wind field over the Baltic Sea.

6.2.2 Wind climate modelling

In an ideal climate study, the model runs should represent all weather conditions. But this would require an unrealistic large number of simulations. Since the MIUU-model is rather computer-time consuming to run, some compromises have to be made. The parameters of greatest importance to the flow have to be identified and varied in order to cover an as wide range of atmospheric conditions as needed in order to get an accurate description of the wind climatology. The parameters judged to be of most importance to the wind field are (based on comparisons between modelled and observed average winds): Geostrophic wind (strength and direction), thermal stratification (through the daily temperature variation), surface roughness, topography, and land-sea/lake temperature differences (Bergström 2002).

The horizontal air pressure gradient, i.e. the geostrophic wind, is the primary driving force of the wind. Using only the mean geostrophic wind speed in the simulations would reduce the effect of thermal stratification, because the daily stability variations are much larger with a low geostrophic wind speed compared to a high one. This effect is sometimes very large, and this is why it is important to include simulations with different geostrophic wind speeds. Therefore model runs with three values of the geostrophic wind speed (5, 10, and 15 m/s) for 8 wind directions have been used in earlier investigations of the wind climate made with the MIUU-model (Bergström, 1996, Sandström, 1997).

Here 4, 9, and 14 m/s were used instead, as this was judged to be somewhat more representative for the actual geostrophic wind distribution in the Scandinavian area, and also 16 wind directions were used instead of 8 in order to better resolve topographical and coast-line flow modifications.

The air temperature shows both clear annual and daily variations, which also must be included in the simulations. To limit the number of model runs, but still include the annual variations, 4 months (January, April, July and October) have in earlier investigations been selected to represent the four seasons, which is sufficiently accurate for the purpose of modelling the wind climate. A monthly average soil temperature has been used as input to the surface energy balance routine, which estimates the surface temperatures over land. To include the spatial differences, data from a number of weather stations have been used and the data have been interpolated within the model domain. The mean temperature is also allowed to vary with wind direction. Typically winds from the northern sector are colder than winds from the south in Northern Europe. Thus the mean temperature for different directions was also estimated. The daily variation of sea surface temperature is small compared with the variations of the air

temperature. Therefore, model runs were made with the seasonal mean sea surface temperature at each grid point, with no daily variation but including a spatial variation. Although it is important to keep the daily variation in air temperature, it is accurate enough to use the average sea surface temperature at the lower model boundary.

Summing up, for each season, runs were made with three values of the geostrophic wind speed, and with 16 wind direction sectors, summing up to 192 model runs to cover the most important parameters determining the boundary layer wind climate. Each simulation was made for a 30-hour time period, of which only the last 24 hours were used, allowing for 6 hours initialisation. The background flow for each model run is specified as a geostrophic wind constant in time but with a with variation with height (thermal wind) following climatological averaged estimated from radio-soundings in the area. Also the initial potential temperature and humidity profiles were taken from climatologically averaged radio-sonde data for the different seasons.

All simulations are finally weighted together using climatological statistics of the geostrophic wind. This gives the climatological averages for each month, grid point, and height. The annual mean wind speed may then be calculated by weighting the four individual months together. Thus, the result from a study of the climatological wind field may be presented as the mean wind speed (annual or seasonal), or wind energy potential, at different heights. The wind speed distribution and the corresponding Weibull parameters may also be determined. It should be pointed out that the MIUU model uses no local wind measurements as input, but it is of course important to validate the results against observations.

6.2.3 Model domain

When mapping the wind resources of a limited area, like Sweden, earlier investigations have shown the importance of including surrounding sea and mountain areas in order to get accurate results, see e.g. (Källstrand *et al.* 2000). Therefore it is not sufficient to just include Sweden in the modelled area. The Baltic Sea and the surrounding land areas must be included for example to adequately take into account the influence from marine low-level jets and thermally driven flows evolving due to temperature differences between land and sea Bergström (2002). Also the Scandinavian mountain range has a great impact in the wind pattern over Sweden, and must consequently be included into the model domain.

Due to this it was judged necessary to include the whole of Scandinavia, together with the Baltic Sea and the Bothnian Sea, including surrounding land areas, into the model domain, and to make a set of runs using 5 km horizontal resolution in order to make it possible to cover this large area. The model area covering Southern Scandinavia can be seen in Figure 6.8. Outside the 5 km grid spacing areas, shown in Figure 6.8 a region with gradually expanding grid distances was used to increase the modelled area even further but at the same time limiting the number of grid points. Typically this boundary region was chosen to be about 200-300 km wide.

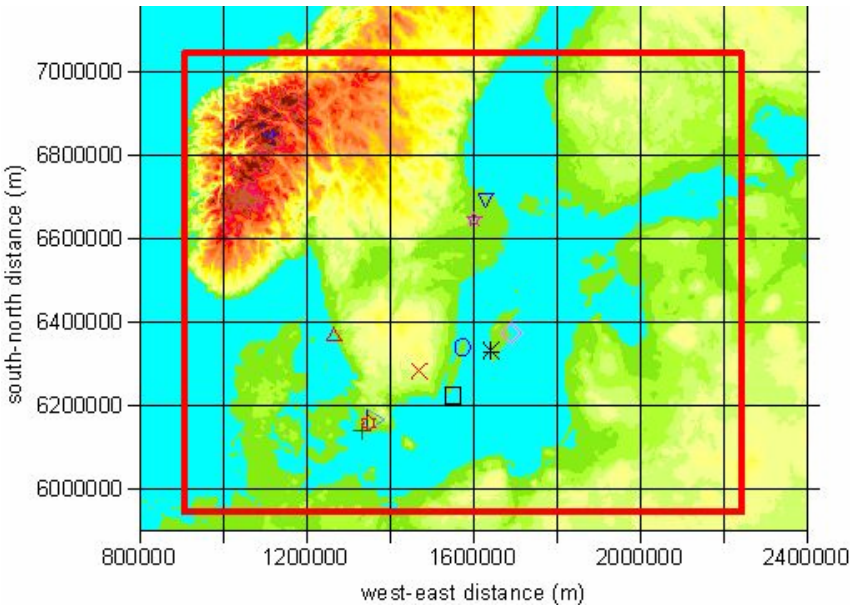

Figure 6.8 Map over Southern Scandinavia and the Baltic Sea area showing the 5 km model domain. Markers show locations of 12 observation sites used for model verification.

6.2.4 Geostrophic wind statistics

In order to be able to weight the results from the different model runs together into the final wind climate estimate, statistics of the horizontal air pressure gradient, i.e. the geostrophic wind, is needed. The geostrophic wind components are then given by

$$u_g = -\frac{1}{\rho f}\cdot\frac{\partial p}{\partial y}; \quad v_g = \frac{1}{\rho f}\cdot\frac{\partial p}{\partial x} \qquad (1)$$

where p is sea level pressure, ρ is air density, and f the Coriolis parameter.

To calculate the geostrophic wind from the air pressure data, simultaneous observations at three sites are needed. For Southern Scandinavia observations taken at Visby, Göteborg, and Lund have been used. Pressure data from the weather stations at these sites have been thoroughly checked and homogenized, see (Schmith *et al.* 1997). The location of these pressure observations sites are shown in Figure 6.9.

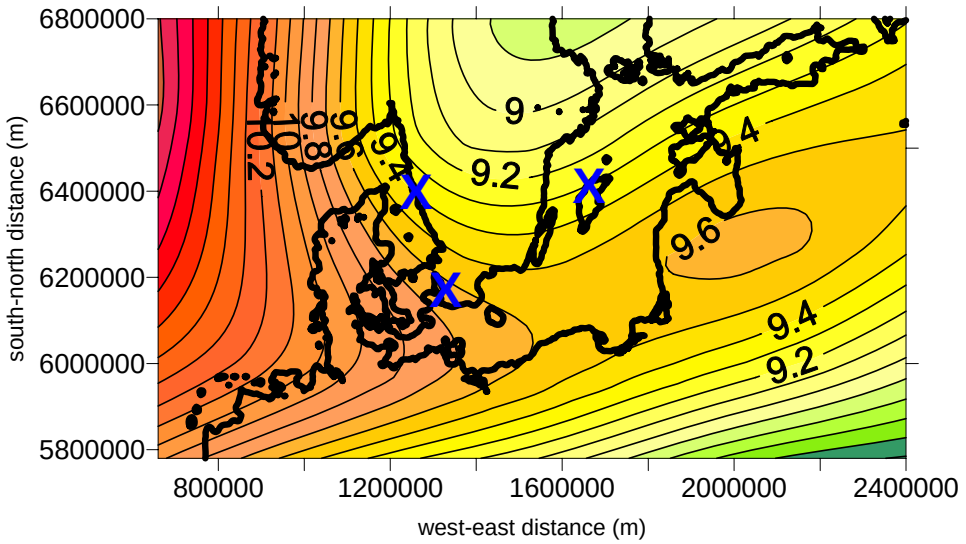

Figure 6.9 Annual average geostrophic wind speed over the Scandinavian area as estimated from NCEP/NCAR 850 hPa geo-potential height data four times per day 1948 to 2006. The crosses mark the location of the sites from which surface pressure data were used to estimate geostrophic winds (Visby, Göteborg and Lund).

The geostrophic winds vary, however, with geographical locations, and also with time, see (Johansson & Bergström 2004). Thus e.g. the annual average estimated from Bodö, Härnösand, and Haparanda is 8.7 m/s, while the annual average calculated from the pressure observations at Visby, Göteborg, and Lund is 9.7 m/s. This geographical variation should be taken into account when weighting together the model results. As the number of weather stations with reliable and homogenized surface pressure data is limited, and not evenly geographically distributed, the use of global atmospheric reanalysis data would be an interesting alternative. Two such datasets have been tested, the ERA40 reanalysis data from ECMWF using the European global circulation model, and the reanalysis data from NCEP/NCAR using the American global circulation model.

NCEP/NCAR data for the years 1948-2006 was used here having data four times per day with a longitudinal and latitudinal resolution of 2.5°. Coordinates approximately corresponding to the pressure observation sites were chosen from the reanalysis data sets, and the mean sea level pressure reanalysis data was used to determine the geostrophic wind every six hours. These results were then compared to the geostrophic winds estimated from surface pressure data. The two estimates compare well both for Southern and Northern Scandinavia. The averages agree to within 0.1 m/s from each other, although the individual observations are somewhat scattered. In (Johansson & Bergström 2004) it was shown that the distribution of the differences in geostrophic wind for the Southern Scandinavian sites as estimated using sea level pressure observations or NCEP/NCAR data to more than 70% agree within ±2 m/s and almost 90% differ by less than ±3 m/s. Also the distributions of geostrophic wind speed itself agree well comparing results using the two methods to calculate the geostrophic wind, as was also shown in Bergström (2004). We may thus conclude that geostrophic winds calculated from NCEP/NCAR data agree well with results using weather station data, both for the northern and for the southern area.

The variation in annual average geostrophic wind speed over Scandinavia and the Baltic Sea area as estimated using 850 hPa pressure heights from the NCEP/NCAR reanalysis data and the result is shown in Figure 6.9. The geostrophic wind was estimated using data from three points at a time, forming triangles from which the north-south and west-east gradients of the air pressure was determined, where after the geostrophic wind components were calculated using Eq. (3.2). These three points were separated by 2.5° in latitude and 5° in longitude.

The results show an area with higher values of the geostrophic wind speed over Southern Scandinavia and in over the southern parts of the Baltic Sea, where the averages reach 9.5 to 10 m/s. From this maximum the geostrophic wind decreases northwards to an area with a minimum below 9 m/s over Northern Scandinavia and the northern parts of the Bothnian Sea. Further to the west over the North Sea and the Atlantic Ocean the numbers increase to between 10.5 and 11 m/s. It is obvious that the Scandinavian mountain range has a great influence upon the geostrophic wind field on the average. The minimum over central and northern Scandinavia is located in lee of the mountains and in the north centred above the mountains. The general patterns in the average field are probably related to the typical cyclone paths in the area. We conclude that the agreement with the results from the NCEP/NCAR data and the two sets of geostrophic winds calculated from surface pressure observation data are good.

To estimate the wind climate from the MIUU-model runs detailed geostrophic wind speed statistics (dependent on month and wind direction) are needed. Instead of determining all these detailed statistics for each model grid points using NCEP/NCAR data, geostrophic winds from Visby-Göteborg-Lund were used for the Southern Scandinavia runs. Thus the first wind climate estimates from the climatological weighting of the MIUU-model results are arrived at assuming the same average geostrophic wind speed over either Southern Scandinavia.

As this is obviously not true (cf. figure 6.9), we need to account for the geographical variations after the first climatological weighting. This is done by making a second weighting. The resulting average winds are simply, at each grid point, multiplied with a factor estimated as the ratio between the average geostrophic wind at the individual grid points and the average geostrophic wind speed as given by the geostrophic wind data calculated using observations from Visby-Göteborg-Lund, as these latter were originally used to weight the model output together to get the wind climate.

6.2.5 Results - wind climate in Sweden

The model runs using 5 km horizontal grid spacing have been used to estimate the wind resources over the Southern Scandinavian sea areas. The resulting annual average wind speed is presented in Figure 6.10 for the height 100 m. It is important to remember, however, that the results are based on model estimates with a 5 km grid spacing in the horizontal, why smaller terrain features, which may well influence the wind climate, are absent in the results.

At 100 m height the model results show offshore average wind speed over the Baltic Sea which is 8.8-9.6 m/s. The highest values are found in the south-eastern part. Over Kattegatt and Skagerack, the sea areas between Denmark, Norway, and Sweden, the average wind are typically between 8.6 and 9.0 m/s, while the modelled average wind speed over the easternmost parts of the North Sea are the highest in the modelled area and reaches as most 10.5 m/s southwest of Norway.

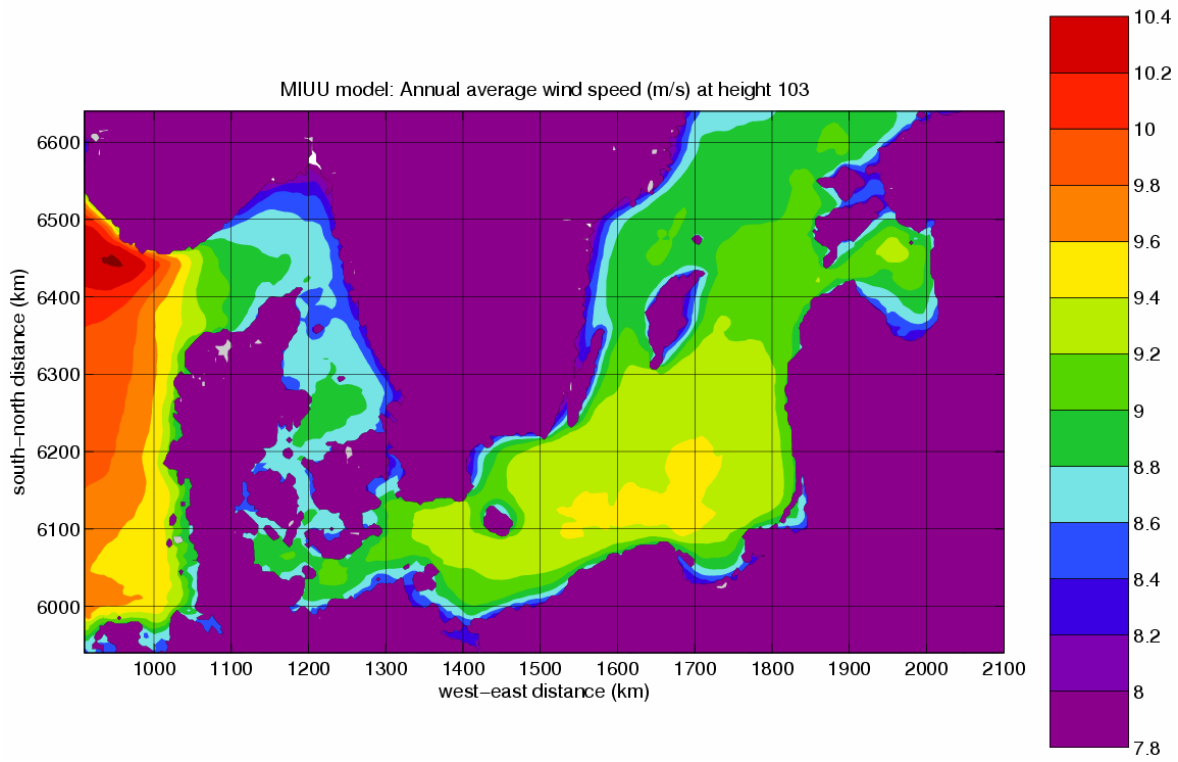

Figure 6.10 Annual average wind speed at 103 m height as estimated from MIUU-model results based on a 5 km grid resolution.

6.2.6 Model verifications

In earlier investigations, where the MIUU-model was used with a 9 km horizontal resolution over the Baltic Sea area, the results have shown good agreement with observations, cf. Bergström, 1996; Sandström, 1997; and Bergström, 2002. The new results with the 5 km resolution have also been verified against wind measurements, mostly in coastal areas. Altogether 12 sites have been used, and their locations are given in figure 6.8.

A comparison between modelled and observed annual average wind speed is shown in Figure 6.11. As can be seen the agreement is good, deviations being of the order a few tenths of m/s. The maximum differences found is 0.4-0.5 m/s at the site marked by blue circles. Comparing with figure 6.8, we see that this site is located on the northern part of the narrow island Öland, which is here only about 10 km wide. Remembering that the model resolution is 5 km in the horizontal, the wind modifications due to the narrow island will not be caught by the model in full. The same arguments may generally apply to all comparisons between modelled winds and observations whenever the observations may be influenced by local effects on a scale smaller than what is resolved by the model results.

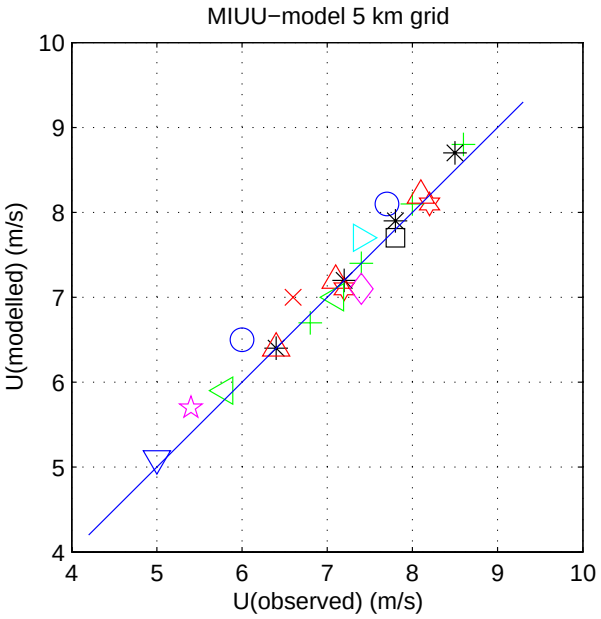

Figure 6.11 Annual average wind speed modeled with the MIUU-model on a 5 km horizontal resolution plotted against observations at the sites shown in Figure 6.8.

6.2.7 Results from QuikSCAT and SAR in Sweden

Maps of mean wind speed from QuikSCAT and Envisat ASAR were calculated for parts of the southern Baltic Sea. Figure 6.12 shows the mean wind speed from QuikSCAT during 8 years.

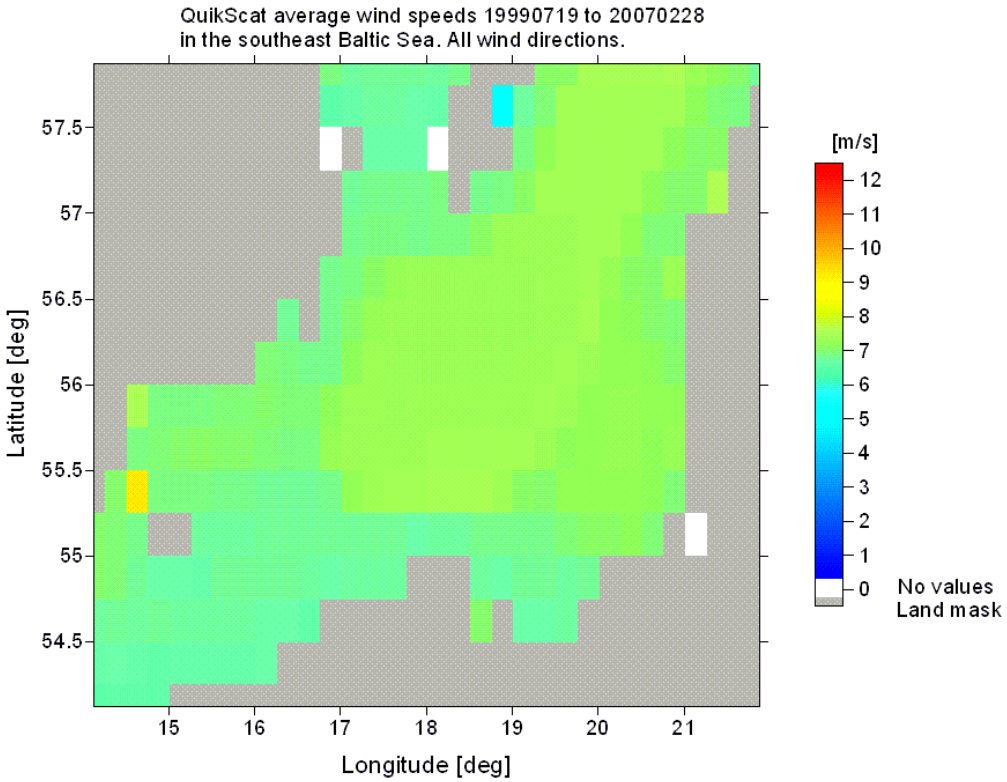

Figure 6.12 Mean wind speeds observed in the Baltic Sea from QuikSCAT during 8 years.

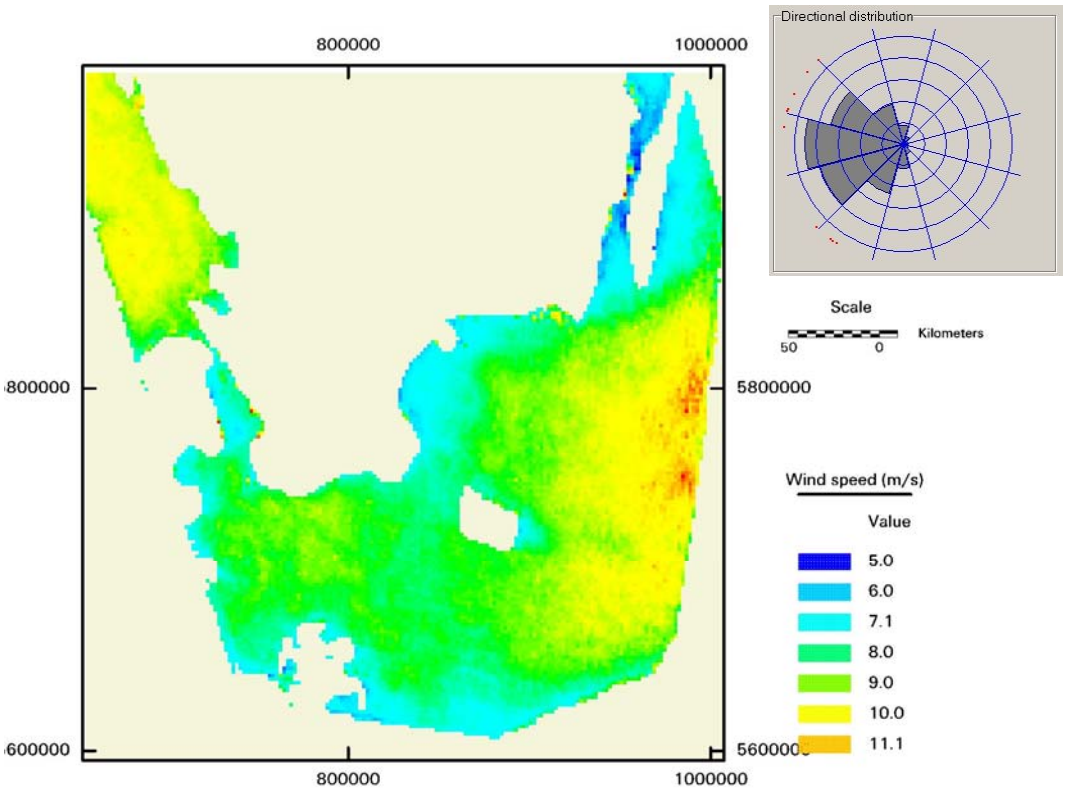

Figure 6.13 Mean wind speed from 10 overlapping Envisat ASAR wind maps of the southern Baltic Sea. The wind rose is from 55°N and 13°E near the island Bornholm.

The mean speed from 10 Envisat ASAR wind maps overlapping for the region of the Baltic Sea south of Sweden is shown in figure 6.13. It appears that only cases of winds from the west were included.

Wind speed maps from 94 Envisat ASAR WSM scenes were used to calculate mean wind speed in the south-east Baltic Sea. In figure 6.14 the result of mean wind speed for all grid cells with more than 50 samples is shown. The wind rose at latitude 55° and longitude 20° is shown. 83 samples were found at this location.

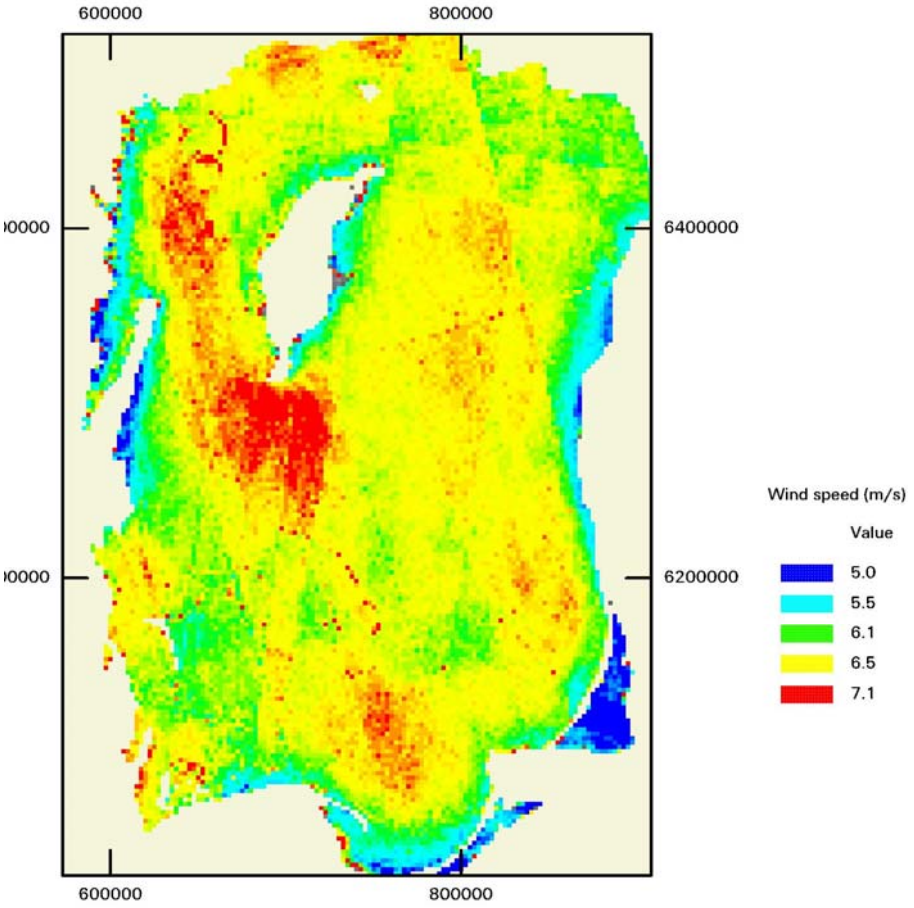

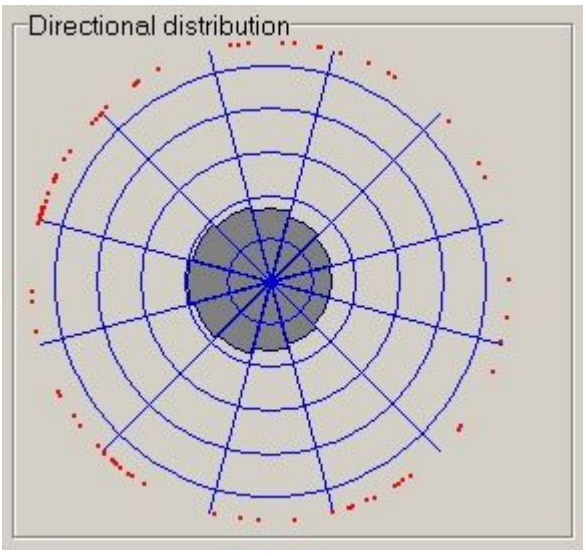

Figure 6.14 Mean wind speed map calculated from more than 50 Envisat ASAR scenes covering the south-eastern Baltic Sea. The wind rose is from 55°N and 20°E in the south east.

7 Wind-indexing

7.1 Introduction

The wind index was calculated at Energi- og Miljødata (EMD). Briefly described the monthly energy production from a number of wind turbine generators is compared to the same wind turbine generators' expected long-term average monthly production based on the longer production period.

$$Wind-index = \frac{Actual-monthly-production}{Long-term-monthly-production}$$

Reference http://www.vindstat.dk/PDF_sider/Windindex_DK_new_short.pdf.

The wind-index is used for giving information on the expected wind energy production in a given period compared to long-term estimates. This is important when planning new wind farms where local measurements typically only are available for a shorter period, as well as when checking the performance of existing wind farms.

As example the wind-index for January 2007 is shown in figure 7.1. It is seen in figure 7.1 that the wind power production was 124% larger than average for this month compared to long-term statistics. This is very high as can be identified from figure 7.2.

At the site http://www.vindstat.dk/PDF_sider/Vindindex_aktuel.pdf it is possible to view the wind-index during the latest 12 months per region, the annual yearly variations for 5 years and the mean, maximum and minimum for 10 years. The results are shown in figure 7.2.

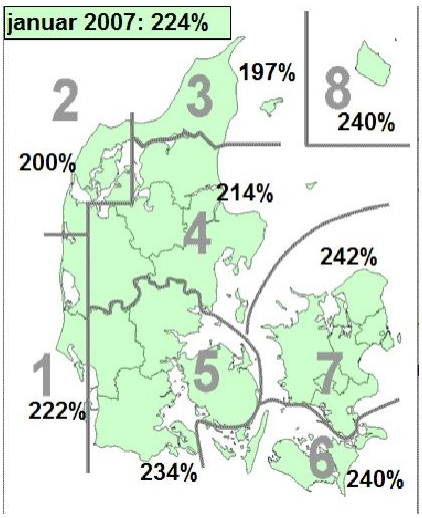

Figure 7.1 Wind-index for Denmark January 2007 from EMD http://www.vindstat.dk/

Vindens energiindhold lokalt seneste 12 måneder

Om-råde	Feb. 06	Mar. 06	Apr. 06	Maj. 06	Jun. 06	Jul. 06	Aug. 06	Sep. 06	Okt. 06	Nov. 06	Dec. 06	Jan. 07	Gns.
1	58	84	93	112	61	30	40	87	81	160	155	222	98,6
2	65	82	86	97	69	37	42	86	70	153	156	200	95,3
3	69	71	82	87	63	42	36	81	68	145	170	197	92,5
4	64	78	84	97	59	35	35	85	73	146	161	214	94,3
5	63	96	91	108	51	30	39	82	89	144	166	234	99,4
6	62	94	82	106	44	27	56	80	96	146	172	240	100,5
7	56	79	82	103	43	28	43	87	92	141	177	242	97,8
8	60	101	79	89	39	26	53	76	100	131	182	240	98,0
Gns.	62	86	85	100	54	32	43	83	84	146	168	224	97,1

Vindens energiindhold på landsplan

	Jan.	Feb.	Mar.	Apr.	Maj.	Jun.	Jul.	Aug.	Sep.	Okt.	Nov.	Dec.	Gns.
2002	146	178	139	66	76	102	68	50	54	106	79	102	97,2
2003	145	43	85	110	68	89	49	75	71	81	87	145	87,3
2004	93	94	118	80	98	100	64	63	113	116	106	130	97,9
2005	196	113	96	83	71	76	51	72	63	72	99	122	93,0
2006	82	62	86	85	100	54	32	43	83	84	146	168	85,2
2007	**224**												**223,5**

Månedsfordeling baseret på seneste 10 år

Gns.	137	132	111	90	80	81	58	62	82	110	103	121	97,4
Min.	78	43	85	61	68	54	32	24	54	72	66	88	85,2
Max.	224	224	142	145	100	102	110	101	118	186	146	168	115,1

Figure 7.2 Wind-index values per month per region for year 2006 and January 2007 (upper panel), wind-index values per month for Denmark for years 2002-2006 (middle panel), and monthly mean, minimum and maximum wind-index for Denmark during 10 years. From EMD http://www.vindstat.dk/PDF_sider/Vindindex_aktuel.pdf. The column to the far right (gns. is average).

One of the challenges in wind-indexing is to identify accurate and reliable long-term wind data series for the analysis. This is to establish the long-term average (trend analysis). For the long-term level a wind-index shall be 100% by definition. However for defining the long-term period, there is no unique definition. Meteorological long-term periods normally are defined for 30 years but we have not yet a 30-year period with wind-index calculation. Traditional meteorological ground measurements are used. Also climate model results like NCEP/NCAR, available for each 6 hour. A processed version (MM5 Mesoscale model) is available named as World Wind Atlas (WWA) is used. The climate model data has in general the problem that near surface wind phenomena are not represented. E.g. this means that for warmer regions with much temperature induced wind flow, the data becomes almost useless. Maybe newer models might compensate for this.

From satellites only SSM/I have a series of relevant length (19 years) and reasonably sampling per day (a few per day).

7.2 Wind-index results using SSM/I

For wind index calculation it is important that the number of observations is large and that the data are accessible in near-real-time (NRT) or within a couple of days. For passive microwave (SSM/I) there is a NRT product at the web. The NRT SSM/I wind maps are recalculated in the following weeks and the fully processed SSM/I wind maps are uploaded about 3 weeks after recording. A test was made in the SAT-WIND project on the differences between the NRT SSM/I and the final product. The differences are small, e.g. changes were found near sea ice margins and near hurricane centers and squall lines (heavy tropical rain). In other words, the changes found have to do with the sea ice margin and precipitation flags. Both things are typically found outside the Danish area. Hence it will be possible to rely on the NRT product for wind index calculation in the present study. The wind climate was calculated from the fully processed wind maps.

The SSM/I Pathfinder data products include the daily geophysical data and time-averaged data as follows in table 7.1.

Table 7.1 Available averaged wind products from SSM/I.

daily	orbital data mapped to 0.25 degree grid, data overwritten by later data
3-day	average of 3 days ending on file date
weekly	average of 7 days ending on the Saturday file date
monthly	average of all data within month

The wind-index experiment with SSM/I wind speed data was made for two sites, one in the North Sea and one in the Baltic Sea (see figure 5.15). For each of these two sites observations from four grid cells were extracted. The extracted data files *.dat looked as shown in table 7.2. Here were data from 4 data points, for the latitude and longitude shown in the first two lines. The Field column is YYYYMMDD. The time columns are HHMM, the time the recording was made. -1639 mean “no data” also shown as -999 in the wind speed column. Figure 7.3 presents the number of valid wind observations in the entire dataset.

Table 7.2. Example of wind data extract from SSM/I for the analysis.

longitude	18.25	18.5	18.25	18.5	18.25	18.5	18.25	18.5
latitude	55.75	55.75	56	56	55.75	55.75	56	56
field	time	time	time	time	wspd	wspd	wspd	wspd
19870709	-1639	-1639	-1639	-1639	-999	-999	-999	-999
19870709	1724	1724	1724	1724	7.8	8.2	8.6	9
19870710	312	312	318	318	11.4	11.4	11.2	11
19870710	1712	1712	1712	1712	9.6	7.8	7.2	5.6
19870711	442	442	442	442	8.4	9	9.6	9.8

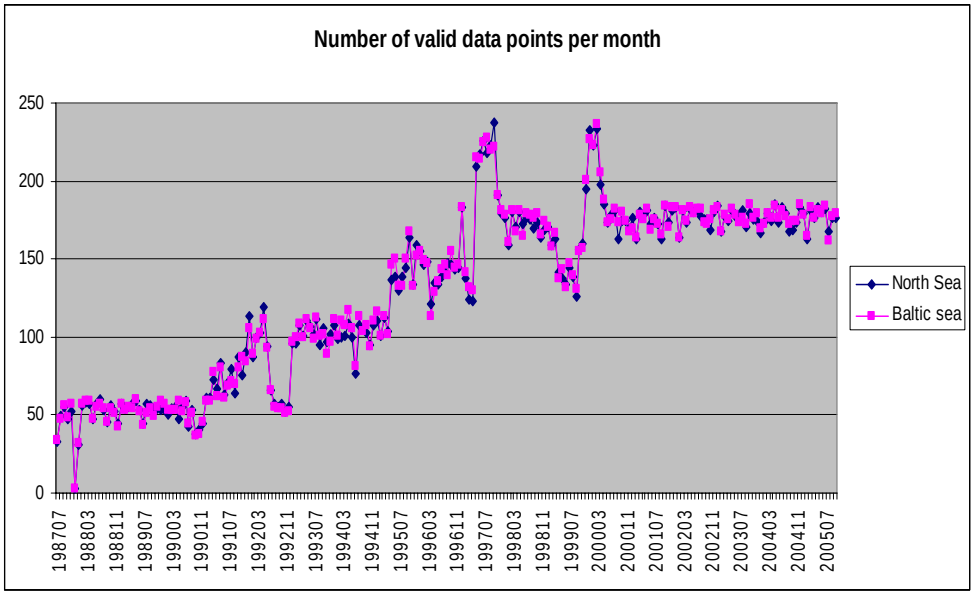

Figure 7.3 From 1987-1990 typically 2 data points per day increases to 6 data points per day from around year 2000 – in-between some changes we do not know the reasons for, but probably the periods with many data are based on more satellites operating in parallel.

From the wind speeds of the 4 neighboring grid cells, the average was taken because then most possible records were obtained, even if only one of the 4 points was available. For each of the mean wind speeds a wind index was calculated based on simply squared wind speed with a "power curve limiter" at 15 ms^{-1}, meaning that at wind speeds above 15 ms^{-1} the wind index simply was set to 15^2.

The resulting long-term average wind speeds based on all approved SSM/I data for the 18 year of data analyzed, the mean wind speeds were 7.7 ms^{-1} for the Baltic Sea and 8.3 ms^{-1} for the North Sea. The data relates to 10m above sea level. The variation in mean wind speed per month during 18 years is graphed figure 7.4 for the Baltic Sea and the North Sea. In the Baltic Sea the monthly minimum was below 4 ms^{-1} and the maximum was around 12 ms^{-1}. For the North Sea the respective values were 5 ms^{-1} and 13 ms^{-1}.

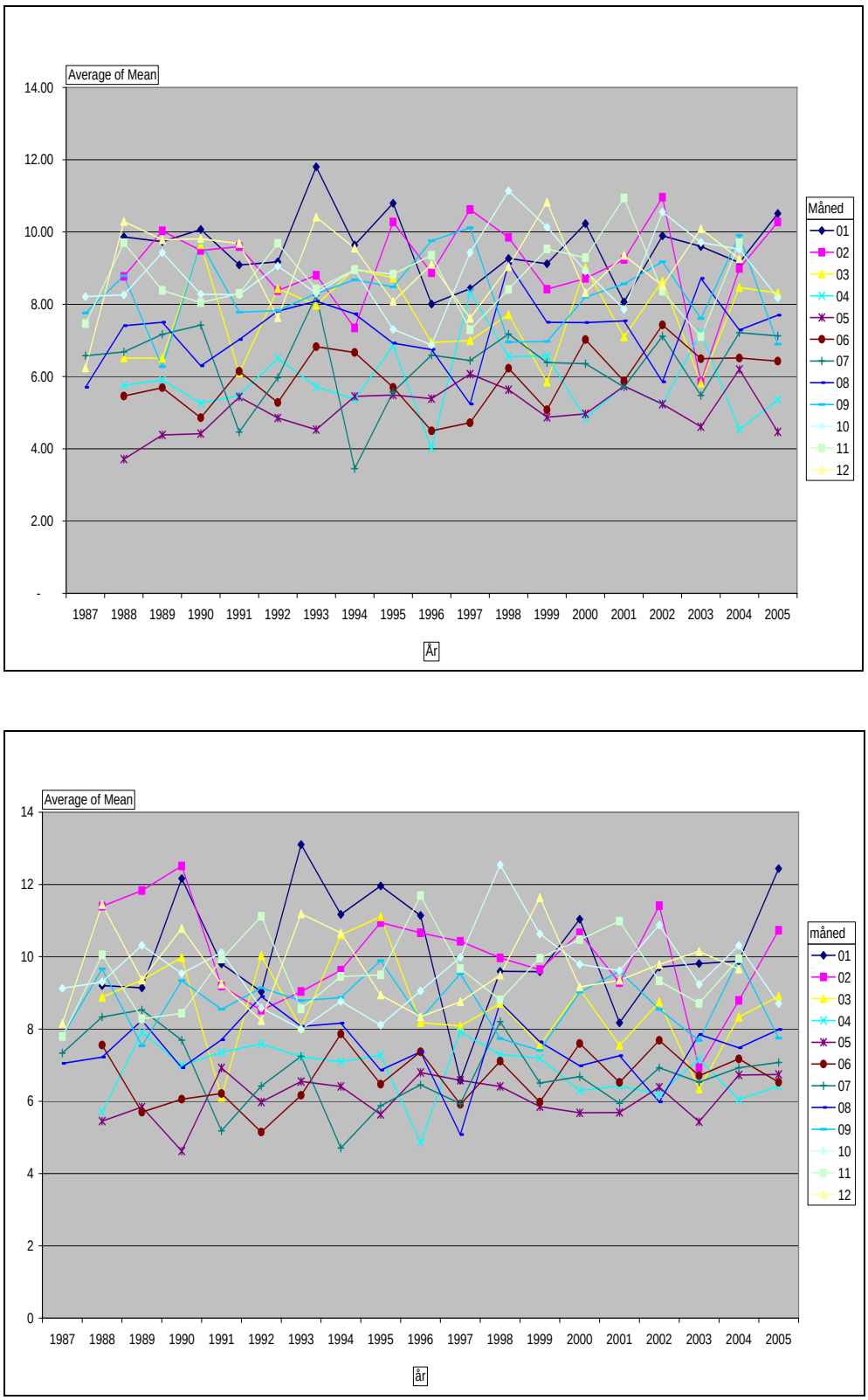

Figure 7.4 Monthly mean wind speeds from SSM/I during 18 years for the Baltic Sea (top panel) and the North Sea (bottom panel). Wind speed for 10 m above sea level.

Calculation of the wind-index includes the following. To get an offshore wind farm relevant wind-index, the SSM/I wind speed data were extrapolated to 80m above sea level with an assumed logarithmic profile and a shear of 0.1. This gave a scaling factor of 1.23. The results presented in figures 7.5 to 7.10 are based on this. The results are shown in figure 7.5 for the North Sea and the Baltic Sea. In this graph also the EMD-ver.06 wind-index is included.

The very first observation from figure 7.5 was that the decreasing trend in the EMD-ver.06 onshore wind turbine generators (WTG)-based index was NOT seen in the offshore indexes.

The second observation was that there were correlations regarding low and high winds during the years. Especially from 1998-2005 there was a good correlation. This is important because in this period the onshore WTG-index had a very high accuracy (i.e. it was based on many relative large turbines). At the same time there were many SSM/I observations (6 data points per day) thus a relatively high level of quality. Before 1998 the data sources were of poorer quality for the WTG-index. Also there were less SSM/I data points per day.

The very interesting issue for both present and future offshore projects is if this really tells us that the offshore wind energy variations are much less than we have seen onshore. It would then mean that the future energy production expectation must be considered as around 100% based on last 5 years, whereas the onshore expectations are 7% below average.

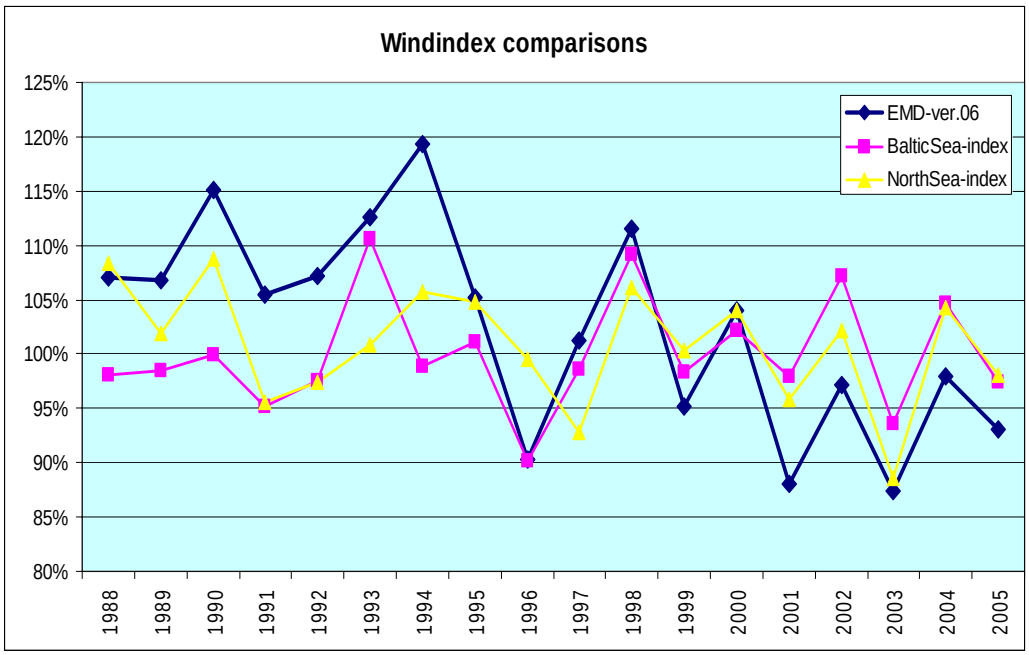

Figure 7.5 Comparison of EMD-ver.06 Danish WTG-based index with SSM/I wind-indexes from the Baltic Sea and the North Sea.

Comparison to Nysted offshore wind farm wind-index was done. The Nysted offshore wind farm is located south of the island Lolland in the Danish part of the Baltic Sea. The monthly comparison with the wind-index at Nysted offshore wind farm based on local measurements near the wind farm is presented in figure 7.6 jointly with the SSM/I wind-index and the EMD-ver.06 WTG-index.

The graph in figure 7.6 indicated that the long-term level of the Nysted wind-index might be too low. Taking an average of the entire period with Nysted experience gave for the SSM/I wind-index an average of 102.5 while Nysted was 98 on average. This made a 5% difference, so the Nysted wind-index might be increased with 5% to make it long-term representative. Or in other words, the long-term production expectations for Nysted should be 5% less than the state-of-the-art expectations.

There was observed a strangely low observation from the SSM/I wind-index for the Baltic Sea in May 2005.

A linear regression was made for the SSM/I Baltic Sea and the Nysted wind-indexes. The correlation (R^2) was only 0.4 so no conclusion could be drawn. The distance between Nysted and the site in the Baltic Sea was large and the winds at Nysted were affected more by land. Similarly a linear regression between Nysted wind-index and the onshore WTG-index was made. R2 = 0.9. But the trend line showed that the interception was not at (0,0). The scatterplots and linear regression results are shown in figure 7.7.

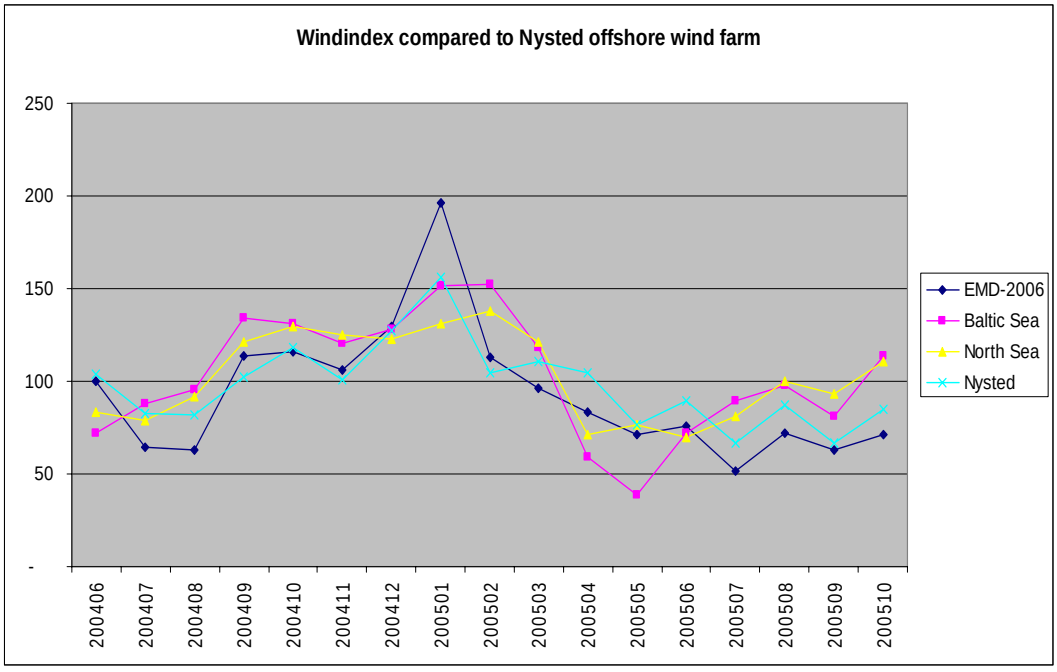

Figure 7.6 Comparison of the monthly wind-index at Nysted offshore wind farm based on local measurements near the wind farm, the SSM/I wind-index and the EMD-ver.06 WTG-index. Nysted data were kindly provided by DONG energy.

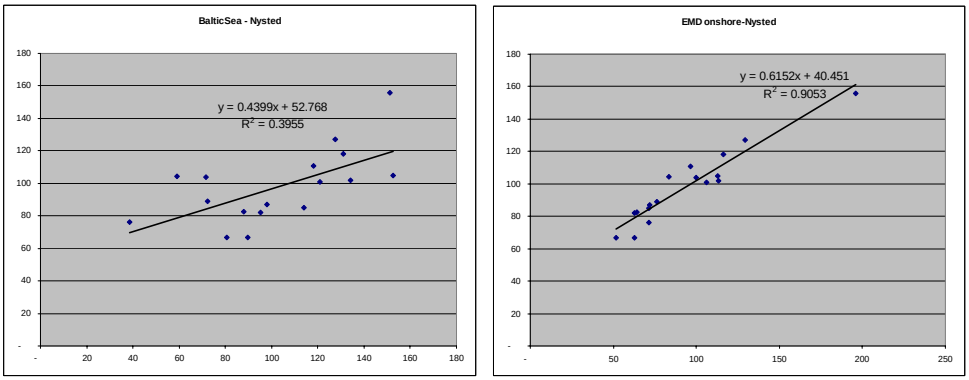

Figure 7.7 Scatterplots and linear regression results between the wind-indexes from SSM/I in the Baltic Sea and Nysted wind-index (left panel) and between EMD-onshore WTG-index and Nysted wind-index.

Monthly long-term comparison was made between the EMD-ver.06 WTG wind-index and the SSM/I wind-indexes from the North Sea and the Baltic Sea. The data are shown in figure 7.8. From the figure two important things were found:

- When the onshore WTG-index was very high, the offshore wind-index did not give similarly high values. This is logical because the offshore wind climate is so much better on average that very windy months do not give much extra (due to power curve saturation characteristic).
- For the low wind months the opposite phenomenon was expected because the offshore wind never became "poor" compared to onshore. This could also be seen as a general trend. However, there are several low wind months with less offshore SSM/I wind-index than onshore. This might be based on that the low wind speeds were not detected accurately in the SSM/I data (or some other systematic problem with these data). This should be investigated further by comparing raw measurement time series. Data for this was not available in the present project.

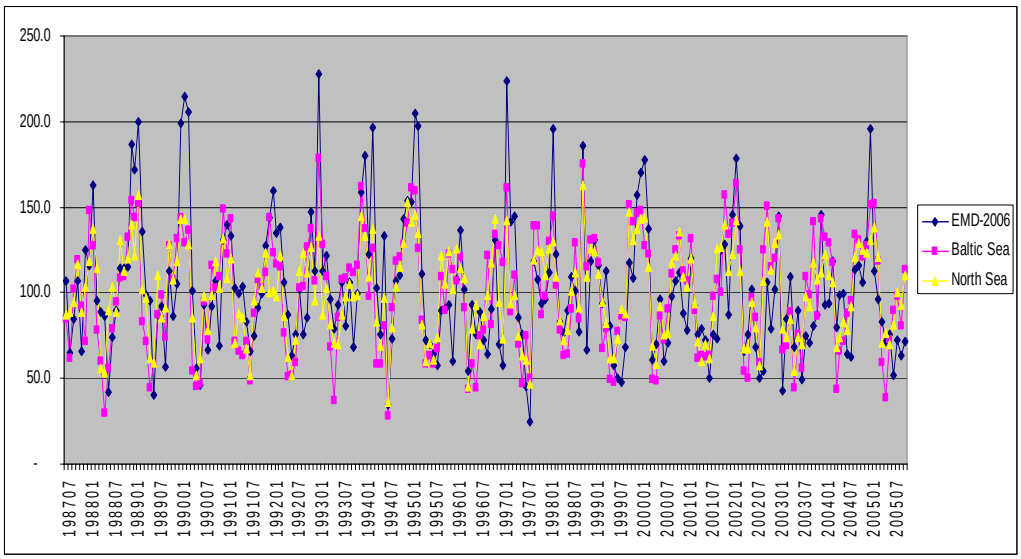

Figure 7.8 Comparison of the monthly EMD-ver.06 WTG onshore index and the SSM/I wind-indexes from the Baltic Sea and the North Sea.

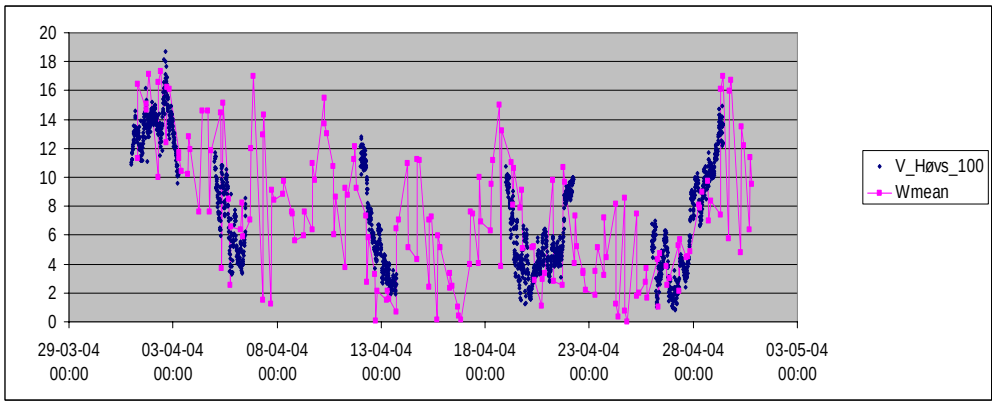
20
18
16
14
12
10
8
6
4
2
0
29-03-04 00:00
03-04-04 00:00
08-04-04 00:00
13-04-04 00:00
18-04-04 00:00
23-04-04 00:00
28-04-04 00:00
03-05-04 00:00
V_Høvs_100
Wmean

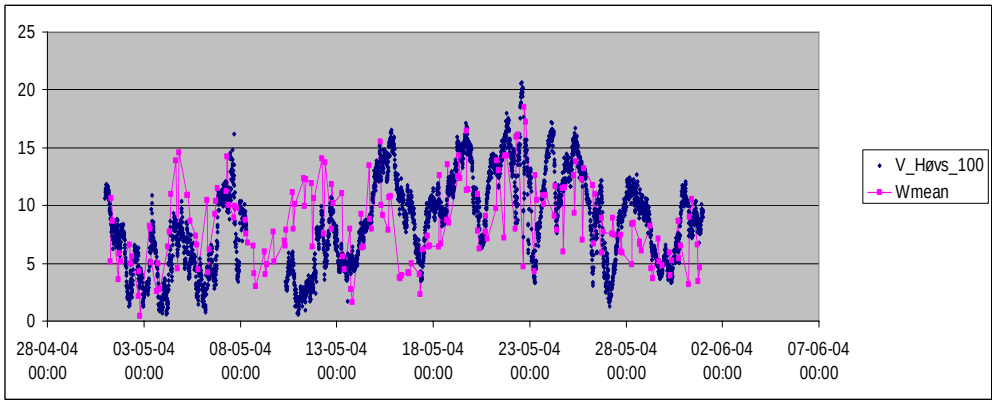
25
20
15
10
5
0
28-04-04 00:00
03-05-04 00:00
08-05-04 00:00
13-05-04 00:00
18-05-04 00:00
23-05-04 00:00
28-05-04 00:00
02-06-04 00:00
07-06-04 00:00
V_Høvs_100
Wmean

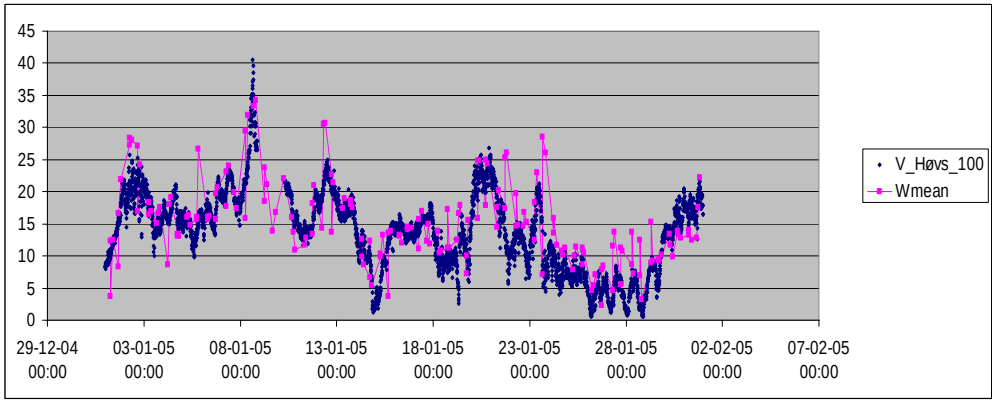
45
40
35
30
25
20
15
10
5
0
29-12-04 00:00
03-01-05 00:00
08-01-05 00:00
13-01-05 00:00
18-01-05 00:00
23-01-05 00:00
28-01-05 00:00
02-02-05 00:00
07-02-05 00:00
V_Høvs_100
Wmean

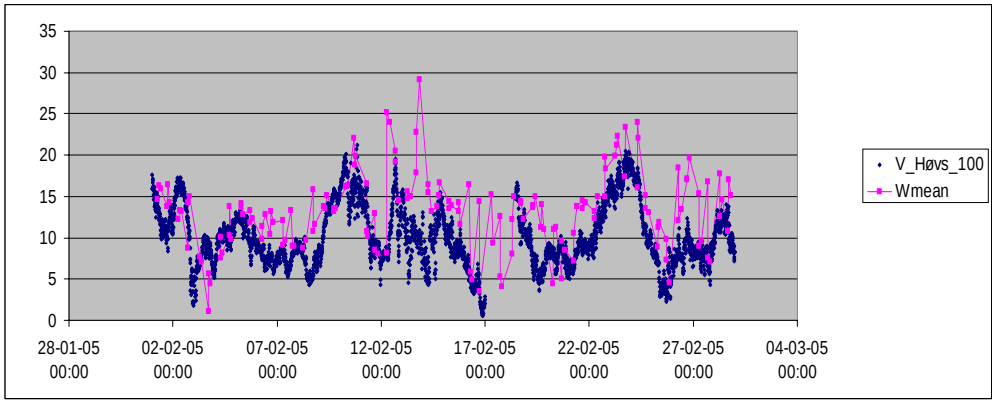
35
30
25
20
15
10
5
0
28-01-05 00:00
02-02-05 00:00
07-02-05 00:00
12-02-05 00:00
17-02-05 00:00
22-02-05 00:00
27-02-05 00:00
04-03-05 00:00
V_Høvs_100
Wmean

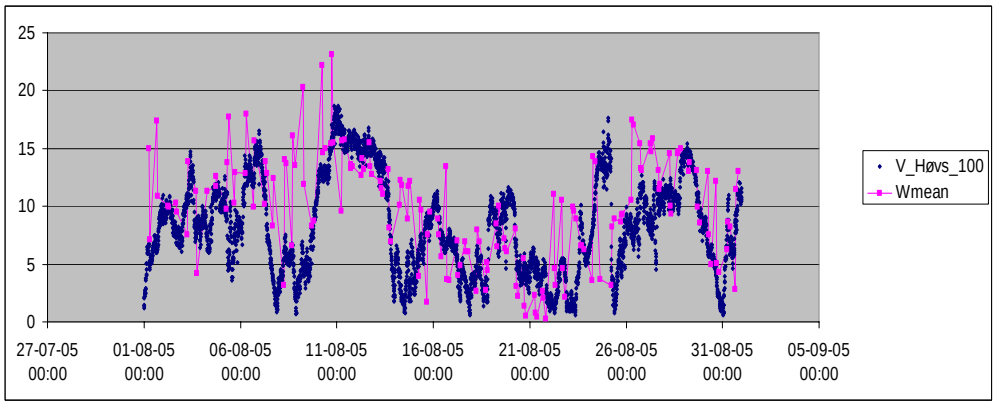

Figure 7.9 Wind speed observed at Høvsøre meteorological mast at 100 m (V_Hovs_100) in ms^{-1} and SSM/I from the North Sea extrapolated to 80m above seal level (Wmean).

Comparison of wind data from the meteorological mast at Høvsøre (Risø) at the coast of Jutland (~1.5 km inland) and the SSM/I North Sea wind speed were done. Examples from the period January 2004 to October 2005 are graphed in figure 7.9.

Wind speed observations from Høvsøre and SSM/I observed at the same times (6 times per day) are presented in figure 7.10. It was found that the agreement was relatively better in January 2005 than in February 2005. The difference in wind speed was calculated and presented with the wind direction observed at Høvsøre. The result is also shown in figure 7.10.

From figure 7.10 it is interesting to see how most of January had very similar (high) wind speeds at the two sites, while the difference was around 5 ms^{-1} for half of February (taken as 6 period average values per day). The wind direction could explain part of the wind speed differences. The differences were larger for easterly winds.

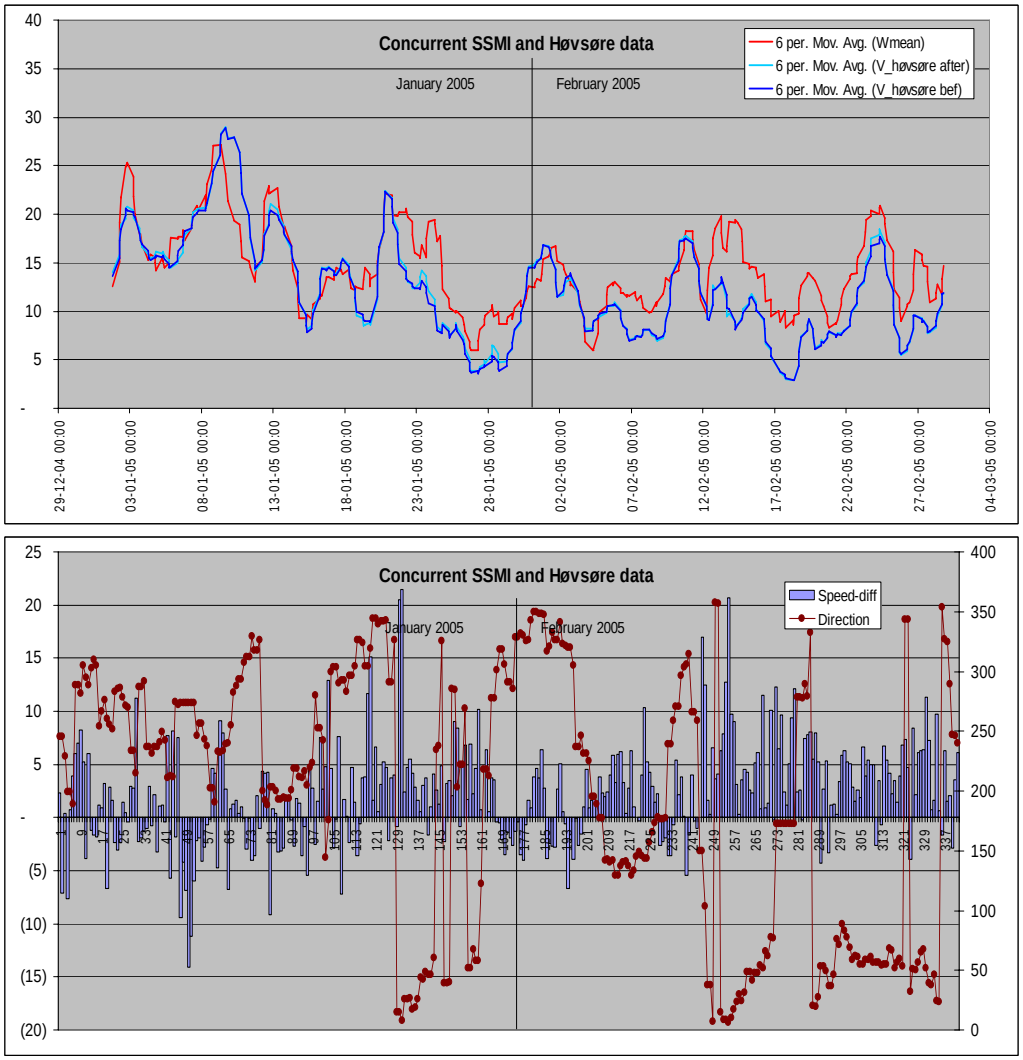

Figure 7.10 Wind speed (moving average) observed at Høvsøre meteorological mast at 100 m and from SSM/I in the North Sea extrapolated to 80 m for two months. Only concurrent observations are included (top panel). Difference in wind speed SSM/I minus Høvsøre data and the wind direction observed at Høvsøre (bottom panel).

The average wind speed for each of the five months (shown in figure 7.9) were calculated for only concurrent observations, i.e. those that were observed 6 times per day at Høvsøre at the same time as the SSM/I wind data were collected in the North Sea. The result is presented in figure 7.11.

From figure 7.10 it was indicated that wind direction could partly explain the agreement/disagreement between the two data sources. Therefore a directional analysis was made for each of the 5 months. The difference in wind speed as a function of wind direction is presented in table 7.3. For westerly winds the wind speed difference was relatively low, while the difference was relatively high for easterly and northerly winds probably due to the sheltering of Jutland and Norway, respectively. Høvsøre is more 'sheltered' than the North Sea. When the wind came from the west, there was almost no

difference in the wind speed. This gave good confidence to the SSM/I wind speed data. There is for sure a potential in the SSM/I wind speed data as a source for wind-index calculations offshore and probably also for production estimation offshore.

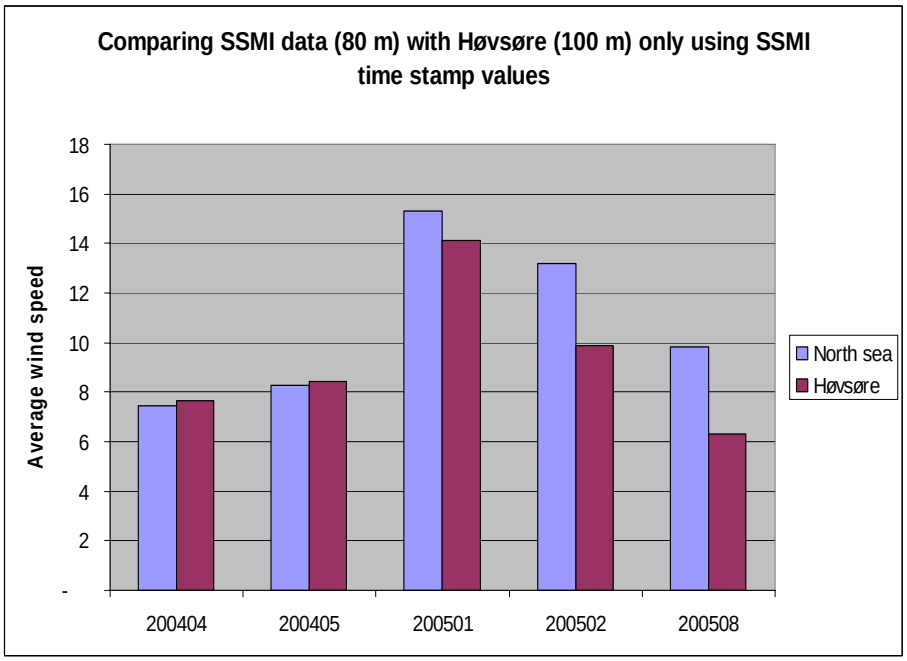

Figure 7.11 Monthly average wind speed from concurrent (same time stamp) wind speed observations from SSM/I in the North Sea (extrapolated to 80 m above sea level) and wind speed from Høvsøre meteorological mast at 100 m.

Table 7.3 The average difference in wind speed between SSM/I observed in the North Sea and Høvsøre meteorological data grouped in the main wind directions.

	North	East	South	West
200404			0,9	2,1
200405	0,7		2,5	
200501	2,6	3,4	1,6	0,3
200502	3,4	4,1	3,8	0,9
200508	4,2		6,1	0,4

8 Discussion

Wind maps from 19 different satellite sensors all capable of mapping ocean winds have been described, obtained and analyzed in the SAT-WIND project. The data include passive microwave wind speed maps from SSM/I and AMSR-E, passive microwave polarimetric wind vector maps from WindSat, scatterometer wind vector maps from ERS SCAT, NSCAT, QuikSCAT and Midori-2, altimeter wind speed maps from ERS-1 and -2, Topex/Poseidon, GFO-1 and Jason-1 and SAR wind vector maps from ERS-2 and Envisat.

In summary, the most frequently recorded ocean wind maps are from passive microwave. These maps, however, contain only wind speed. Currently 6 observations per day are available.

Scatterometer wind maps are also frequent recorded (twice per day). Scatterometer wind maps contain wind vectors hence this data source is very important.

Altimeter data are very sparse, difficult (or costly) to access and only contain wind speed. Therefore altimeter winds are of less interest. However one clear advantage is that altimeter winds are recorded 'randomly' in time (non-sun-synchronous orbit).

Passive microwave polarimetric wind maps resemble scatterometer data but are still of research quality because the data are very new. WindSat is the first sensor of this type. It means that calibration and re-processing of the wind maps will take place. However in the future it is anticipated that passive microwave polarimetric wind maps will compete in quality with scatterometer wind maps.

SAR wind maps are very different from all the above wind observations. First of all, the spatial resolution is more than an order of magnitude higher (compare 25 km by 25 km grid cells to 400 m by 400 m grid cells). This means that SAR wind maps provide observations much closer to the shoreline. SAR wind maps directly cover the offshore areas of interest for wind farming which typically is beyond a 3 km coastal zone. At this high spatial resolution however, one wind map only covers an area of 100 km by 100 km. This may be too small for some applications, e.g. for mapping the Danish Seas. For this task the low-resolution SAR from the wide swath mode seems ideal. Here each wind map covers 400 km by 400 km. The grid resolution is reduced to around 2 km by 2 km.

For all satellite wind map products except SAR, it is necessary to model the open ocean wind statistics into the coastal - wind farming - zone as the grid resolution is too coarse for a true coastal wind mapping. The low resolution wind maps 'blank' out the coastal zone. For SAR the wind maps provide directly spatial wind resource statistics at the location of interest.

The advantages and limitations of the five types of satellite wind maps are listed in table 8.1.

Table 8.1 Wind maps for wind resource mapping: advantages and limitations

	Advantages	Limitations
SAR (high-resolution)	Cover the coastal area Wind vector Long time-series High spatial resolution	Costly for commercial use Very few (3) new observations per month Only available morning and evening
SAR (wide swath mode)	Cover the coastal area Wind vector Good spatial resolution Fairly long time-series	Costly for commercial use Few (8) new observations per month Only available morning and evening
Scatterometer	Long time-series Wind vector Two daily recordings No cost	Only available morning and evening
Passive microwave	Very long time-series Six daily recordings No cost	Only wind speed
Passive microwave polarimetric	Wind vector	Research quality, further calibration of wind algorithm is needed Only available morning and evening
Altimeter	Random sampling times Long time-series	Only wind speed Few data Cost for commercial use

Validation of how accurately a certain single ocean wind speed or wind vector observation was observed from satellite sensors was addressed for SAR, scatterometer (QuikSCAT and ERS SCAT) and altimeter (ERS-2 and Topex and Poseidon). In situ observations from Horns Rev in the North Sea were used for all satellite data types and from Östergarnsholm in the Baltic Sea for QuikSCAT only. The overall finding is that there may be some bias and the rms. error on wind speed is above 1 ms^{-1}. A typical rms. value is around 1.1 to 1.5 ms^{-1}. This type of accuracy does not favor offshore satellite wind observations as a stand-alone solution in wind engineering. The accuracy is too low.

Comparison results on monthly and year time-scale from sensors that observe ocean wind speed frequently (SSM/I 6 times per day; AMSR-E twice per day; QuikSCAT twice per day) were found to be attractive for wind resource mapping. In particular, SSM/I show potential in wind-indexing.

The advantage of QuikSCAT is the 8-year long time-series and that it is the wind vector observed. The example from Denmark and Cape Verde clearly show the significant difference, readily mapped from satellite observations at a global scale. Unfortunately QuikSCAT does not map the coastal area so modeling to the near-coastal zone is necessary. WAsP can be used.

Envisat ASAR was the most promising data set for studies of the coastal wind speed variations in Denmark and Sweden. Comparison results between QuikSCAT mean wind speed maps, Envisat ASAR wind speed maps and KAMM/WAsP and MIUU wind climate maps indicate small-scale variations in wind speed offshore not (yet) fully captured by state-of-the-art wind resource models.

9 Conclusion

The goal of the SAT-WIND project was to verify the applicability of satellite wind maps derived from passive microwave, altimeter, scatterometer and imaging SAR technologies for wind energy tools for wind resources and wind-indexing. This has been achieved. The study area was the Danish Seas including the North Sea, interior seas and the Baltic Sea.

Wind maps from 19 different satellite sensors all capable of mapping ocean winds have been described, obtained and analyzed in the SAT-WIND project. The data include passive microwave wind speed maps from SSM/I and AMSR-E, passive microwave polarimetric wind vector maps from WindSat, scatterometer wind vector maps from ERS SCAT, NSCAT, QuikSCAT and Midori-2, altimeter wind speed maps from ERS-1 and -2, Topex/Poseidon, GFO-1 and Jason-1 and SAR wind vector maps from ERS-2 and Envisat.

There were basically three levels of comparison. The first was to in situ meteorological data and wind power production, i.e. long-term wind-indexing. The second was satellite wind speed inter-comparison during time. The third was offshore mean wind speed maps compared to maps of mesoscale model results in Denmark and Sweden.

In general, the results were good. It was clear that comparison results to in situ meteorological observations were best for onshore flow in near-neutral stability because this is the conditions closest to that of the geophysical model functions. However, also for all other conditions (non-neutral and offshore flow) the satellite wind data appeared suited for wind mapping. The offshore mast data from DONG energy at Horns Rev were excellent for the present validation study.

The wind-indexing results based on SSM/I were very interesting, and may be of importance in offshore wind-indexing. In case the offshore wind resource is truly characterized by less amplitude in winds and also contains higher winds than on land, it is good news to the offshore wind power industry.

The mean wind speed maps from QuikSCAT and Envisat for offshore regions in Denmark and Sweden indicate a more complex pattern of spatial variability than state-of-the-art wind resource models indicate. The overall comparison indicates that satellite offshore wind maps contain information relevant in offshore wind engineering.

The wind resource results are not as accurate as in situ observations and cannot be used as stand-alone for offshore siting. The satellite wind data and maps appear useful in (pre)-feasibility wind resource estimation and in wind-indexing for offshore wind farms.

Acknowledgements

Funding from the Danish Technical Research Council (STVF) Sagsnr. 2058-03-0006, for the SAT-WIND project is greatly appreciated as well as the funding from Strategic Research Council for SAT-WIND-SMV, Sagsnr. 2104-05-0084 for tool development in cooperation with a small-medium size private company, GRAS A/S. The cooperation

with Lars Boye Hansen is greatly appreciated. Satellite data from the European Space Agency (Cat. 1 EO-1356 and EO-3644) projects are acknowledged including access to Envisat rolling data archive. WindSat data from NASA's Jet Propulsion Laboratory are acknowledged. We are also thankful to all institutes that allow free access to satellite-based ocean wind maps based on QuikSCAT, NSCAT, Midori-2, AMSR-E and SSM/I satellite observations. These include PODAAC, CERSAT at IFREMER and Remote Sensing Systems (RSS). Wind maps from ERS SCAT and altimeter (ERS, Topex/Poseidon, GFO-1 and Jason-1) were received from ARGOSS. We are very thankful to Han Wensink at ARGOSS for this. The brand new ALOS PALSAR scene from JAXA/ ESA-ADEN agreement (EO-3729) we appreciate. Our cooperation with Frank Monaldo and Don Thompson at Johns Hopkins University, Applied Physics Laboratory, Maryland, USA for hosting Ph.D. student Merete. B. Christiansen is greatly appreciated as well as access to the JHU/APL near-real-time software. Offshore meteorological data provided by DONG energy are acknowledged. Also the cooperation with Hans Bergström at Uppsala University is greatly appreciated. The work with the MIUU model was financed by the Swedish Energy Agency, project number 20484-1. As the initial work with satellite SAR for offshore wind mapping was started in EU-WEMSAR (ERK6-CT-1999-00017) and followed up in ESA EOMD EO-windfarm (CT 17736/03/I-IW) the cooperation in and funding of the projects are acknowledged.

Reference List

Adrian, G. & Fiedler, F. (1991). Simulation of unstationary wind and temperature fields over complex terrain and comparison with observations. *Beitrage Physical Atmosphere*, 64, 27-48.

Aicken, W. T., Stapleton, N. R., Scott, J. C. & Barrett, E. C. Use of satellite microwave imagery in the assessment of wind resoruces for optimal siting of offshore wind farms. 2002. Paris. Global Wind Power 2002.
Ref Type: Conference Proceeding

Badger, J., Barthelmie, R., Frandsen, S. & Christiansen, M. B. Mesoscale modelling for an offshore wind farm. 1-6. 2006. Brussels, European Wind Energy Association. European Wind Energy Conference and Exhibition, Athens, 2006.
Ref Type: Conference Proceeding

Barthelmie, R. J. & Pryor, S. C. (2003). Can satellite sampling of offshore wind speeds realistically represent wind speed distributions. *Journal of Applied Meteorology*, 42, 83-94.

Beal, B., Young, G. S., Monaldo, F., Thompson, D. R., Winstead, N. S. & Scott, C. High Resolution Wind Monitoring with Wide Swath SAR: A User's Guide. 2004.
Ref Type: Report

Bergström, H. (1996). A climatological study of boundary layer wind speed using a meso--scale higher-order closure model. *J.Appl.Meteor.*, 35, 1291-1306.

Bergström, H. (2002). Boundary-Layer Modelling for Wind Climate Estimates. *Boundary-Layer Meteorology*, 25, 289-299.

Bergström, H. & Källstrand, B. Measuring and modelling the wind climate in a mountain valley in northern Sweden. 2000. Proceedings, Boreas V, 29 Nov.-1 DEc.

2000, Levi, Finland.
Ref Type: Conference Proceeding

Bergström, H. & Källstrand, B. Estimating Wind Potential in a Complex Terrain Arctic Mountain Valley. 842-845. 2001. München, WIP-Renewable Energies. Proceedings of EWEC2001, Copenhagen, 3-7 July 2001.
Ref Type: Conference Proceeding

Christiansen, M. B. & Hasager, C. B. (2005a). Wake effects of large offshore wind farms identified from satellite SAR. *Remote Sensing of Environment*, 98, 251-268.

Christiansen, M. B. & Hasager, C. B. Wake studies around a large offshore wind farm using satellite and airborne SAR. 2005b. Skt. Petersburg, Russia, 20-24 June 2005. 31st International Symposium on Remote Sensing of Environment (ISRSE).
Ref Type: Conference Proceeding

Christiansen, M. B. & Hasager, C. B. (2006). Using airborne and satellite SAR for wake mapping offshore. *Wind Energy*, 9, 437-455.

Christiansen, M. B., Hasager, C. B. & Monaldo, F. (2006a). Offshore winds observed from space. Issues for planning of offshore wind farms. *WindTech Int.*, 2, 6-9.

Christiansen, M. B., Koch, W., Horstmann, J. & Hasager, C. B. (2006b). Wind resource assessment from C-band SAR. *Remote Sensing of Environment*, 105, 68-81.

Du, Y., Vachon, P. W. & Wolfe, J. (2002). Wind direction estimation from SAR images of the ocean using wavelet analysis. *Canadian Journal of Remote Sensing*, 28, 498-509.

Dyer, A. (1974). A review of flux-profile relationships. Boundary-Layer Meteorology. *Boundary-Layer Meteorology*, 7, 363-372.

Enger, L. (1990). Simulation of dispersion in moderately complex terrain. Part A: The fluid dynamic model. *Atmos.Environment*, 24A, 2431-2446.

Enger, L. & Grisogono, B. (1998). The response of Bora-type flow to sea surface temperature. *Quarterly Journal of the Royal Meteorological Society*, 124, 1227-1244.

Enger, L., Koracin, D. & Yang, X. (1993). A numerical study of boundary-layer dynamics in a mountain valley. Part 1: Model validation and Sensitivity Experiments. *Boundary-Layer Meteorology*, 66, 357-394.

Fichaux, N. & Ranchin, T. (2002). Combined extraction of high spatial resolution wind speed and direction from SAR images: a new approach using wavelet transform. *Canadian Journal of Remote Sensing*, 28, 510-516.

Figa-Saldana, J., Wilson, J. J. W., Attema, E., Gelsthorpe, R., Drinkwater, M. R. & Stoffelen, A. (2002). The advanced scatterometer (ASCAT) on the meteorological operational (MetOp) platform: A follow on for European wind scatterometers. *Canadian Journal of Remote Sensing*, 28, 404-412.

Frank, H., Rathmann, O., Mortensen, N. & Landberg, L. The Numerical Wind Atlas, the KAMM/WAsP Method. Risø-R-1252(EN), 1-60. 2001. Roskilde, Denmark.
Ref Type: Report

Frank, H. P. & Landberg, L. (1997). Modelling the wind climate of Ireland. *Boundary-Layer Meteorology*, 85, 359-378.

Gerling, T. W. (1986). Structure of the surface wind field from the SEASAT SAR. *Journal of Geophysical Research,* 91, 2308-2320.

Hasager, C. B. Wind energy mapping using synthetic aperture radar. 259-265. 2000. Germany, EUMETSAT. Proceedings of Fifth International Winds Workshop. 28-2-0003.
Ref Type: Conference Proceeding

Hasager, C. B., Astrup, P., Christiansen, M. B., Nielsen, M. & Barthelmie, R. J. Wind resources and wind farm wake effects offshore observed from satellite. 1-10. 2006a. Proceedings of the European Wind Energy Conference and Exhibition (EWEC) 2006, Athens, Greece.
Ref Type: Conference Proceeding

Hasager, C. B., Astrup, P., Nielsen, M., Barthelmie, R. J., Christiansen, M. B., Pryor, S. C., Nielsen, P. & Sørensen, P. B. SAT-WIND project. First yearly report. 1-53. 2005a. Roskilde, Denmark, Risø National Laboratory. Risø-I-2294(EN).
Ref Type: Report

Hasager, C. B., Barthelmie, R. J., Christiansen, M. B., Nielsen, M. & Pryor, S. C. Quantifying offshore wind resources from satellite wind maps: study area the North Sea. 29-33. 2004a. Proceedings of the European Wind Energy and Exhibition Conference (EWEC) 2004, 22-26 November 2004, London, UK.
Ref Type: Conference Proceeding

Hasager, C. B., Barthelmie, R. J., Christiansen, M. B., Nielsen, M. & Pryor, S. C. (2006b). Quantifying offshore wind resources from satellite wind maps: study area the North Sea. *Wind Energy,* 9, 63-74.

Hasager, C. B., Christiansen, M. B., Barthelmie, R. J., Skriver, H. & Sørensen, P. B. SAR-WAKE results. 2005b. Roskilde, Denmark. Risø-R-1506(EN).
Ref Type: Report

Hasager, C. B., Christiansen, M. B., Peña, A., Badger, J., Antoniou, I., Nielsen, M., Astrup, P. & Courtney, M. (2007). Advances in offshore wind resource estimation.

Hasager, C. B., Dellwik, E., Nielsen, M. & Furevik, B. (2004b). Validation of ERS-2 SAR offshore wind-speed maps in the North Sea. *International Journal of Remote Sensing,* 25, 3817-3841.

Hasager, C. B., Nielsen, M., Astrup, P., Barthelmie, R. J., Dellwik, E., Jensen, N. O., Jørgensen, B. H., Pryor, S. C., Rathmann, O. & Furevik, B. (2005c). Offshore wind resource estimation from satellite SAR wind field maps. *Wind Energy,* 8, 403-419.

Hasager, C. B., Nielsen, M. & Christiansen, M. B. Quantitative remote sensing: Horns Rev wind farm case study. 2004c. SP-572 Envisat/ERS Symposium Proceedings, 6-10 September 2004, Salzburg, Austria.
Ref Type: Conference Proceeding

Hasager, C. B., Nielsen, M. & Christiansen, M. B. Satellite wind resource mapping: State-of-the-art on method and results. 69-75. 2006c. Rome (IT). Offshore wind and other marine renewable energies in Mediterranean and European seas. Proceedings. OWEMES 2006.
Ref Type: Conference Proceeding

Johansson, C. & Bergström, H. Variability in the energy content of the wind over Scandinavia, a 101-year perspective. 21-25. 2004. Proceedings EWEC2004, 21-25 November 2004, London.
Ref Type: Conference Proceeding

Källstrand, B., Bergström, H., Højstrup, J. & Smedman, A. S. (2000). Mesoscale wind field modifications over the Baltic Sea. *Boundary-Layer Meteorology*, 95, 161-188.

Koch, W. (2004). Directional analysis of SAR images aiming at wind direction. *IEEE Transactions on Geoscience and Remote Sensing*, 42, 702-710.

Koracin, D. & Enger, L. (1994). A numerical study of boundary-layer dynamics in a mountain valley. Part 2: Observed and simulated characteristics of atmospheric stability and local flows. *Boundary-Layer Meteorology*, 69, 249-283.

Kramer, H. J. (1996). *Observation of the Earth and its environment*. Berlin: Springer.

Kramer, H. J. (2002). *Observation on the Earth and Its Environement. Survey of missions and sensors*. Berlin: Springer.

Monaldo, F. (2000). The Alaska SAR demonstration and near-real-time synthetic aperture radar winds. *John Hopkins APL Technical Digest*, 21, 75-79.

Monaldo, F., Kerbaol, V., Clemente-Colón, P., Furevik, B., Horstmann, J., Johannessen, J., Li, X., Pichel, W., Sikora, T. D., Thomson, D. J. & Wackerman, C. The SAR measurement of ocean surface winds:an overview. ESA SP-565, 15-32. 2003. ESA. Proceedings of the Second Workshop Coastal and Marine Applications of SAR, 2-12 September 2003, Svalbard, Norway.
Ref Type: Conference Proceeding

Monaldo, F., Thompson, D. R., Pichel, W. & Clemente-Colón, P. (2004). A systematic comparison of QuickSCAT and SAR ocean surface wind speeds. *IEEE Transactions on Geoscience and Remote Sensing*, 42, 283-291.

Monaldo, F. M., Thompson, D. R., Beal, R. C., Pichel, W. G. & Clemente-Colón, P. (2001). Comparison of SAR-derived wind speed with model predictions and ocean byou measurements. *IEEE Transactions on Geoscience and Remote Sensing*, 39, 2587-2600.

Mortensen, N., Heathfield, D. N., Landberg, L., Rathmann, O., TROEN, I. & Petersen, E. L. Wind Atlas Analysis and Wind Atlas Analysis and Application program:WAsP 7.0 Help Facility. ISBN 87-550-2667-2, 1-277. 2000. Roskilde, Risø National Laboratory.
Ref Type: Report

Mortensen, N. G., Hansen, J. C., Badger, J., Jørgensen, B. H., Hasager, C. B., Georgy Youssef, L., Said Said, U., Abd El-Salam Moussa, A., Akmal Mahmoud, M., El Sayed Yousef, A., Mahmoud Awad, A., Amd-El Raheem Ahmed, M., Sayed, M. A. M., Hussein Korany, M. & Adb-El Baky Tarad, M. Wind Atlas for Egypt, Measurements and Modelling 1991-2005. 1-258. 2005. New and Renewable Energy Authority, Egyptian Meteorological Authority and Risø National Laboratory. ISBN 87-550-3493-4.
Ref Type: Report

Nielsen, M., Astrup, P., Hasager, C. B., Barthelmie, R. J. & Pryor, S. C. Satellite information for wind energy applications. Risø-R-1479(EN), 1-57. 2004. Roskilde,

Denmark, Risø National Laboratory. Ref Type: Report

Owinoh, A. Z., Hunt, J. C. R., Orr, A., Clark, P. K. R., Fernando, H. J. S. & NIEUWSTADT, F. T. M. (2005). Effects of changing surface heat flux on atmospheric boundary-layer flow over flat terrain. *Boundary-Layer Meteorology,* 116, 331-361.

Pryor, S. C., Nielsen, M., Barthelmie, R. J. & Mann, J. (2004). Can satellite sampling of offshore wind speeds realistically represent wind speed distributions? Part II Quantifying uncertainties associated with sampling strategy and distribution fitting methods. *Journal of Applied Meteorology,* 43, 739-750.

Sandström, S. (1997). Simulations of the Climatological Wind Field in the Baltic Sea Area using a Mesoscale Higher-Order Closure Model. *J.Appl.Meteor.,* 36, 1541-1552.

Schmith, T., Alexandersson, H., Iden, K. & Toumenvirta, H. North Atlantic-European pressure observations 1868-1995 (WASA dataset 1.0; CD-ROM included). 1997. Denmark, Danish Meteorological Institute. Technical report 97-3. Ref Type: Report

Sempreviva, A. M., Larsen, S. E., Mortensen, N. G. & Troen, I. (1990). Response of Neutral Boundary-Layers to Changes of Roughness. *Boundary-Layer Meteorology,* 50, 205-225.

Shimada, T., Kawamura, H. & Shimada, M. (2003). An L-band Geophysical Model Function for SAR wind retrieval using JERS-1 SAR. *IEEE Transactions on Geoscience and Remote Sensing,* 41, 518-531.

Shimada, T., Kawamura, H., Shimada, M. & et al. (2004). Evaluation of &&JERS-&&1 &&SAR images from a coastal wind retrieval point of view. *IEEE Transactions on Geoscience and Remote Sensing,* 42, 491-500.

Smedman, A., Högström, U. & Bergstrom, H. (1996). Low level jets – a decisive factor for offshore wind energy siting in the Baltic Sea. *Wind Engineering,* 20, 137-147.

Sommer, A. Offshore measurements of wind and waves at Horns Rev and Laesoe, Denmark. 65-79. 2003. Athena. OWEMES 10-12 April 2003, Naples, Italy. Ref Type: Conference Proceeding

Stoffelen, A. & Anderson, D. L. T. (1997). Scatterometer data interpretation: Estimation and validation of the transfer fuction CMOD4. *Journal of Geophysical Research,* 102, 5767-5780.

Thompson, D. R., Monaldo, F. M., Beal, R. C., Winstead, N. S., Pichel, W. G. & Clemente-Colón, P. (2001). Combined estimates improve high-resolution coastal wind mapping. *EOS, Transactions, American Geophysical Union,* 82, 1-3.

Wentz, F. J. A well calibrated ocean algorithm for SSM/I. 101395, 1-34. 1995. Santa Rosa, CA, Remote Sensing Systems. RSS Tech. Report 101395. Ref Type: Report

Appendix A (List of SAT-WIND publications)

PUBLISHED

Review journals

1. Hasager, C.B.; Barthelmie, R.J.; Christiansen, M.B.; Nielsen, M.; Pryor, S.C.. (2006), Quantifying offshore wind resources from satellite wind maps: Study area the North Sea. Wind Energy v. 9 p. 63-74

2. Christiansen, M.B.; Koch, W.; Horstmann, J.; Hasager, C.B.; Nielsen, M.. (2006), Wind resource assessment from C-band SAR. Remote Sens. Environ. v. 105 p. 68-81

3. Hasager, C.B.; Nielsen, M.; Astrup, P.; Barthelmie, R.J.; Dellwik, E.; Jensen, N.O.; Jørgensen, B.H.; Pryor, S.C.; Rathmann, O.; Furevik, B.R.. (2005), Offshore wind resource estimation from satellite SAR wind field maps. Wind Energy v. 8 p. 403-419

Non-reviewed journals

4. Christiansen, M.B.; Hasager, C.B.; Monaldo, F., Offshore winds observed from space. Issues for planning of offshore wind farms. Windtech Int. (2006) **2** (no.5) , 6-9

5. Monaldo, F.M., Thompson, D.R., Winstead, N.S., Pichel, W.G., Clemente-Colón, P. and Christiansen, M.B. 2005 Ocean wind field mapping from Synthetic Aperture Radar and its application to research and applied problems. Johns Hopkins APL Technical Digest, vol. 26, no. 2., p. 102-113

6. Hasager, C.B., Remote sensing at Risø National Laboratory. EARSeL Newsl. (2005) (no.63), 20

Reports

7. Hasager, C. B., Astrup, P., Nielsen, M., Christiansen, M. B., Badger, J., Nielsen, P., Sørensen, P. B., Barthelmie, R. J., Pryor, S. C. & Bergström, H. SAT-WIND Final report. Risø-R-1586(EN), 1-131. 2007. Roskilde, Denmark, http://www.risoe.dk/rispubl/VEA/ris-r-1586.htm

8. Nielsen, M.; Astrup, P.; Hasager, C.B.; Barthelmie, R.J.; Pryor, S.C., *Satellite information for wind energy applications.* Risø-R-1479(EN), Roskilde, Denmark (2004) 57 p. http://www.risoe.dk/rispubl/VEA/ris-r-1479.htm

9. Hasager, C. B., Astrup, P., Nielsen, M., Barthelmie, R. J., Christiansen, M. B., Pryor, S. C., Nielsen, P., and Sørensen, P. B. *SAT-WIND project. First yearly report.* Risø-I-2294(EN). Roskilde, Denmark (2005) 53 p.

Conference proceeding papers

10. Hasager, C.B.; Astrup, P.; Christiansen, M.B.; Nielsen, M.; Barthelmie, R.J. (2006), Wind resources and wind farm wake effects offshore observed from satellite. In: Proceedings (online). 2006 European Wind Energy Conference and Exhibition, Athens (GR), 27 Feb - 2 Mar 2006. (European Wind Energy Association, Brussels) 10 p.

11. Hasager, C.B.; Nielsen, M.; Christiansen, M.B (2006),., Satellite wind resource mapping: State-of-the-art on method and results. In: Offshore wind and other marine renewable energies in Mediterranean and European seas. Proceedings. OWEMES 2006. European seminar, Rome (IT), 20-22 Apr 2006. (ENEA, Roma) p. 69-75

12. *Christiansen, M.B.; Hasager, C.B.*, Wind energy applications of synthetic aperture radar. In: Combined preprints (CD-ROM). 86. AMS annual meeting, Atlanta, GA (US), 29 Jan - 2 Feb 2006. (American Meteorological Society, Boston, MA, 2006) 6 p.

13. *Hasager, C.B.; Christiansen, M.B.; Nielsen, M.; Barthelmie, R.J.*, Using satellite data for mapping offshore wind resources and wakes. In: Proceedings (CD-ROM). Copenhagen offshore wind conference 2005, Copenhagen (DK), 25-28 Sep 2005. (Copenhagen Offshore Wind, Copenhagen, 2005) 10 p.

14. Hasager, C.B.; Nielsen, M.; Astrup, P. (2005), Remote sensing for wind energy applications. In: Proceedings (CD-ROM). 31. International symposium on remote sensing of environment: Global monitoring for sustainability and security, St. Petersburg (RU), 20-24 Jun 2005. (Nansen International Environmental and Remote Sensing Centre, St. Petersburg) 3 p.

15. Hasager, C.B.; Nielsen, M.; Christiansen, M.B.; Barthelmie, R.J.; Astrup, P., Advances on wind energy resource mapping from SAR. In: Abstract book. SEASAR 2006 - Advances in SAR oceanography from ENVISAT and ERS missions, Rome (IT), 23-26 Jan 2006. (European Space Agency, Paris, 2006) http://earth.esa.int/workshops/seasar2006/proceedings/

16. *Hasager, C.B.; Nielsen, M.; Christiansen, M.B.*, Quantitative remote sensing: Horns Rev wind farm case study. In: Proceedings (CD-ROM). 2004 Envisat and ERS symposium, Salzburg (AT), 6-10 Sep 2004. (European Space Agency, Paris, 2005) 4P17-1 (6 p.)

17. *Hasager, C.B.; Nielsen, M.; Christiansen, M.B.*, RWT tool: Offshore wind energy mapping from SAR. In: Proceedings (CD-ROM). 2004 Envisat and ERS symposium, Salzburg (AT), 6-10 Sep 2004. (European Space Agency, Paris, 2005) (SP-572) 2P14-2 (6 p.)

18. Barthelmie, R.J.; Giebel, G.; Jørgensen, B.H.; Badger, J.; Pryor, S.C.; Hasager, C.B., Comparison of corrections to site wind speeds in the offshore environment: Value for short-term forecasting. In: *Scientific Proceedings CD-ROM. 2004 European Wind Energy Conference and Exhibition, London (GB), 22-25 Nov 2004*. (European Wind Energy Association, Brussels, 2005), 9 p.

19. Hasager, C.B.; Barthelmie, R.J.; Christiansen, M.B.; Nielsen, M.; Pryor, S.C., Quantifying offshore wind resources from satellite wind maps: Study area the North Sea. *In: Scientific proceedings. 2004 European Wind Energy Conference and Exhibition, London (GB), 22-25 Nov 2004.* (European Wind Energy Association, London, 2004) p. 29-33

20. Hasager, C.B.; Christiansen, M.B., Coastal wind mapping from satellite SAR: Possibilities and limitations. I*n: Conference proceedings. 4. Study conference on BALTEX, Gudhjem (DK), 24-28 May 2004. Isemer, H.-J. (ed.)*, (International BALTEX Secretariat, Geesthacht, 2004) (International BALTEX Secretariat publication, no. 29) p. 21-22

Conference abstracts

21. Hasager, C.B., Astrup, P., Nielsen, P., Christiansen, M.B., Nielsen, M., 2007 Satellite ocean surface winds in offshore wind engineering. European Geosciences Union (EGU) General Assembly. Vienna (Austria), 16-20 April 2007, http://www.cosis.net/abstracts/EGU2007/01605/EGU2007-J-01605.pdf

22. Hasager, C.B.; Christiansen, M.B.; Nielsen, M., SAR wind mapping. In: Abstract book. 2. International symposium on recent advances in quantitative remote sensing (RAQRS 2), Torrent (ES), 25-29 Sep 2006. (Universitat de Valencia, Valencia, 2006) p. 168-169

23. Hasager, C.B.; Christiansen, M.B.; Nielsen, M., Wind climate in the Danish Seas observed from the Envisat satellite. EGU General Assembly 2006, Vienna (AT), 2-7 Apr 2006. Geophys. Res. Abstr. (CD-ROM) (2006) 8 (no.Abstr. EGU06-A-03132)

24. Hasager, C.B.; Nielsen, M.; Pryor, S.C., Offshore wind resource assessment through satellite images. EGU General Assembly 2004, Nice (FR), 25-30 Apr 2004. Geophys. Res. Abstr. (CD-ROM) (2004) 6

25. Hasager, C.B.; Nielsen, M.; Christiansen, M.B.; Barthelmie, R.J.; Astrup, P., Advances on wind energy resource mapping from SAR. In: Abstract book. SEASAR 2006 - Advances in SAR oceanography from ENVISAT and ERS missions, Rome (IT), 23-26 Jan 2006. (European Space Agency, Paris, 2006) 1 p.

26. Hasager, C.B.; Nielsen, M.; Astrup, P.; Christiansen, M.B.; Barthelmie, R.J., SAT-WIND: Mapping the offshore wind resources near Denmark using satellite observations. EGU General Assembly 2005, Vienna (AT), 24-29 Apr 2005. Geophys. Res. Abstr. (CD-ROM) (2005) 7

27. Hasager, C.B., Satellite SAR applied in offshore wind resource mapping: Possibilities and limitations. In: Abstracts (CD-ROM). 35. COSPAR scientific assembly 2004, Paris (FR), 18-25 Jul 2004. (CNES, Paris, 2004)

Public information

Information on the SAT-WIND project may be found at the SAT-WIND homepage

http://risoe-staged.risoe.dk/Research/sustainable_energy/wind_energy/projects/sat-wind.aspx

Appendix B (Bitmap color scale)

Scatterometer image color scale

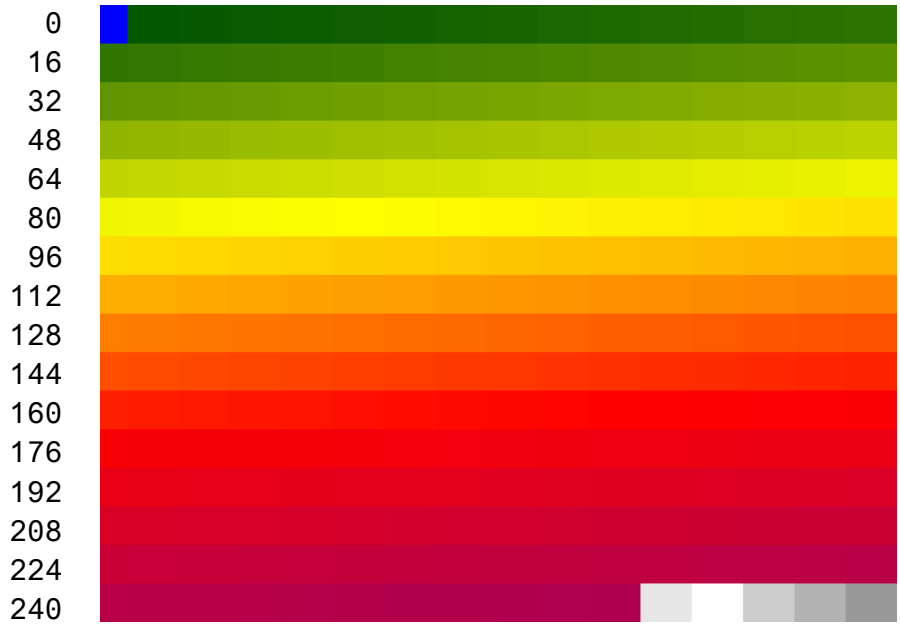

The colors applied to the scatterometer bitmaps are blue for pixel value 0, from dark green over lighter green, yellow, orange, and red to somewhat violet for values 1 to 250, and 5 shades of gray for the flag values 251 to 255.

Appendix C (Technical details on SAR systems)

Technical details on SAR systems

From http://www.nap.edu/html/ssb_html/SAR/sartab11.htm

Comparison of SAR Systems

Parameter	ERS-1	ERS-2	SIR-C	SIR-C/X-SAR	Rad-arsat	Envisat (ASAR)	JERS-1	PALSAR	MIR-PRI-RODA	ALMAZ-1	MITI SAR-2
Radar band	C	C	C, L	X	C	C	L	L	L,S	S	L
Polarization	VV	VV	all	VV	HH	HH,VV, HV	HH	HH or VV HV or VH	*	HH	HH
Look angle (degrees)	24	24	- 17-60 ^	17-60	10-60	20-45	35	20-55	35	30-60	20-45
Resolution (m) / per number of looks	25/4	25/4	25/4	25/4	10-100/1-8	30/4	18/3	10-100/1-8	*	15/2	10-100/*
Swath width (km)	100	100	15-100	15-40	50-500	50-400	76	70-250	120	20-45	50-500
System sensitivity (dB)	-25	-25	-50	-22	-23	*	-20	-25	*	*	-25
Altitude (km)	790	785	225	225	790	600	568	700	394	300	700
Simultaneous frequencies	1	1	3	3	1	1	1	1	2	1	1
Simultaneous polarizations	1	1	4	4	1	2	1	2	*	1	1
Orbit inclina-tion (degree)	97.7	97.7	57	57	98.6	100	93.7	98	51.6	72.7	97.7
Bandwidth (MHz)	13.5	13.5	10, 20	10, 20	12-30	14	15	30	*	*	50
Data rate (Mbps)	105	105	90 or 46 per channel	45	105 (direct) 85 (recorded)	100	60	240	*	*	240
Launch date	07/91	04/95	04, 10/94	04, 10/94	11/95	1999	02/92	08/2002	TBD	03/91	2004
Design lifetime (yrs)	3	3	11 days	11 days	5	5	2	3-5	2	2	3-5

* Information unavailable

NOTE: dB = decibels; HH = horizontal horizontal polarization; HV = horizontal vertical polarization; VH= vertical horizontal polarization; VV = vertical vertical polarization; Mbps = megabits per second; TBD = to be determined.

SOURCE: Jet Propulsion Laboratory, Working Group Draft Report, JPLD-13945, Jet Propulsion Laboratory, Pasadena, California, p. 12.

Mission

To promote an innovative and environmentally sustainable technological development within the areas of energy, industrial technology and bioproduction through research, innovation and advisory services.

Vision

Risø's research **shall extend the boundaries** for the understanding of nature's processes and interactions right down to the molecular nanoscale.

The results obtained shall **set new trends** for the development of sustainable technologies within the fields of energy, industrial technology and biotechnology.

The efforts made **shall benefit** Danish society and lead to the development of new multi-billion industries.

Risø’s research is aimed at solving concrete problems in the society.

Research targets are set through continuous dialogue with business, the political system and researchers.

The effects of our research are sustainable energy supply and new technology for the health sector.